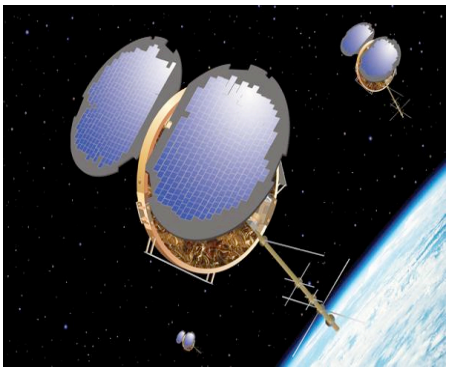

COSMIC

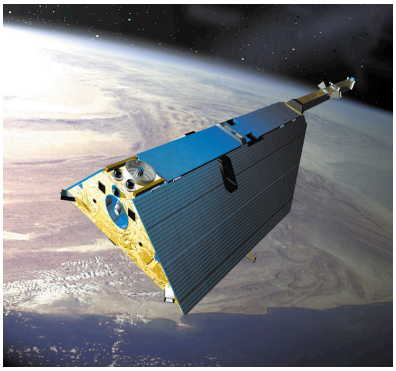

CHAMP

YEAR 2 BI-ANNUAL PROJECT REPORT (from 12/01/2012 to 05/30/2013)
NOAA Award number: NA10NES4400002

# Construction of Consistent Microwave Sensor Temperature Records and Tropopause Height Climatology using MSU/AMSU Measurements, GPS RO Data, and Radiosonde Observations


**Principal Investigator:**
Shu-Peng (Ben) Ho (303-497-2922, spho@ucar.edu)

**Co-Investigators:**
Cheng-Zhi Zou ((301) 763-8042 x156, cheng-zhi.zou@noaa.gov)
Ying-Hwa Kuo ((303) 497-8910, kuo@ucar.edu)

**National Center for Atmospheric Research**
**P.O. Box 3000, Boulder, CO 80307 USA**

# 1. Introduction

In this report, we summarize the continuous efforts since the last report (submitted in December 2012) for this project. The work undertaken to date is detailed in Section 2. We list presentations and publications since December 2012 in section 3.

# 2. Progress on Proposed Studies

***Continued efforts since the last report have focused on: 1) Refining AMSU Ch9 processing method, 2) Refining AMSU Ch7 (Temperatures of Tropopause/Stratosphere – TTS) calibration algorithm, 3) Refining the method to construct the global tropopause height climatology using GPS radio occultation data.***

### 2.1 Construction AMSU/MSU TLS climate data records from 1978 to 2010

#### a. Refining AMSU Ch9 processing method and the results from 2001 to 2012

During the performance period, we continue refining the calibration algorithm. A sequence of processing steps is implemented to use the RO data to calibrate the AMSU TLS and merge the calibrated TLS among multiple AMSU missions. The procedure consists of the following steps:

i) Forward calculation of the AMSU TLS using RO temperature profiles

ii) Data Matching : To avoid the spatial and temporal representation errors, we collocate AMSU pixels with each RO profile within 30 minutes and 100 km. AMSU pixels with a satellite viewing angle ranging from -15 degrees to 15 degrees are all included in this study to increase the number of AMSU pixels in our comparison.

iii) Calculation of the calibration coefficients: The quality of the RO temperatures over the vertical range of AMSU Ch9 weighting function leads to comparable brightness temperatures $TLS^{RO}$. The highly linear relationship between $TLS^{RO}$ and the measured AMSU brightness temperatures ($TLS^{AMSU}$) permits calibration via a simple linear fit.

iv) Merging Procedures: Prior to the application of the linear calibration, daily means of the AMSU Ch9 brightness temperatures for each NOAA orbiter on a 2.5 degree $\times$ 2.5 degree grid are calculated. Only AMSU pixels with a satellite viewing angle ranging from -15 degrees to 15 degrees are included in the binning procedure.

Using above procedures, monthly means of AMSU TLS can be generated for each NOAA orbiters on a 2.5 degree $\times$ 2.5 degree grid. Fig. 1 depicts the time series TLS differences for N16, N18, N19, Aqua, and Metop-A relative to those of N15 globally (Fig. 1a), for the northern high-altitudes (Fig. 1b), and for the southern mid-latitudes (Fig. 1c), respectively. Both the intersatellite biases

among the missions and the possible location- and time- (e.g., scene-) dependent biases are largely eliminated. The mean Aqua-N15 TLS anomaly is more obvious in the north high-latitudes (Fig. 1b). Because the Aqua orbit does not drift in local time after launch, the possible 0.2 K Aqua-N15 TLS anomalies may be due to the combined effect of the N15 orbit drift of local time and the SZA-related bias. Because all of the AMSU TLS are calibrated against RO data from 2001 to 2010, the global mean time series of intersatellite biases for N16-N15, N18-N15, N19-N15, Aqua-N15, and Metop-A-N15 are equal to (0.01, 0.00, 0.06, 0.09, 0.03)K with the standard deviation of (0.12, 0.11, 0.11, 0.12, 0.14)K, respectively.

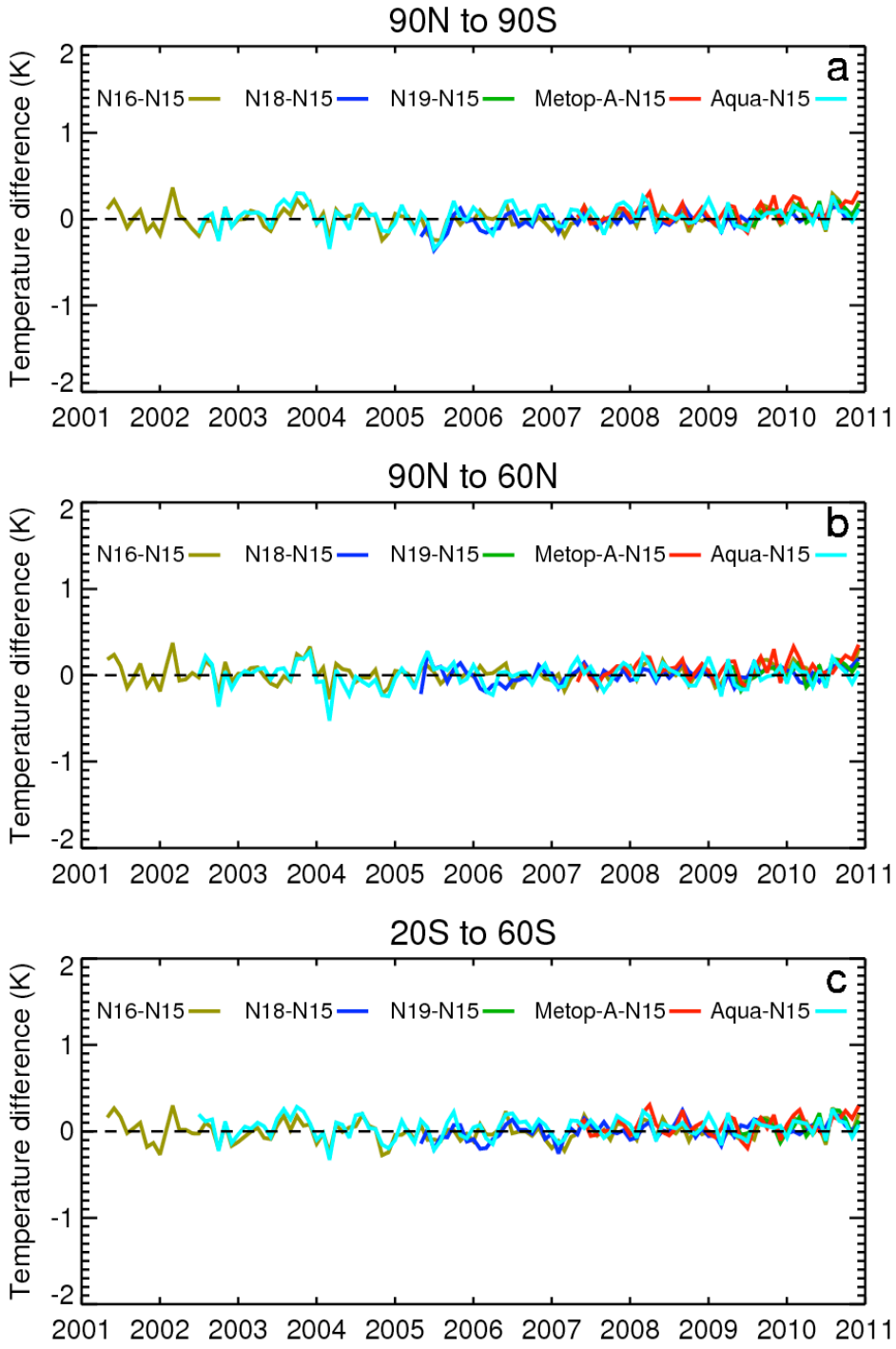


Figure 1. The time series of the calibrated monthly TLS mean differences for N16, N18, N19, Aqua, and Metop-A relative to those of N15 for (a) the entire globe (90ºN to 90ºS), (b) the 90ºN to 60ºN zone, and (c) the 20ºS to 60ºS zone.

### b. AMSU TLS Anomaly Climatology and Trends

By merging the daily TLS from all the available missions from the same month, we construct the monthly TLS CDR from 2001 to 2010. Fig. 2 depicts the merged de-seasonalized TLS anomalies ($\Delta TLS^{Deseason}$) for the globe, the northern high-latitudes, the northern mid-latitudes, the Tropics, the southern mid-latitudes, and the southern high-latitudes, respectively. The mean monthly TLS climatology for each region is computed from January 2002 to December 2010. The global trend during this period is equal to -0.17 K/decade. The TLS anomalies trend for each of the northern high-latitudes, the northern mid-latitudes, the Tropics, the southern mid-latitudes, and the southern high-latitudes is equal to 0.01 K/decade, 0.025 K/decade, 0.01 K/decade, -0.179 K/decade, and -1.037 K/decade, respectively.

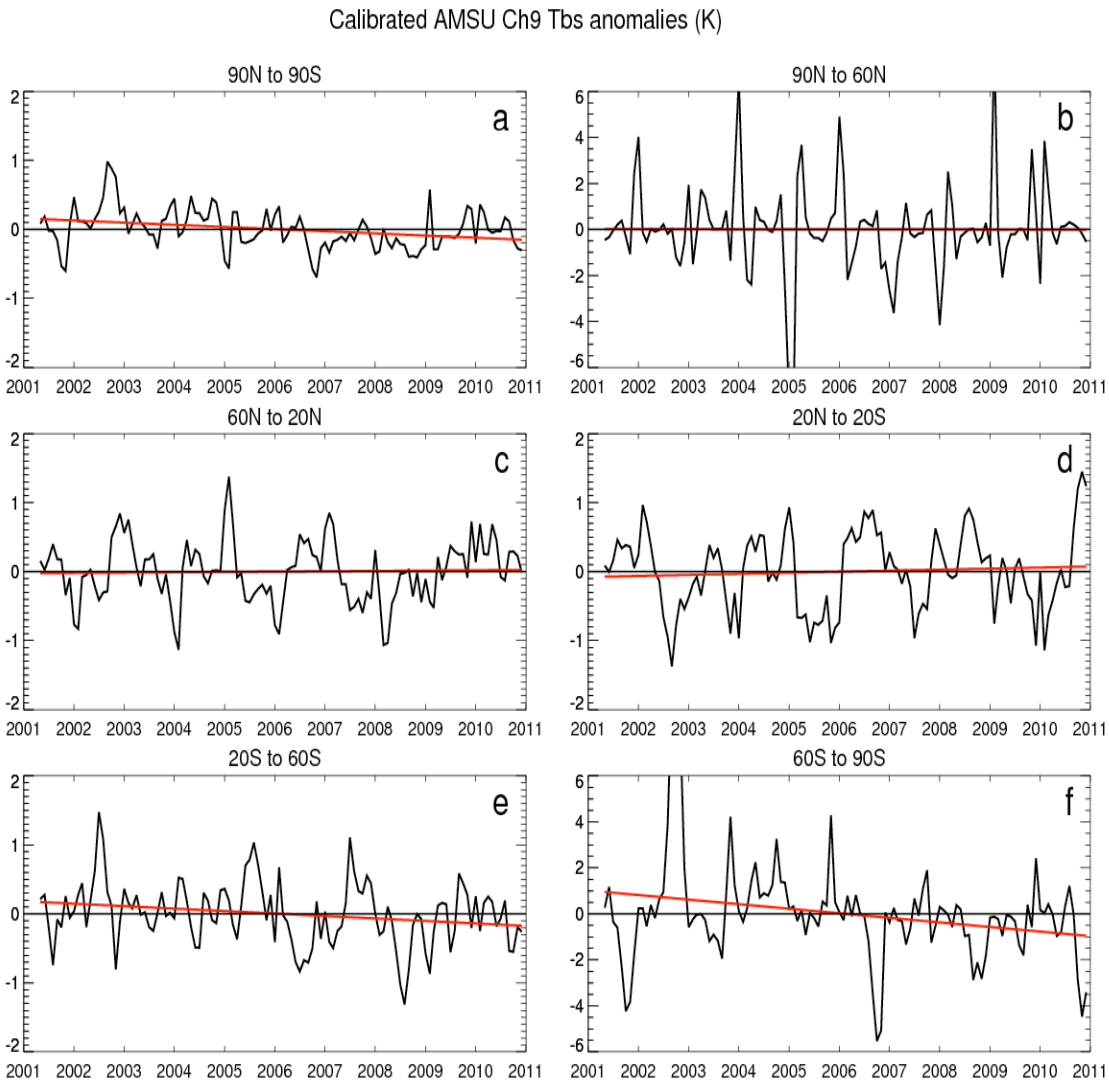


Figure 2. The merged de-seasonalized TLS anomalies ($\Delta TLS^{Deseason}$) for (a) the entire globe (90ºN to 90ºS), (b) the 90ºN to 60ºN zone, (c) the 60ºN to 20ºN zone, (d) the 20ºN to 20ºS zone, (e) the 20ºS to 60ºS zone, and (f) the 60ºS to 90ºS zone.

**c. Using the Simultaneous nadir overlapping (SNO) method and RO calibrated AMSU Ch9 and MSU ch4 from 2001 to 2010 to calibrate the MSU data from 1978 to 2001**

Before applying the consistent calibration method from 1978 to 2012, we first apply SNO method to the MSU data from 1978 to 2000. This is to use the collocated MSU data from different NOAA missions when their field of views (FOVs) are collocated in terms of time and locations. Details are not described here. Then using the collocated MSU-MSU TLS pairs, we define the calibration coefficients for the collocation pairs. The inter-satellite biases between two missions are generated in Figure 3. We separate the inter-satellite biases into six latitudinal zones. The very close to zero monthly mean inter-satellite biases between NOAA9-NOAA10, NOAA8-NOAA9, NOAA7-NOAA8, NOAA6-NOAA7, NOAA11-NOAA10, NOAA12-NOAA11, and NOAA14-NOAA12 give us confidence for our approaches.

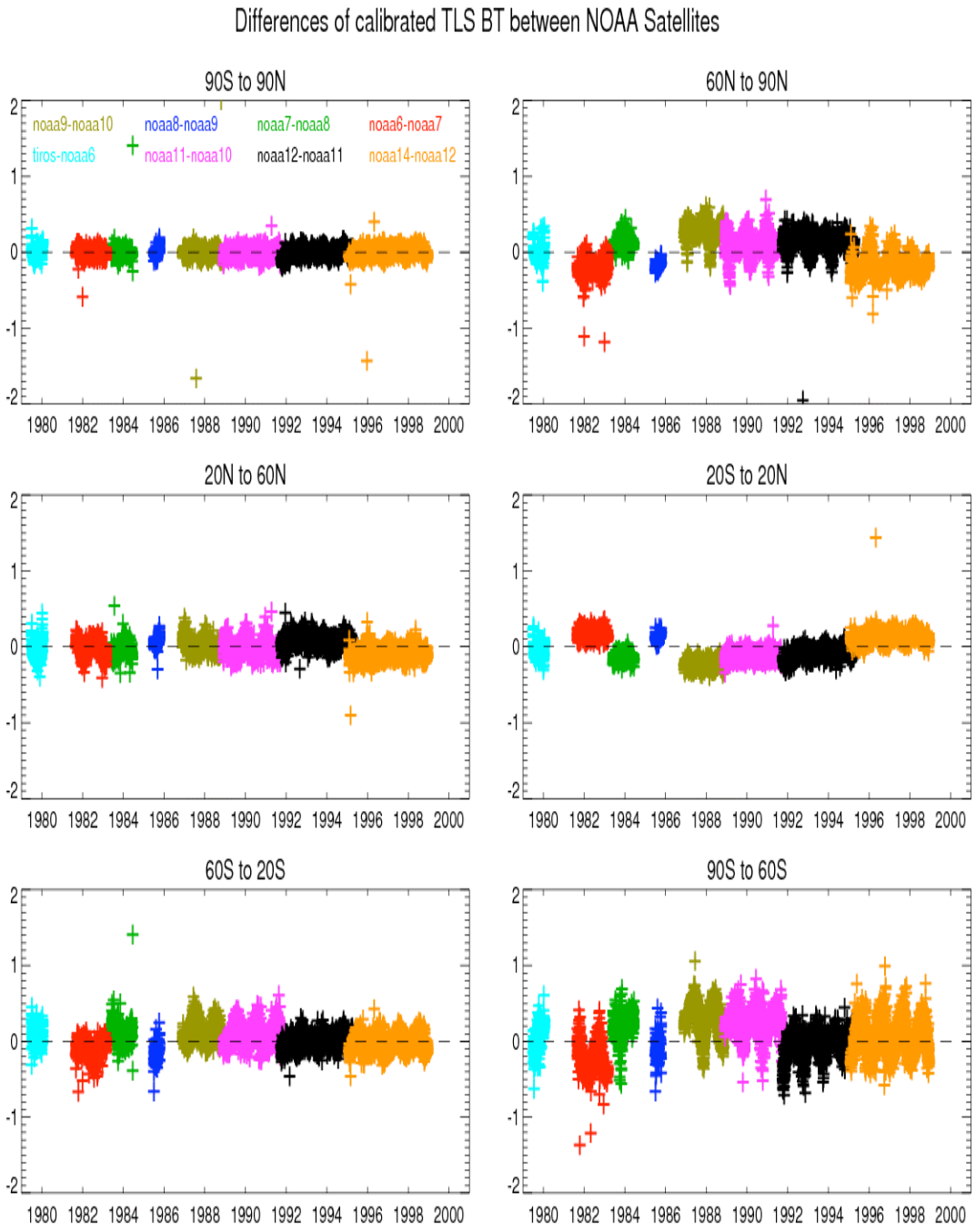


Fig. 3 The time series of the calibrated monthly TLS mean differences for NOAA9-NOAA10, NOAA8-NOAA9, NOAA7-NOAA8, NOAA6-NOAA7, NOAA11-NOAA10, NOAA12-NOAA11, and NOAA14-NOAA12 for (a) the entire globe (90ºN to 90ºS), (b) the 90ºN to 60ºN zone, (c) the 20ºN to 60ºN zone, (d) the 20ºS to 20ºN zone, (e) the 60ºS to 20ºS zone, and (f) the 90ºS to 60ºS zone.

## 2.2 Refining AMSU Ch7 (Temperatures of Tropopause/Stratosphere – TTS) calibration algorithm

In this study, we use COSMIC and CHAMP data to identify high quality radisodonde types and use temperature profiles from those radiosonde types to calibrate brightness temperatures for the temperature of troposphere stratosphere (TTS) from Advanced Microwave Sounding Unit (AMSU). Five types of Vaisala radiosonde data from the year of 2001 to 2010 were used to calibrate Temperatures of Tropopause/Stratosphere (TTS) taken from AMSU microwave measurements from different satellites for potential improvements of tropopause and Stratosphere temperature trend analysis. Five types of Vaisala RS80 and RS90 radiosondes data collected from 2001 to 2010 are used to simulate Channel 7 (TTS) brightness temperatures (Tbs) for AMSU instruments on board NOAA15, 16, 18, 19 and Metop-A. Using radiosonde simulated AMSU Tbs, we calibrate AMSU TTS from different NOAA missions in the same month. A new microwave sensor temperature record in the lower stratosphere and troposphere from 2001 to 2010 is constructed. The derived TTS record is compared with the available TTS datasets generated by other groups. The causes of the TTS differences among these datasets are discussed. Fig. 3 The scattering plot for the monthly collocated RAOB simulated TTS comparing to the collocated NOAA TLS. Figure 4 show the time series of AMSU ch7 Tbs between NOAA16-NOAA15, NOAA18-NOAA15, NOAA19-NOAA15, Metop-A – NOAA15 for the global (upper left panel), 90º N to 60º N zone (upper right panel), 20º N to 60º N zone (middle left panel), 20º N to 20º S zone (middle right panel), 60º S to 20º S zone (lower left panel), and 90º S to 60º S zone (lower right panel). The inter-satellite biases among missions give us the confidence of this approach.

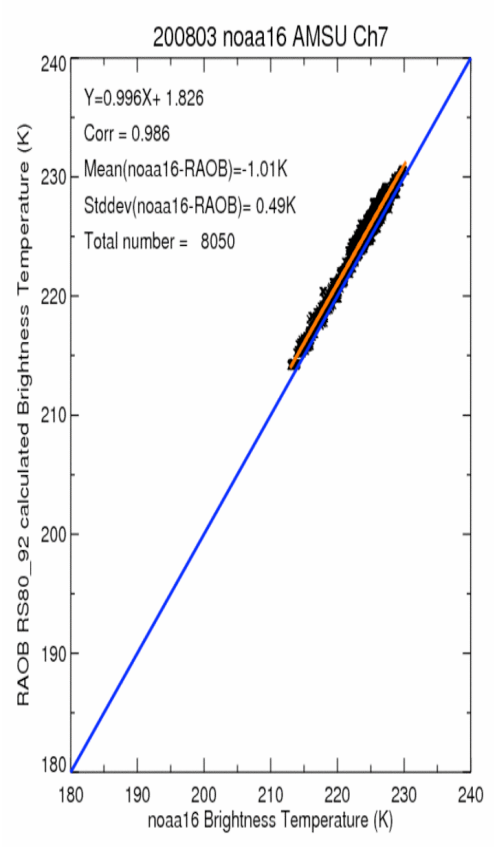


Fig. 3 The scattering plot for the monthly collocated RAOB simulated TTS comparing to the collocated NOAA TLS.

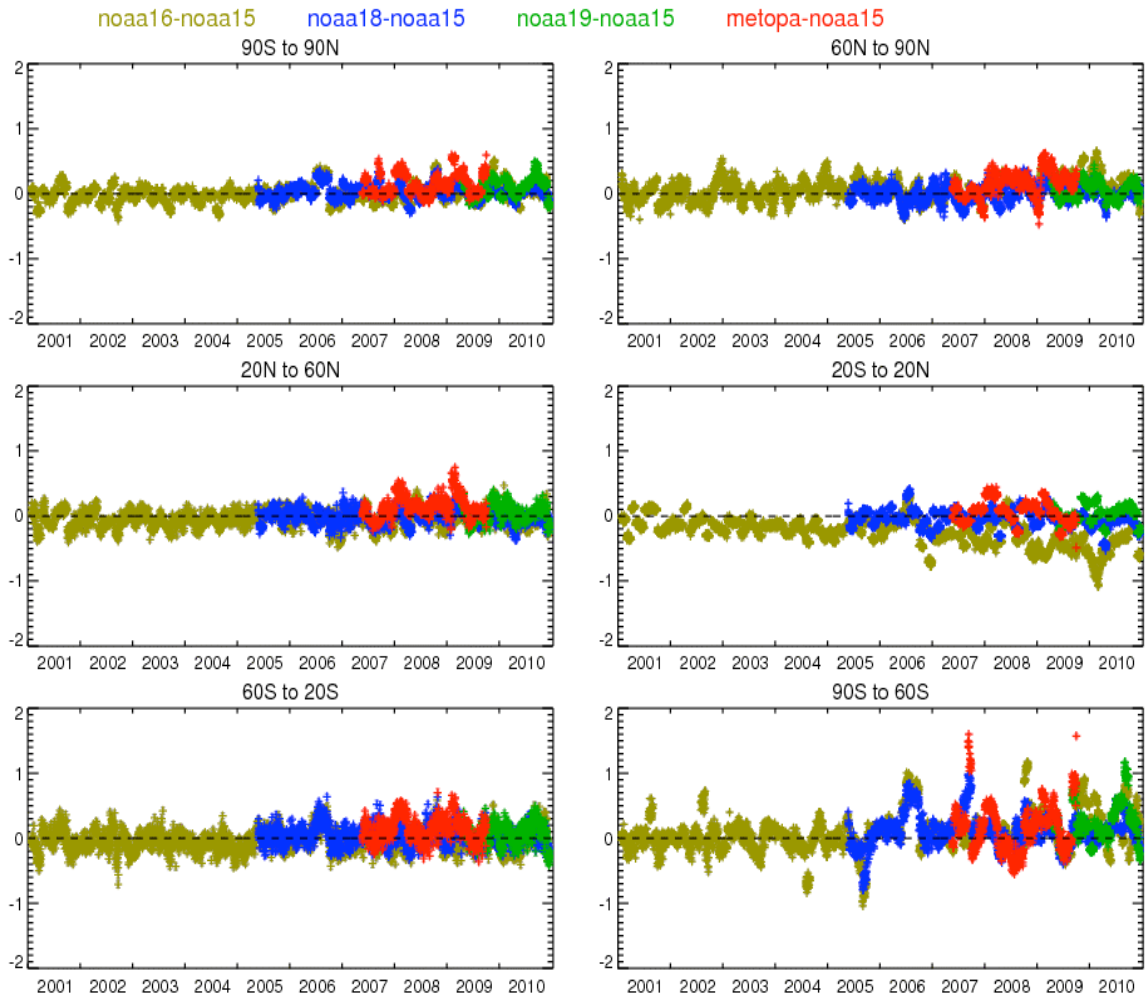


**Figure 4.** The time series of AMSU ch7 Tbs between NOAA16-NOAA15, NOAA18-NOAA15, NOAA19-NOAA15, Metop-A – NOAA15 for the global (upper left panel), 90º N to 60º N zone (upper right panel), 20º N to 60º N zone (middle left panel), 20º N to 20º S zone (middle right panel), 60º S to 20º S zone (lower left panel), and 90º S to 60º S zone (lower right panel).

## 2.3 Refining the method to Construct the Global Tropopause Height Climatology using GPS Radio Occultation Data

We proposed to use COSMIC and CHAMP temperature profiles to detect the tropopause height from May 2001 to December 2012. The monthly mean climatology (MMC) for temperature from 2001 to 2012 was constructed. Then we use reanalysis data to remove the sampling errors for CHAMP and COSMIC temperature profiles. Then we use the temperature MMC to determine the tropopause height MMC.

### a. Remove the temperature sampling error in the MMC

According to the definition of the tropopause, although very small bias in temperature profile may result to large bias in tropopause height. So in this study we generate the temperature MMC (Monthly zonal mean climatologies) which are used to generate the tropopause height after removing the sampling errors. The NCEP, ERA-Interim and MERRA reanalysis data are used in this study.

We use the method of ‘‘binning and averaging’’ to generate the temperature MMC. The dry profiles from CDAAC/COSMIC for CHAMP and COSMIC are used. In this study, zonal bins of 5° latitudinal width were defined at a Mean Sea Level (MSL) altitude grid with vertical resolution of 200 meters. To reduce sampling errors in temperature MMCs, MMCs are all updated for each mission by subtracting the sampling errors (similar to [*Ho et al.*, 2009]). The sampling errors are estimated using the above-mentioned reanalysis data.

We used the following approaches:

i) the reanalysis temperature profiles are interpolated to the times and locations of each GPS profiles for CHAMP and COSMIC;

ii) the interpolated temperature profiles for different missions are binned to the monthly mean climatologies as original GPS temperature MMC respectively (denoted as $\overline{MMC_{Int}}$). The MMC are also generated from original reanalysis grid data (denoted as $\overline{MMC_{grid}}$). Then sampling error of MMC (MSE) is defined as

$$MSE = \overline{MMC_{Int}} - \overline{MMC_{Grid}} .$$

The new MMC (denoted as $MMC^{NEW}$) for each month and mission are then defined as

$$MMC^{NEW} = \overline{MMC_{Grid}} - MSE .$$

### b. Detection of the tropopause height using COSMIC and CHAMP temperature profiles

The tropopause is defined as lapse rate tropopause (LRT) in this study. According to the standard World Meteorological Organization (WMO) [1957] definition, the tropopause is defined as “the lowest level at which the lapse rate decreases to 2°C/km or less, and the average lapse rate from this level to any level within the next higher 2°C/km does not exceed 2°C/km”. Using the original and new MMCs for the CHAMP and COSMIC, we generate the tropopause heights for CHAMP and COSMIC in all month and latitude bins. According to the research of Ho et al. (2009), the reanalysis data such as NCEP can reproduces synoptic short-term (less than one month) changes and spatial variation which are the dominant cause of sampling error in GPS RO data especially for CHAMP.

### c. Time Series of tropopause heights

Fig. 5 summarizes the results for the time series of tropopause height calculated from the temperature climatology. As mentioned above, we use NCEP, ERA-Interim and MERRA reanalysis data interpolated to RO profiles to compute the sampling errors.

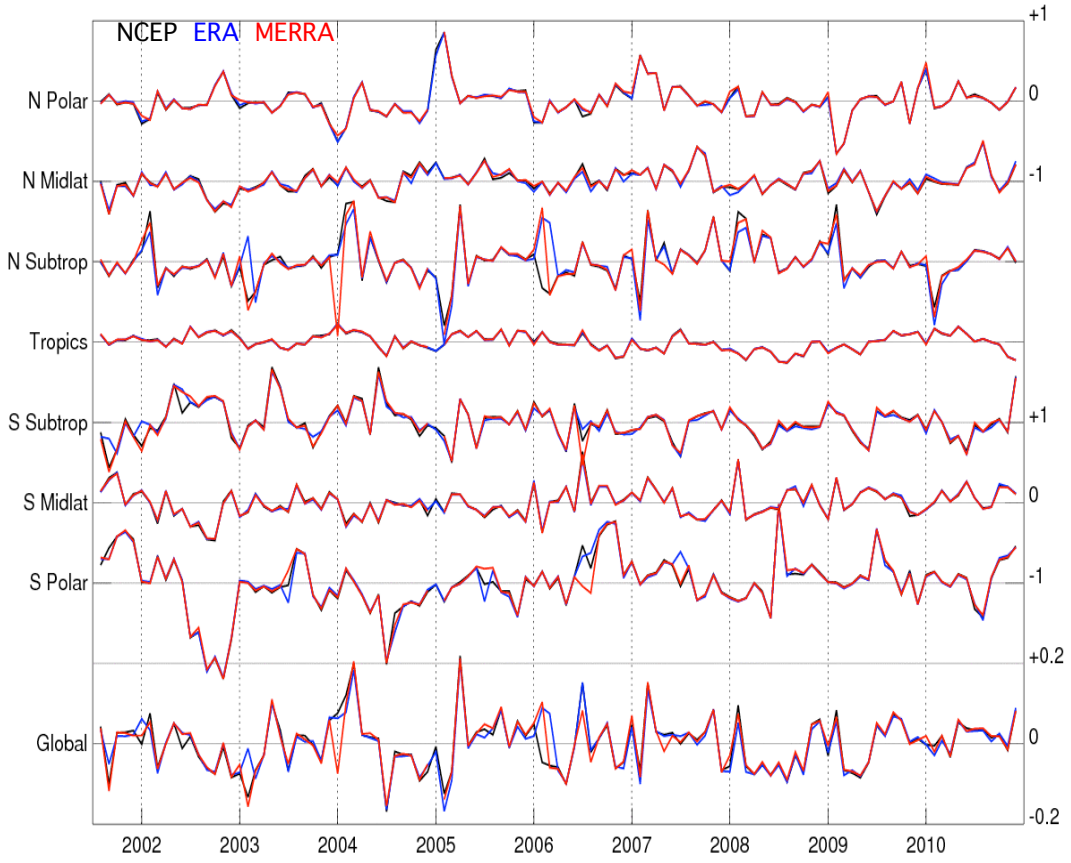


Fig. 5 Monthly anomalies of tropopause heights for different geographical regions and global. Each tick mark on the vertical axis represents 1 km (0.1 km for the global time series, black, NCEP; blue, ERA-Interim; red, MERRA).

The Tropopause height trends [m/yr] based on GPS RO data from May 2001–December 2007 (80 months) from temperature calibrated by different models. (black, NCEP; blue, ERA-Interim; red, MERRA) is shown in Fig. 6.

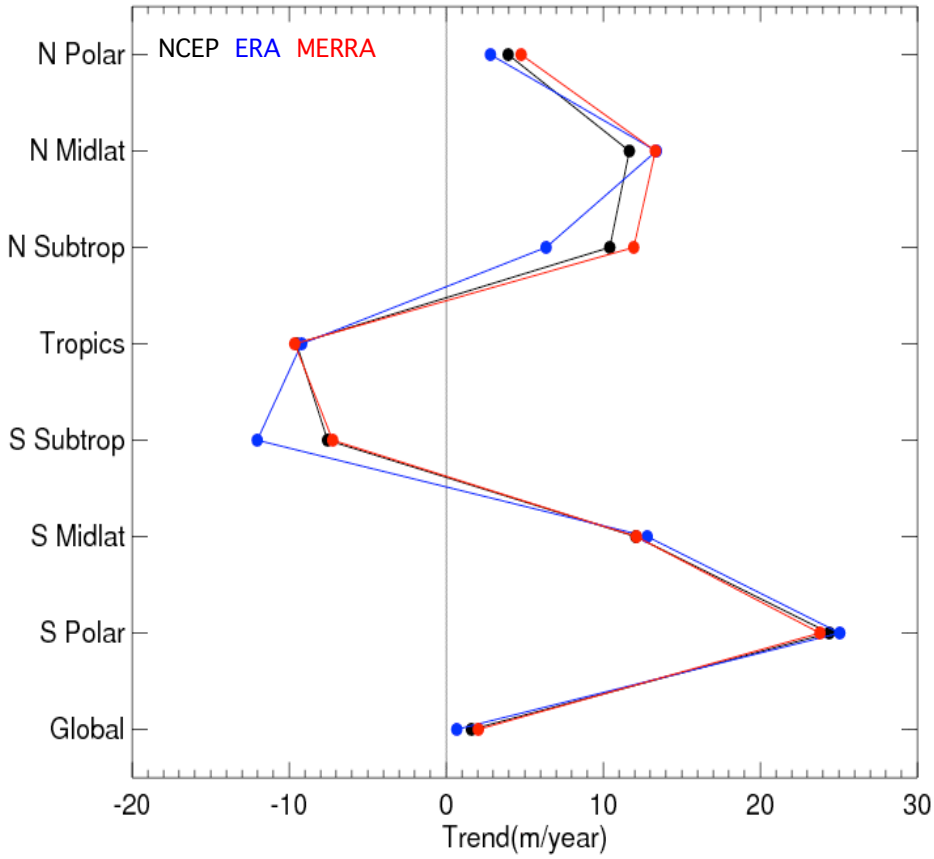


Fig. 6 Tropopause height trends [m/yr] based on GPS RO data from May 2001–December 2007 (80 months) from temperature calibrated by different models. (black, NCEP; blue, ERA-Interim; red, MERRA).

## 3. Presentations and Publications

Related publications and presentations during 2013 are listed:


(1) Ho, S.-P., (2013), Construction of a Consistent Microwave Sensor Temperature Record in the Lower Stratosphere Using Global Positioning System Radio Occultation Data and Microwave Sounding Measurements, *J. Geophy. Research, (submitted).*

(2) Dhaka, S. K., V. Kumar, R. K. Choudhary, S.-P. Ho, and K. K. Reddy (2013), Investigation of new downward propagated motion and tropopause response of polar and tropical region: A case study of 2009 sudden stratospheric warming event, GRL (submitted).

(3) Blackwell W. J., Rebecca Bishop, Clayton Crail, Kerri Cahoy, Brian Cohen, Lidia Cucurull, Pratik Dave, Michael DiLiberto, Neal Erickson, Chad Fish, shu-peng Ho, R. Vincent Leslie, Idahosa A. Osaretin (2013), Radiometer Calibration Using Co-located GPS Radio Occultation Measurements, IEEE TRANSACTIONS ON GEOSCIENCE AND REMOTE SENSING (*submitted*).

(4) Kumar, V., S. K. Dhaka, R. K. Choudhary, S.-P. Ho, and K. K. Reddy (2013), On the occurrence of coldest temperature in stratospheric region and tropical tropopause stability: A study by COSMIC/FORMOSAT-3 satellite measurements, *J. Geophy. Research (submitted).*

(5) Ho, S.-P., X. Yue , Z. Zeng, C. Ao, C.-Y. Huang, E. R. Kursinski, Y.-H. Kuo (2013a), Applications of COSMIC Radio Occultation Data from the Troposphere to Ionosphere and Potential Impacts of COSMIC-2 Data, BAMS, doi: http://dx.doi.org/10.1175/BAMS-D-13-00035.1.

(6) Mears C., J. Wang, S.-P. Ho, L. Zhang, and X. Zhou (2013), Total Column Water Vapor, [In "States of the Climate in 2012]. *Bul. Amer. Meteor. Sci.*, (*in press*).

(7) Teng, Wen-Hsin, Ching-Yung Huang, S.-P. Ho, Ying-Hwa Kuo, and Xin-Jia Zhou (2013), Characteristics of Global Precipitable Water in ENSO Events Revealed by COSMIC Measurements, *J. Geophy. Research,* DOI: 10.1002/jgrd.5037.

(8) Biondi, R., S.-P. Ho, W. Randel, T. Neubert and S. Syndergaard (2013), Tropical cyclone cloud-top heights and vertical temperature structure detection using GPS radio occultation measurements, *J. Geophy. Research,* VOL. 118, 1–13, doi:10.1002/jgrd.50448.

(9) Steiner, A. K., D. Hunt, S.-P. Ho, G. Kirchengast, A. J. Mannucci, B.

Scherllin-Pirscher, H. Gleisner, A. von Engeln, T. Schmidt, C. Ao, S. S. Leroy, E. R. Kursinski, U. Foelsche, M. Gorbunov, Y.-H. Kuo, K. B. Lauritsen, C. Marquardt, C. Rocken, W. Schreiner, S. Sokolovskiy, S. Syndergaard, and J. Wickert (2013), Quantification of Structural Uncertainty in Climate Data Records from GPS Radio Occultation, *ACP* doi:10.5194/acp-13-1469-2013.

(10) Ho, S.-P. and co-authors, Calibration of Temperature Troposphere / Stratosphere from Advanced Microwave Sounding Unit using High Quality Radiosonde Data Identified by Radio Occultation Data, AMS annual meeting, Jan 6-10, Austin TX, U.S.A.

(11) Ho, S.-P., Current Developments on the Applications of COSMIC from the Troposphere to Stratosphere and the Potential Impacts of COSMIC-2 Data, invited seminar given in Department of Atmospheric Science, National Central University, Jan. 29, 2013, Taiwan (invited).

(12) Ho, S.-P., Current Developments on the Applications of COSMIC from the Troposphere to Stratosphere and the Potential Impacts of COSMIC-2 Data, invited seminar given in Research Center for Environmental Changes, Academia Sinica, Jan. 31, 2013, Taiwan (invited).

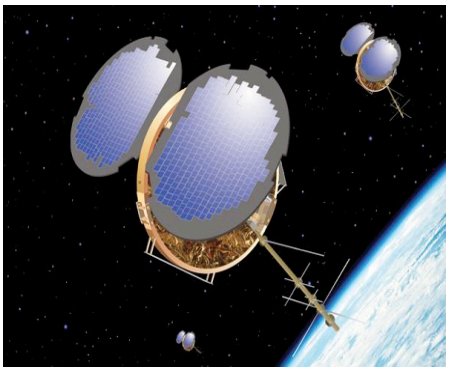

COSMIC

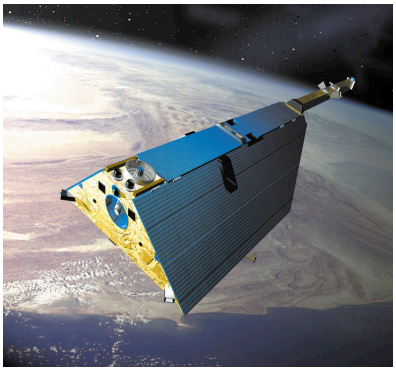

CHAMP

YEAR 3 BI-ANNUAL PROJECT REPORT (from 6/01/2013 to 12/30/2013)
NOAA Award number: NA10NES4400002

# Construction of Consistent Microwave Sensor Temperature Records and Tropopause Height Climatology using MSU/AMSU Measurements, GPS RO Data, and Radiosonde Observations


**Principal Investigator:**
Shu-Peng (Ben) Ho (303-497-2922, spho@ucar.edu)

**Co-Investigators:**
Cheng-Zhi Zou ((301) 763-8042 x156, cheng-zhi.zou@noaa.gov)
Ying-Hwa Kuo **(**(303) 497-8910, kuo@ucar.edu)

**National Center for Atmospheric Research**
**P.O. Box 3000, Boulder, CO 80307 USA**

# 1. Introduction

In this report, we summarize the continuous efforts since the last report (submitted in June 2013) for this project. The work undertaken to date is detailed in Section 2. We list presentations and publications since January 2013 in section 3.

# 2. Progress on Proposed Studies

***Efforts since the last report have focused on 1) refining the method to construct the global tropopause height climatology using GPS radio occultation data, 2) refining AMSU Ch9 processing method and constriction of the AMSU ch9 climate data record from 1978 to 2010, and 3) refining AMSU Ch7 processing method and constriction of the AMSU ch7 climate data record from 1978 to 2010.***

## 2.1 Refining the method to Construct the Global Tropopause Height Climatology using GPS Radio Occultation Data

The tropopause layer represents the boundary between the tropopause and stratosphere. It is an important region of the atmosphere often been examined to understand the stratosphere-troposphere exchange and coupling [*Son et al.*, 2011]. The tropopause recently received more and more attention because long-term change of the global tropopause is a sensitive indicator of global climate change. Studies with reanalysis data and climate model simulations show that tropopause height has increased by several hundred meters in recent several decades. The increases of tropopause height were closely associated with tropospheric warming and stratospheric cooling caused by well-mixed green gas and ozone respectively. In this study, we proposed to use COSMIC and CHAMP temperature profiles to detect the tropopause height from June 2001 to December 2012. The tropopause height is determined by the high resolution COSMIC and CHAMP temperature profiles. However, because the the temporal and spatial resolution of CHAMP (one receiver from 2001 to 2008) is different from those from COSMIC (6 receivers from 2006 to the current), we will need to quantify and remove the possible sampling errors before we can construct the tropopause height climatology. We first use reanalysis data to remove the sampling errors for CHAMP and COSMIC temperature profiles. Then we use the temperature monthly mean climatology (MMC) to determine the tropopause height MMC.

### a. Method to remove the RO sampling errors

We use the method of ‘‘binning and averaging’’ to generate the temperature MMC. COSMIC and CHAMP temperature profiles downloaded from CDAAC are used. In this study, zonal bins of 5° latitudinal width were defined at a Mean Sea Level (MSL) altitude grid with vertical resolution of 200 meters. To reduce

sampling errors in temperature MMC, MMCs are all updated for each mission by subtracting the sampling errors (similar to [*S P Ho et al.*, 2009c]). The sampling errors are estimated using the NCEP, ERA-Interim and MERRA reanalysis data. The following procedures are used:

1) the reanalysis temperature profiles are interpolated to the times and locations of each GPS profiles for CHAMP and COSMIC.

2) the interpolated temperature profiles for different missions are binned to the monthly mean climatologies as original GPS temperature MMC respectively (denoted as $\overline{MMC_{Int}}$). The MMC are also generated from original reanalysis grid data (denoted as $\overline{MMC_{grid}}$). The sampling error of MMC (MSE) is defined as

$$MSE = \overline{MMC_{Int}} - \overline{MMC_{grid}} \qquad (1).$$

The MSE estimated from NCEP, ERA-Interim and MERRA reanalysis are denoted as $MSE_{NCEP}$, $MSE_{ERA_Intrim}$, and $MSE_{MERRA}$, respectively.

3) The new MMC (denoted as $MMC^{NEW}$) for each month and mission are then defined as

$$MMC^{NEW} = \overline{MMC_{Grid}} - MSE \qquad (2)$$

The new MMC computed from $MSE_{NCEP}$, $MSE_{ERA_Intrim}$, and $MSE_{MERRA}$ are denoted as $MMC^{NEW}_{NCEP}$, $MMC^{NEW}_{ERA_Intrim}$, and $MMC^{NEW}_{MERRA}$, respectively.

4) Using the new MMCs for the CHAMP and COSMIC, we generate the tropopause heights for CHAMP and COSMIC in all month and latitude bins.

In this study, the thermal definition of the tropopause (i.e., lapse rate tropopause (LRT)) was used. According to the standard World Meteorological Organization (WMO) [1957] definition, the tropopause is defined as “the lowest level at which the lapse rate decreases to 2°C/km or less, and the average lapse rate from this level to any level within the next higher 2°C/km does not exceed 2°C/km”. It is calculated using the method employed by *Schmidt et al.* [2008] in which the tropopause height is defined exactly at the profile altitude where the above-mentioned WMO criterion is fulfilled for the first time. The bottom level is set to 5 km at the pole and is increased to 10 km at the equator according to the relation 7.5+2.5 (cos2$\varphi$), where $\varphi$ is the latitude. This empirical constraint is applied to avoid noise caused by water vapor in the lowest tropopause. The lapse rate tropopause is applied to each temperature original and new MMC.

Fig. 1 shows the latitude variations of the zonal mean temperature MMC generated with COSMIC data and tropopause height calculated by temperature

MMC. We can see that the variations of temperature lapse rates in tropics are more dramatic than those in other region. According to the definition of lapse rate tropopause height the extra-tropical region are very sensitive to the temperature bias. The large variations are found in the region between tropics and polar region.

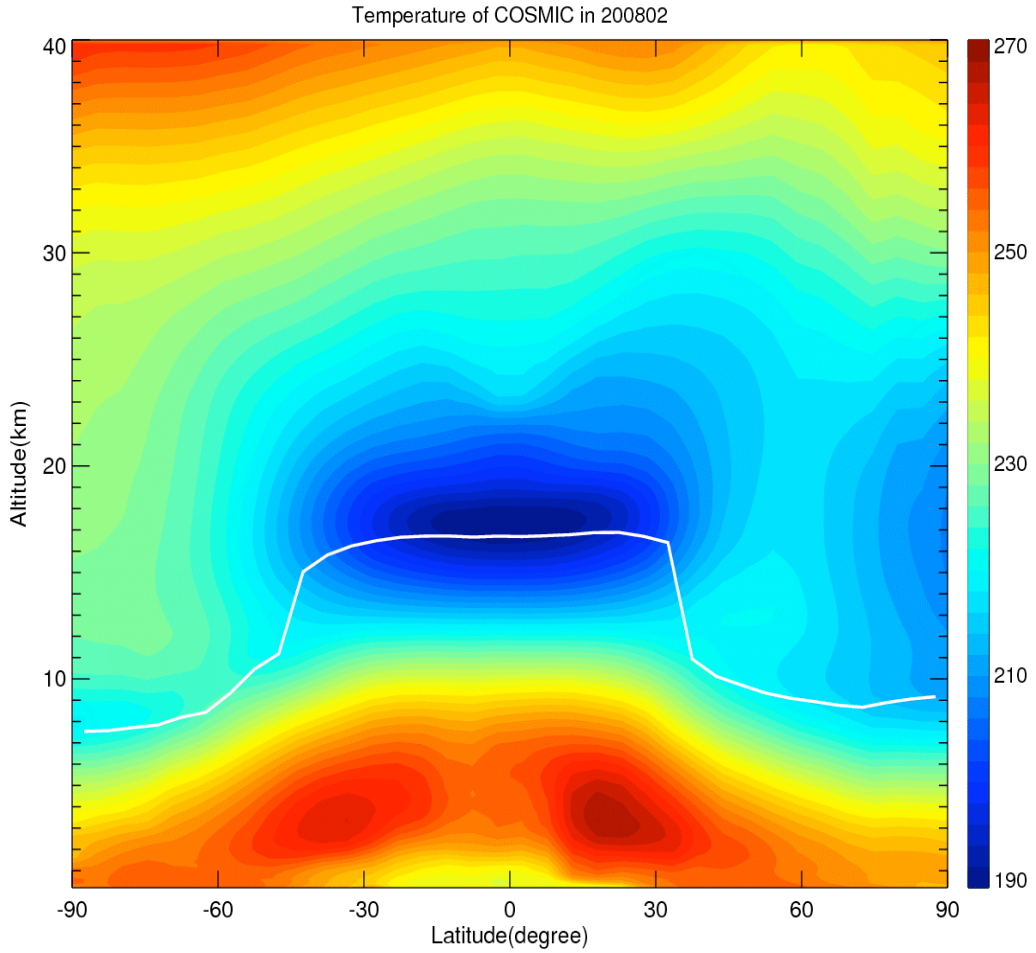


**Figure 1**. Mean monthly mean climatology (MMC) temperature of COSMIC in February 2008. The white line show the tropopause height calculated by the temperature profiles.

### b. Results: sampling error uncertainty of RO temperature profiles from different reanalysis data

Figure 2 shows latitude variations of the zonal mean differences between COSMIC and CHAMP dry temperatures in the troposphere and lower stratosphere in February 2008. The zonal mean statistics was calculated zonal bins of 5° latitudinal width. It illustrates that the large biases occur in middle and high latitude in upper stratosphere and in lower troposphere in tropical region for original temperatures (Figure 2a), which are mainly caused by the relatively large temperature variations and small sampling number. The small biases between CHAMP and COSMIC in tropical region in upper troposphere and stratosphere are caused by small temperature variations in this region. One can recognize that the differences of calibrated temperature (Figure 2b, c) are much smaller that those of original temperature. The larger temperature biases in the lower troposphere are caused by the difference between temperature and dry temperature for nonzero humidity [Kursinski et al., 1997; Marquardt et al., 2003]. The results show that the differences for original temperatures are primarily due to sampling errors among different missions. The sampling error removing method described in 2.1a do remove the sampling error of dry temperature. Although obvious differences occur in the high altitude and high latitude, the calculation of tropopause is not affected because of the relatively lower tropopause heights in that regions.

Note that although the temperatures profiles from NCEP, ERA-Interim, and MERRA are different (no shown), the estimated sampling errors are very similar. This is demonstrated in the time series of the monthly mean of $MSE_{NCEP}$, $MSE_{ERA_Intrim}$, and $MSE_{MERRA}$ for the 8 km to 30 km layer at different latitudinal zones (see Figure 3). This gives the confidence for the sampling error estimates.

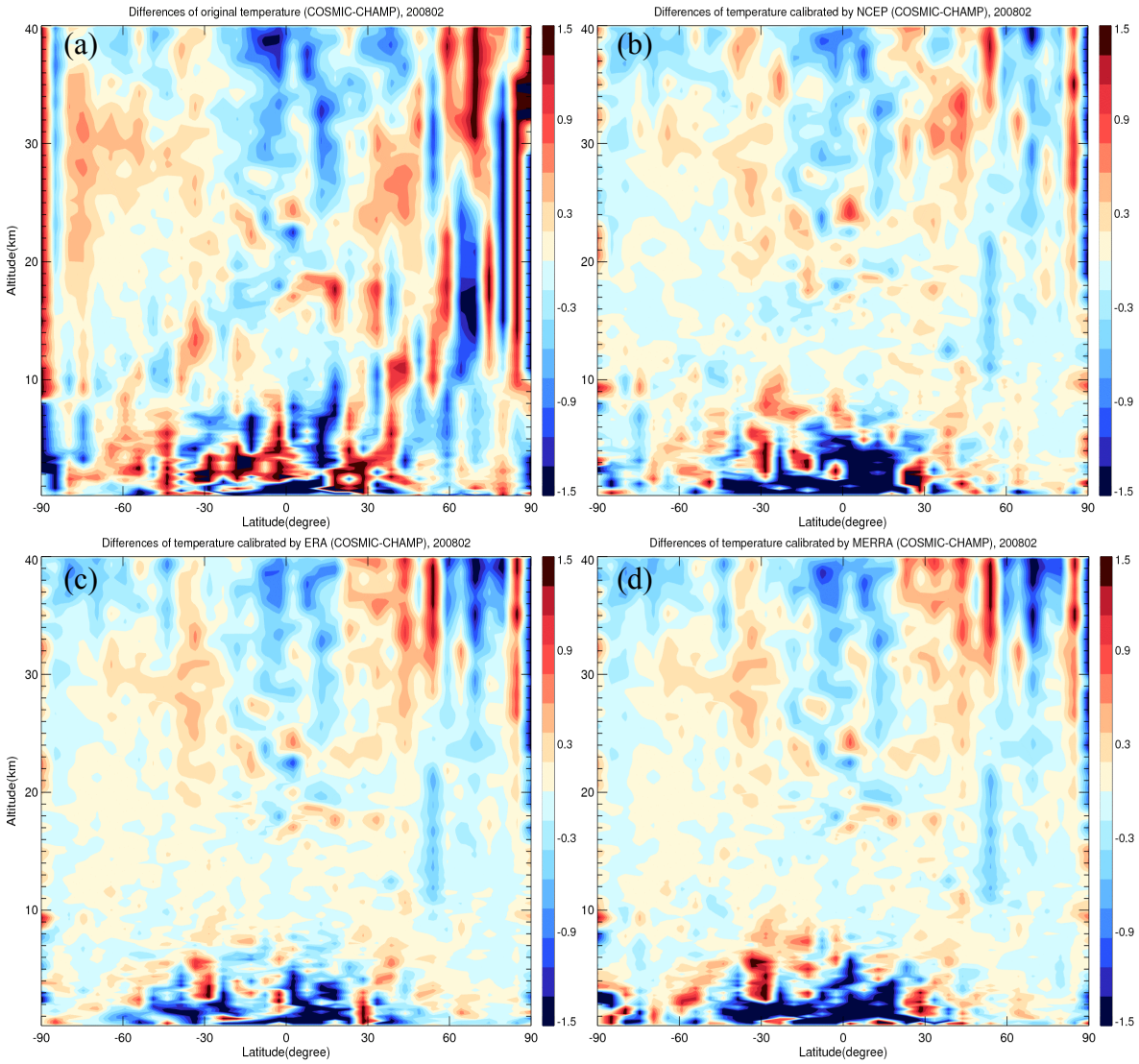


**Figure 2**. Difference in the mean zonal average temperature between COSMIC and CHAMP in February 2008. (a) Original, (b) Calibrated by NCEP, (c) Calibrated by ERA-Interim, (d) Calibrated by MERRA.

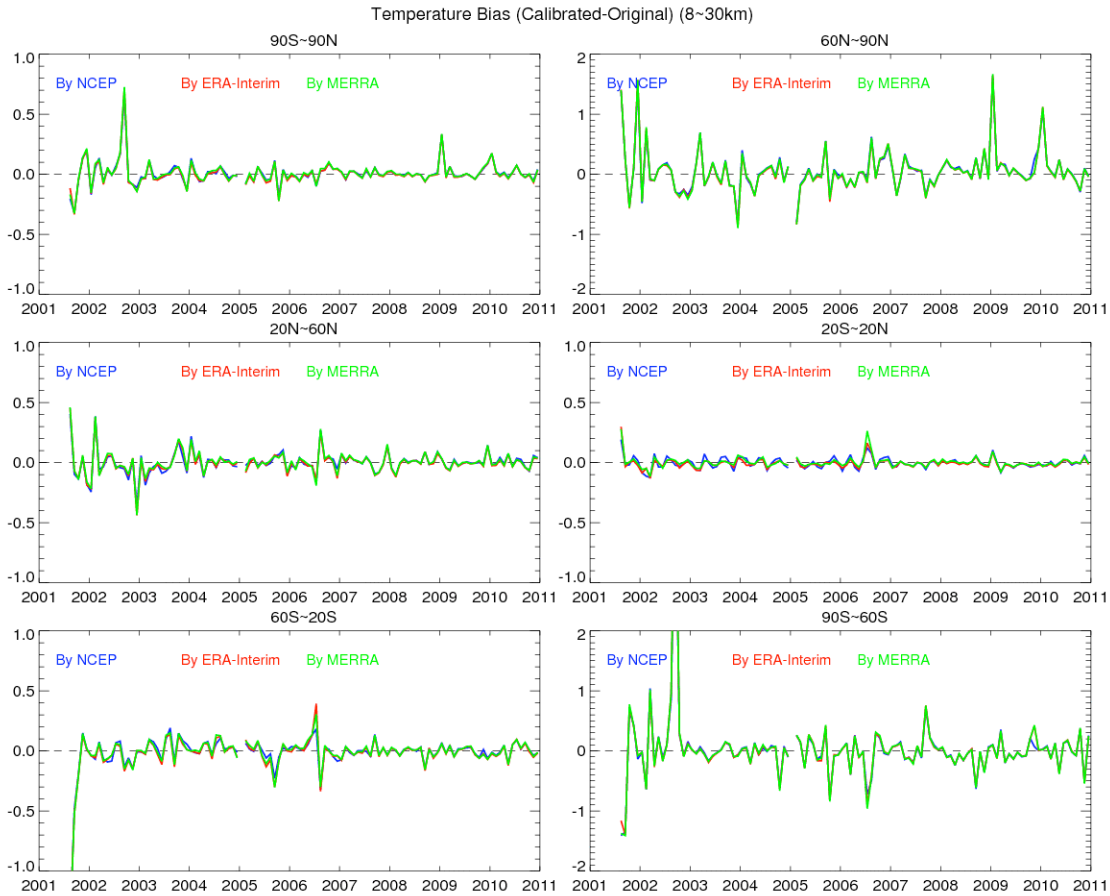


**Figure 3**. The time series of the monthly mean $MSE_{NCEP}$, $MSE_{ERA_Intrim}$, and $MSE_{MERRA}$ for the 8 km to 30 km layer for (a) the entire globe (90ºN to 90ºS), (b) the 90ºN to 60ºN zone, (c) the 20ºN to 60ºN zone, (d) the 20ºS to 20ºN zone, (e) the 60ºS to 20ºS zone, and (f) the 90ºS to 60ºS zone.

### c. Time Series of tropopause heights

Fig. 4 shows the monthly anomalies of tropopause heights from temperature MMC calibrated by different reanalysis data. We can see that the anomalies from different MMCs are nearly the same. The Tropopause height trends [m/yr] based on GPS RO data from May 2001–December 2007 (80 months) from temperature calibrated by different models. Tropopause height trends [m/yr] based on GPS RO data from May 2001–December 2007 (80 months) from temperature calibrated by different models black, NCEP; blue, ERA-Interim; red, MERRA) are shown in Fig. 5. With each method we find the maximum trend in the S Polar region (33-37 m/yr) and the minimum trend (-9 m/yr) in the tropics. Only the tropics and S Subtrop give a negative tropopause height trend. Largest uncertainties occur in the S Subtrop and N Subtrop mainly. The anomalies and trends for global tropopause heights are not simply generated by averaging all latitude bins but multiply weighting coefficient generated by cosine of latitude. The trend for global tropopause height is nearly zero.

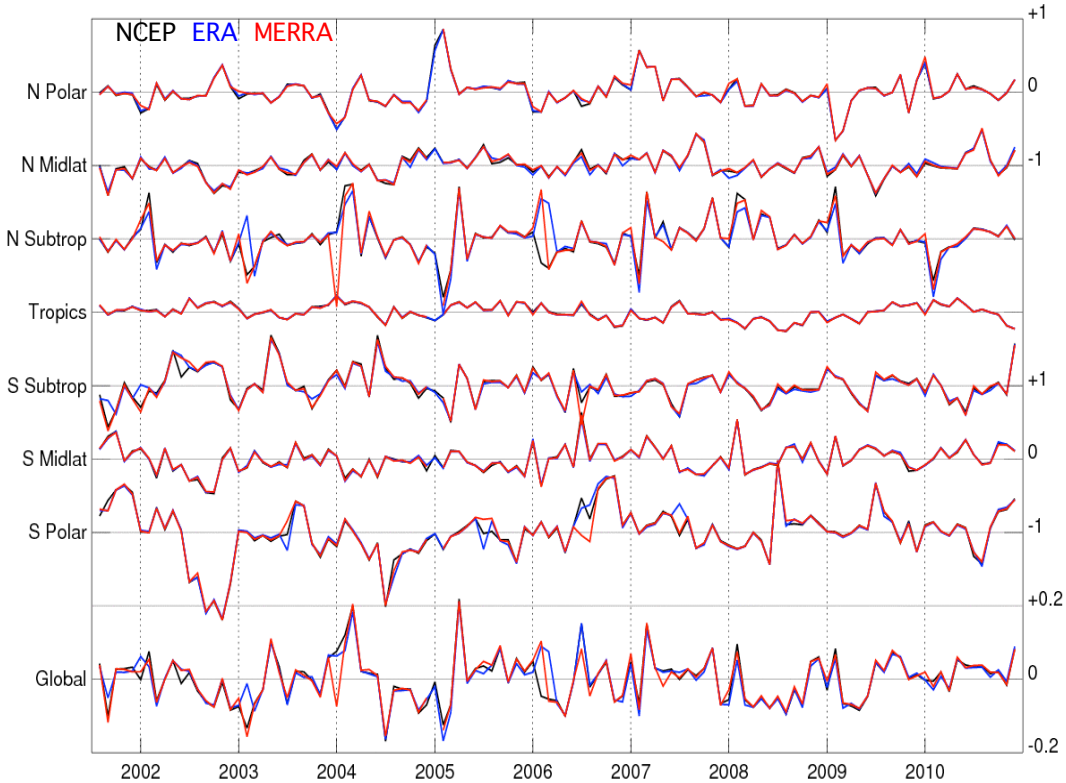


**Figure 4**. Monthly anomalies of tropopause heights for different geographical regions and global. Each tick mark on the vertical axis represents 1 km (0.1 km for the global time series, black, NCEP; blue, ERA-Interim; red, MERRA).

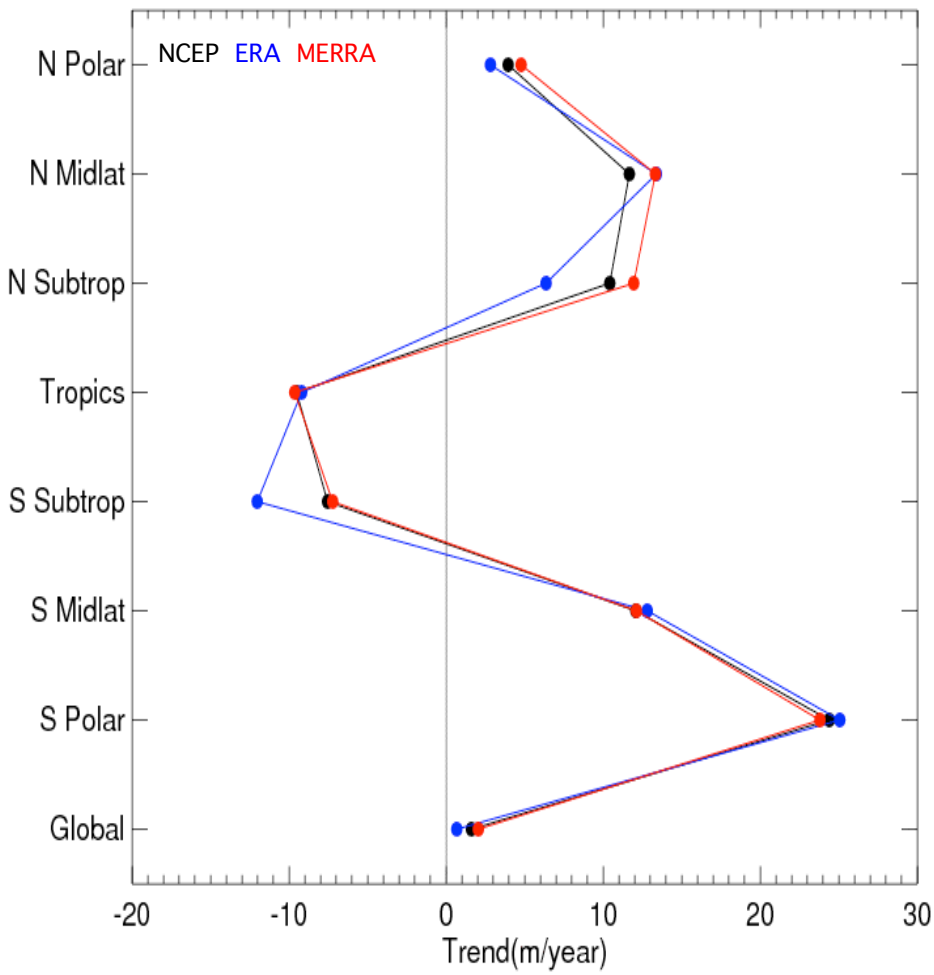


**Figure 5**. Tropopause height trends [m/yr] based on GPS RO data from May 2001–December 2007 (80 months) from temperature calibrated by different models. (black, NCEP; blue, ERA-Interim; red, MERRA).

## 2.2 Construction AMSU/MSU TLS climate data records from 1978 to 2010

During the performance period, we continue refining the calibration algorithm. A sequence of processing steps is implemented to use the RO data to calibrate the AMSU TLS and merge the calibrated TLS among multiple AMSU missions. The RO calibrated AMSU ch9 TLS data sets from 2001 to 2013 is delivered to NCDC. In this performance period, we apply SNO method to the MSU data from 1978 to 2000. Fig. 6 depicts the inter-satellite biases between two missions when they are co-located. No calibration procedures are implemented. The inter-satellite biases between TIROS-N6, N6-N7, N7-N8, N8-N9, N10-N11, N11-N12, N12-N14, N14-N15, N16-N15, N19-N18, N14-RO, N15-RO, and Metop-A-N19 are generated.

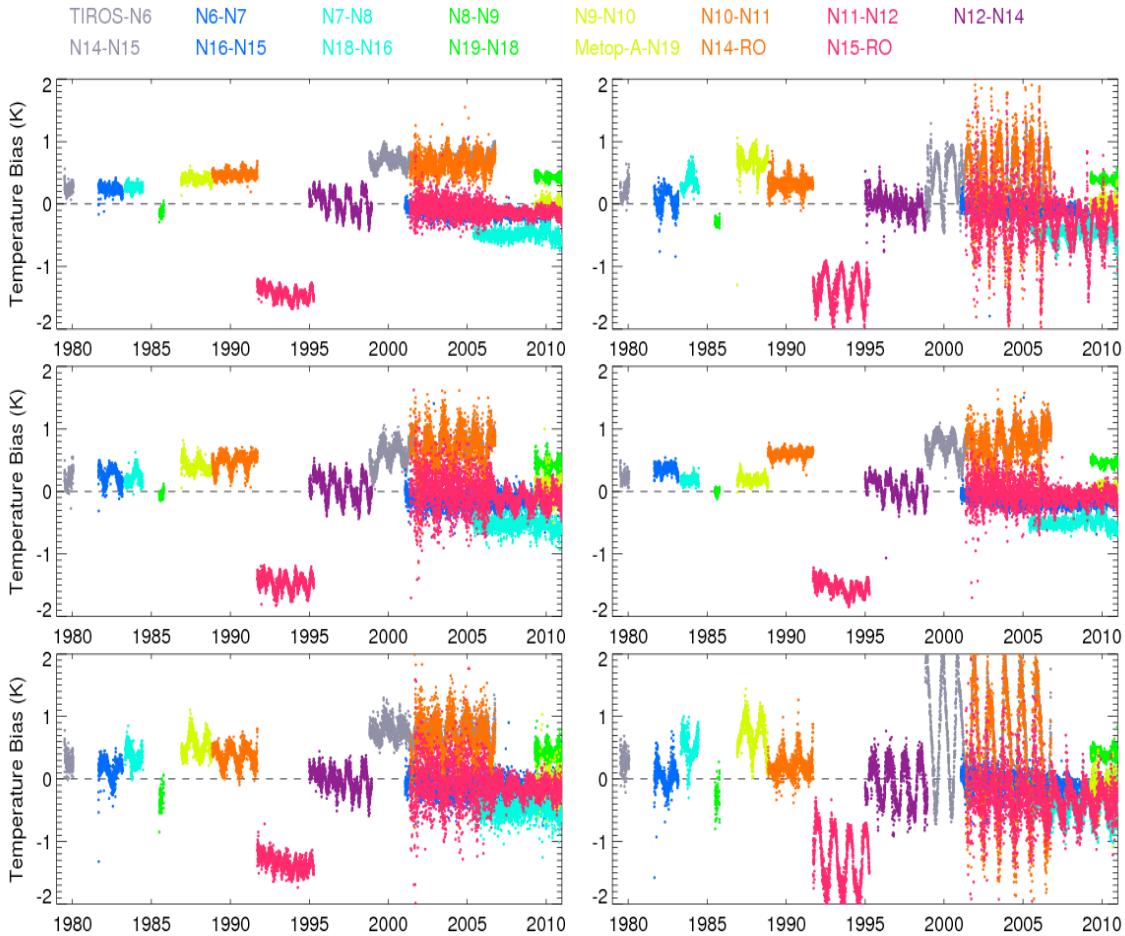


**Figure 6**. The time series of the monthly TLS mean differences for TIROS-N6, N6-N7, N7-N8, N8-N9, N10-N11, N11-N12, N12-N14, N14-N15, N16-N15, N19-N18, N14-RO, N15-RO, and Metop-A-N19 for (a) the entire globe (90ºN to 90ºS), (b) the 90ºN to 60ºN zone, (c) the 20ºN to 60ºN zone, (d) the 20ºS to 20ºN zone, (e) the 60ºS to 20ºS zone, and (f) the 90ºS to 60ºS zone.

Then using the collocated MSU-MSU TLS pairs, we define the calibration coefficients for the collocation pairs. The inter-satellite biases between two missions are generated in Figure 7. We separate the inter-satellite biases into six latitudinal zones. The very close to zero monthly mean inter-satellite biases between TIROS-N6, N6-N7, N7-N8, N8-N9, N10-N11, N11-N12, N12-N14, N14-N15, N16-N15, N19-N18, N14-RO, N15-RO, and Metop-A-N19 give us confidence for our approaches.

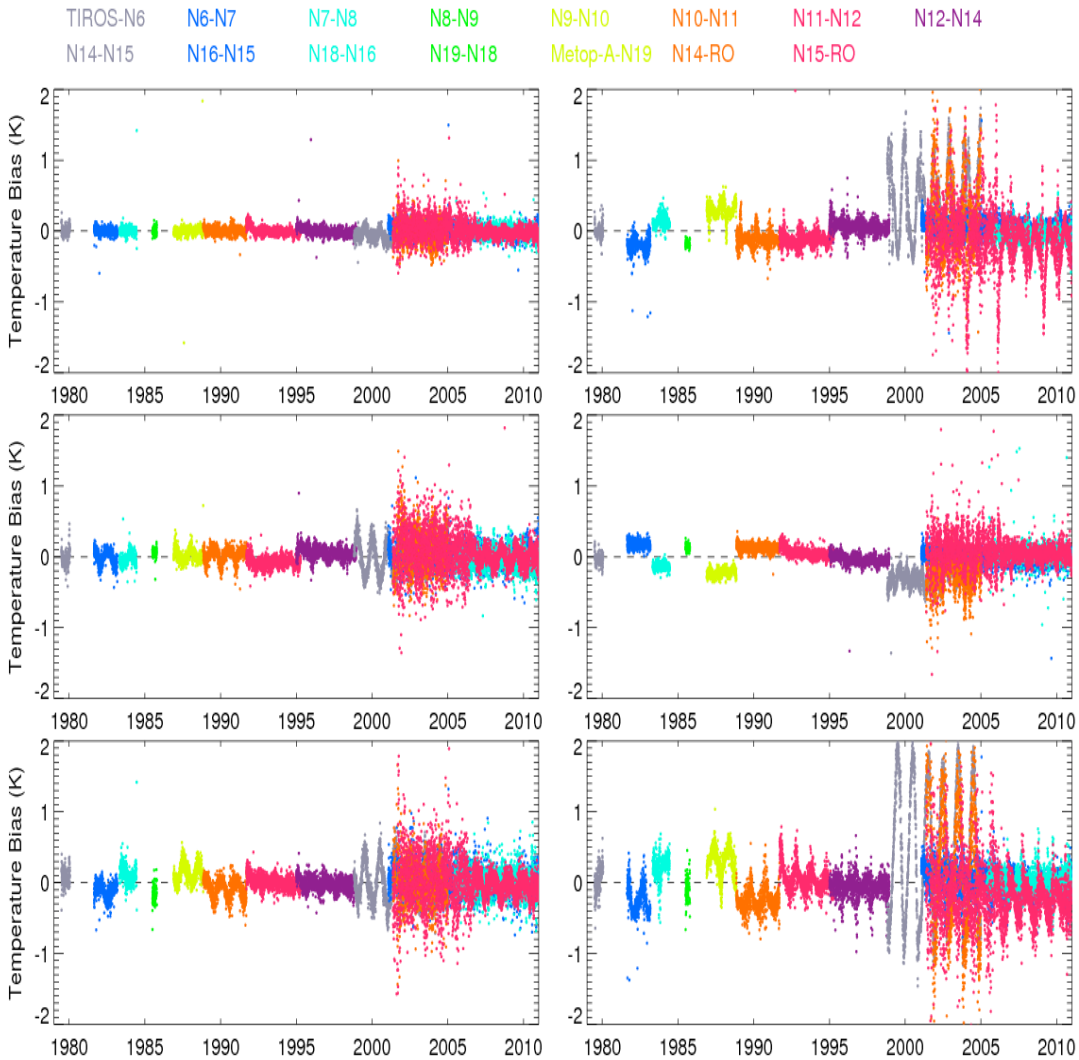


**Figure 7**. The time series of the calibrated monthly TLS mean differences for TIROS-N6, N6-N7, N7-N8, N8-N9, N10-N11, N11-N12, N12-N14, N14-N15, N16-N15, N19-N18, N14-RO, N15-RO, and Metop-A-N19 for (a) the entire globe (90ºN to 90ºS), (b) the 90ºN to 60ºN zone, (c) the 20ºN to 60ºN zone, (d) the 20ºS to 20ºN zone, (e) the 60ºS to 20ºS zone, and (f) the 90ºS to 60ºS zone.

## 2.3 Construction AMSU/MSU TTS climate data records from 1978 to 2010

The method used for calibration of the TTS MSU/AMSU data from 1978 to 2010 us also applying for the AMSU/MSU TTS CDR from 1978 to 2010. We had completed the TTS CDR from 2001 and 2010 and submitted to NCDC this year. Five types of Vaisala radiosonde data from the year of 2001 to 2010 were used to calibrate Temperatures of Tropopause/Stratosphere (TTS) taken from AMSU microwave measurements from different satellites for potential improvements of tropopause and Stratosphere temperature trend analysis. Details are described in the TTS CATBD and are not repeated here. Figure 8 show the time series of AMSU ch7 Tbs between NOAA16-NOAA15, NOAA18-NOAA15, NOAA19-NOAA15, Metop-A – NOAA15 for the global (upper left panel), 90º N to 60º N zone (upper right panel), 20º N to 60º N zone (middle left panel), 20º N to 20º S zone (middle right panel), 60º S to 20º S zone (lower left panel), and 90º S to 60º S zone (lower right panel). The inter-satellite biases among missions give us the confidence of this approach. We are still testing the algorithms to applying the calibrated AMSU ch7 data to calibrate the overlapped MSU TTS data before 2000.

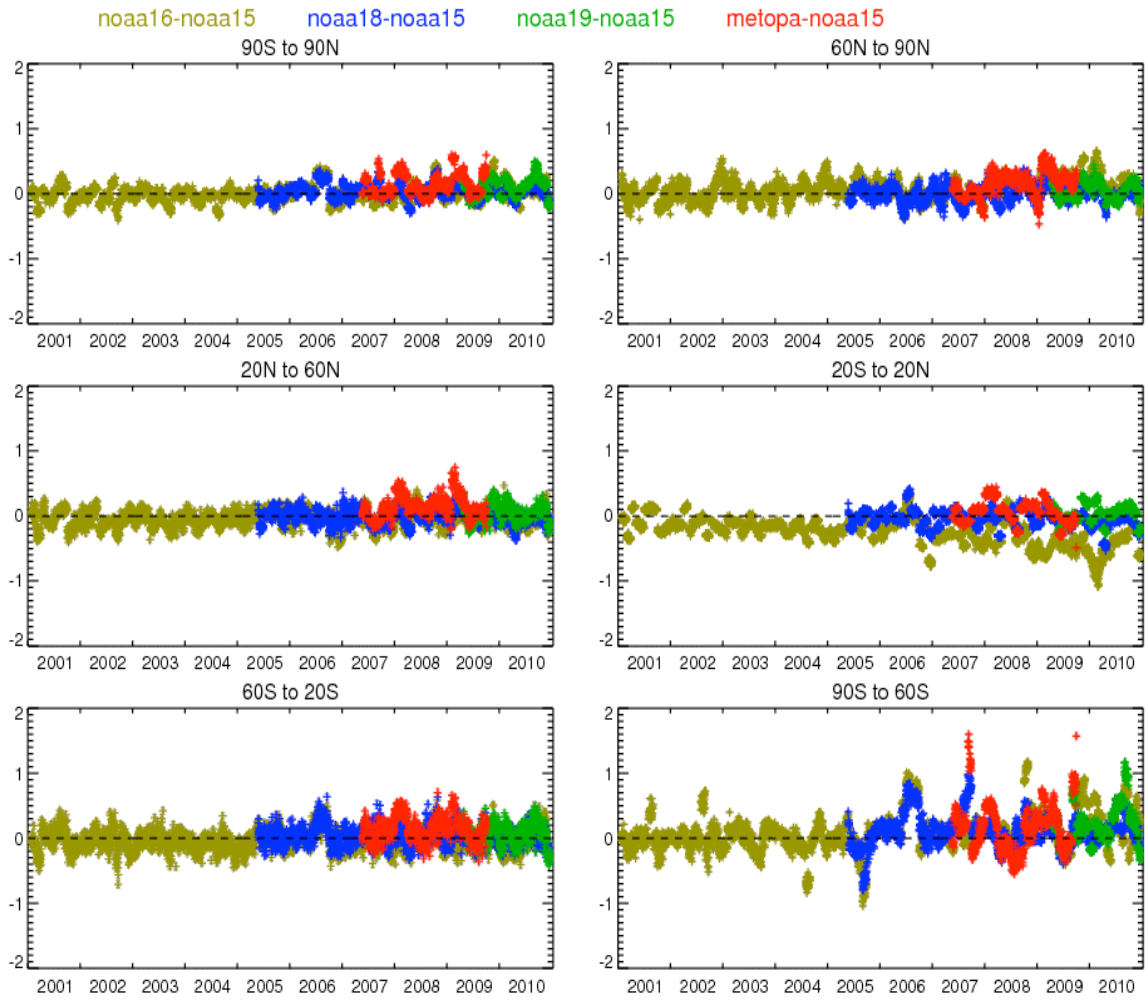


**Figure 8.** The time series of AMSU ch7 Tbs between NOAA16-NOAA15, NOAA18-NOAA15, NOAA19-NOAA15, Metop-A – NOAA15 for the global (upper left panel), 90º N to 60º N zone (upper right panel), 20º N to 60º N zone (middle left panel), 20º N to 20º S zone (middle right panel), 60º S to 20º S zone (lower left panel), and 90º S to 60º S zone (lower right panel).

## 3. Presentations and Publications

Related publications during 2013 are listed:


1) **Ho, S.-P.**, X. Yue , Z. Zeng, C. Ao, C.-Y. Huang, E. R. Kursinski, Y.-H. Kuo (2013a), Applications of COSMIC Radio Occultation Data from the Troposphere to Ionosphere and Potential Impacts of COSMIC-2 Data, BAMS, doi: http://dx.doi.org/10.1175/BAMS-D-13-00035.1.

2) Huang, Ching-yuang, Wen-hsin Teng, **S.-P. Ho**, Y. H. Kuo (2013), Global Variation of COSMIC Precipitable Water over Land: Comparisons with Ground-based GPS Measurements and NCEP Reanalyses, GRL, DOI: 10.1002/grl.50885

3) Blackwell W. J., Rebecca Bishop, Clayton Crail, Kerri Cahoy, Brian Cohen, Lidia Cucurull, Pratik Dave, Michael DiLiberto, Neal Erickson, Chad Fish, **shu-peng Ho**, R. Vincent Leslie, Idahosa A. Osaretin, Radiometer Calibration Using Co-located GPS Radio Occultation Measurements, IEEE TRANSACTIONS ON GEOSCIENCE AND REMOTE SENSING, 2013 (*submitted*).

4) Dhaka, S. K., V. Kumar, R. K. Choudhary, **S.-P. Ho**, and K. K. Reddy (2013), Investigation of new downward propagated motion and tropopause response of polar and tropical region: A case study of 2009 sudden stratospheric warming event, JGR (submitted).

5) Kumar, V., S. K. Dhaka, K. K. Reddy, A. Gupta, S. B. Surendra Prasad, V. Panwar, N. Singh, **Shu-Peng Ho**, and M. Takahashi, Impact of Quasi-Biennial Oscillation on the inter-annual variability of the tropopause height and temperature in the tropics: A study using COSMIC/FORMOSAT-2 observations, Journal of Atmospheric Research (in press).

6) Mears C., J. Wang, **S.-P. Ho**, L. Zhang, and X. Zhou (2013), Total Column Water Vapor, [In “States of the Climate in 2012]. *Bul. Amer. Meteor. Sci.*, (*in press*).

7) **Ho, S.-P**., IPCC AR5 report

8) Mears C., J. Wang, **S.-P. Ho**, L. Zhang, and X. Zhou (2014), Total Column Water Vapor, [In “States of the Climate in 2013]. *Bul. Amer. Meteor. Sci.*, (*in press*).

9) Teng*, Wen-Hsin, Ching-Yung Huang, **S.-P. Ho**, Ying-Hwa Kuo, and Xin-Jia Zhou (2013), Characteristics of Global Precipitable Water in ENSO Events Revealed by COSMIC Measurements, *J. Geophy. Research,* Vol. 118, 1–15, doi:10.1002/jgrd.50371.

10) Biondi*, R., **S.-P. Ho**, W. Randel, T. Neubert and S. Syndergaard (2013), Tropical cyclone cloud-top heights and vertical temperature structure detection using GPS radio occultation measurements, *J. Geophy. Research,* VOL. 118, 1–13, doi:10.1002/jgrd.50448.

11) Steiner, A. K., D. Hunt, **S.-P. Ho**, G. Kirchengast, A. J. Mannucci, B. Scherllin-Pirscher, H. Gleisner, A. von Engeln, T. Schmidt, C. Ao, S. S. Leroy, E. R. Kursinski, U. Foelsche, M. Gorbunov, Y.-H. Kuo, K. B. Lauritsen, C. Marquardt, C. Rocken, W. Schreiner, S. Sokolovskiy, S. Syndergaard, and J. Wickert (2013), Quantification of Structural Uncertainty in Climate Data Records from GPS Radio Occultation, *ACP* doi:10.5194/acp-13-1469-2013.

12) **Ho, S.-P.**, PBL height estimated from COSMIC, CLIPSO, and high resolution Radiosonde during the VOCAL-REx.

13) **Ho, S.-P.**, (2013b), Construction of a Consistent Microwave Sensor Temperature Record in the Lower Stratosphere Using Global Positioning System Radio Occultation Data and Microwave Sounding Measurements, *J. Geophy. Research, (submitted).*

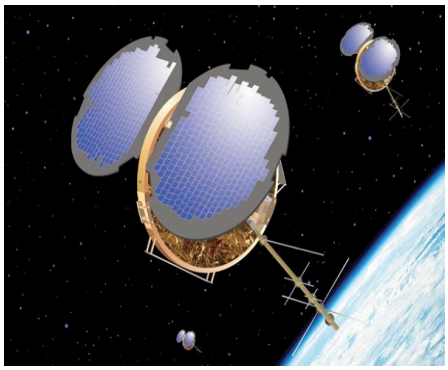

COSMIC

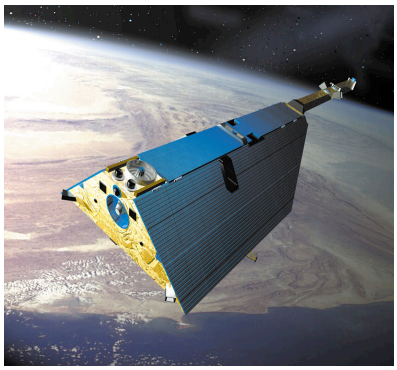

CHAMP

YEAR 3 BI-ANNUAL PROJECT REPORT (from 01/01/2014 to 06/30/2014)
NOAA Award number: NA10NES4400002

# Construction of Consistent Microwave Sensor Temperature Records and Tropopause Height Climatology using MSU/AMSU Measurements, GPS RO Data, and Radiosonde Observations


**Principal Investigator:**
Shu-Peng (Ben) Ho (303-497-2922, spho@ucar.edu)

**Co-Investigators:**
Cheng-Zhi Zou ((301) 763-8042 x156, cheng-zhi.zou@noaa.gov)
Ying-Hwa Kuo ((303) 497-8910, kuo@ucar.edu)

**National Center for Atmospheric Research**
**P.O. Box 3000, Boulder, CO 80307 USA**

# 1. Introduction

In this report, we summarize the continuous efforts since the last report (submitted in December 2013) for this project.

# 2. Progress on Proposed Studies

***Efforts since the last report have focused on 1) refining the AMSU Ch9 processing method and constriction of the AMSU ch9 climate data record from 2001 to 2013, 2) refining the processing method to constructing AMSU ch9/MSU ch4 from 1978 to 2013, 3) refining AMSU ch7 processing method and construction of the AMSU ch7 climate data record from 2001 to 2013, and 4) refining the processing method for AMSU ch7 climate data record and to construct AMSU ch 7 CDR from 1978 to 2013.***

The method to construct the global tropopause height climatology using GPS Radio Occultation (RO) data processed from multiple RO missions are reported in the previous report and is not further mentioned in this report.

## 2.1 AMSU temperature in the lower stratosphere (TLS) results from 2001 to 2013

Using RO temperature profiles derived from multiple RO missions, the AMSU ch9 brightness temperatures (TLS) are calibrated.

Currently, more than 10 year of RO data from multiple RO missions including CHAllenging Minisatellite Payload (CHAMP, launched in 2001), COSMIC (launched in 2006), Gravity Recovery And Climate Experiment (GRACE, launched in 2004), and MetOp/GRAS (launched in 2006) are consistently processed by the COSMIC Data Analysis and Archive Center (CDAAC). The COSMIC, CHAMP, GRACE dry temperature profiles (atmPrf) downloaded from UCAR CDAAC (http://cosmic.cosmic.ucar.edu/cdaac/index.html) are used.

Fig. 1 depicts the inter-satellite biases between two missions when they are co-located. No calibration procedures are implemented. The inter-satellite biases between N16-N15, N18-N15, N19-N15, Metop-A – N!5, and Aqua-N15 are generated.

A sequence of processing steps is implemented to use the RO data to calibrate the AMSU TLS and merge the calibrated TLS among multiple AMSU missions. The procedure consists of the following steps:

i) Forward calculation of the AMSU TLS using RO temperature profiles: The AMSU fast-forward model from the Cooperative Institute for Meteorological Satellite Studies–CIMSS, $MWF_{CIMSS}$ (Hal Woolf, CIMSS, personal communication, 2005), is used in this study. The validation of the microwave

transmittance of this model is described in *Woolf et al.,* [1999]. All the available temperature profiles for COSMIC, CHAMP, and GRACE are first extracted from the CDAAC level2 data and interpolated to the 100 pressure levels of the AMSU fast-forward model. The interpolated temperature profiles from GPS RO missions are then applied to the AMSU fast-forward model to calculate the AMSU Ch9 brightness temperatures. The water vapor profiles are set to zero in the forward calculation.

ii) Data Matching: To avoid the spatial and temporal representation errors, we collocate AMSU pixels with each RO profile within 30 minutes and 100 km. AMSU pixels with a satellite viewing angle ranging from -15 degrees to 15 degrees are all included in this study to increase the number of AMSU pixels in our comparison. To avoid anomalous values due to missing data, differences among the brightness temperatures that are larger than 10 degrees are omitted. To have enough RO profiles, which contain reasonable temporal and spatial coverage, we use three consecutive months of CHAMP data to represent the TLS variation for the middle month. Three monthly running CHAMP-AMSU pairs are used before June 2006, whereas the available CHAMP, COSMIC, and GRACE RO data in the same month are used to match up with the AMSU data after June 2006. Collectively, these matching criteria balance the tradeoff between the quality and the number of the matched measurements.

iii) Calculation of the calibration coefficients: The quality of the RO temperatures over the vertical range of AMSU Ch9 weighting function leads to comparable brightness temperatures $TLS^{RO}$ . The highly linear relationship between $TLS^{RO}$ and the measured AMSU brightness temperatures ( $TLS^{AMSU}$ ) permits calibration via a simple linear fit:

$$TLS^{RO} = \text{SLOPE} \times TLS^{AMSU} + \text{OFFSET} \qquad (2),$$

where the SLOPE and OFFSET values for each month are calculated by minimizing the root mean square between the coincident $TLS^{RO}$ and $TLS^{AMSU}$ values. Hereafter, the RO- simulated TLS for N15, N16, N18, N19, Aqua, and Metop-A are denoted as $TLS^{RO}_{N15}$, $TLS^{RO}_{N16}$, $TLS^{RO}_{N18}$, $TLS^{RO}_{N19}$, $TLS^{RO}_{Aqua}$, and $TLS^{RO}_{Metop-A}$, respectively. The AMSU TLS for N15, N16, N18, N19, Aqua, and Metop-A are denoted as $TLS_{N15}$, $TLS_{N16}$, $TLS_{N18}$, $TLS_{N18}$, $TLS_{Aqua}$, and $TLS_{Metop-A}$, respectively. The calibrated AMSU TLS (i.e., $TLS^{Cal}$) can be obtained by applying the defined slope and offset to the $TLS^{AMSU}$ for the same month. Note that although the derived RO variables (bending angle, refractivity, and dry temperature) are not synchronized to the ultra-stable atomic clocks on the ground, the high precision nature of the raw RO observables is preserved in the inversion chain [*Ho et al.,* 2012]. Since the AMSU fast-forward model cannot introduce additional variability, the precision of these temperature measurements at the altitudes sensitive to AMSU Ch9 results in stable reference values for Ch9 brightness temperatures. To quantify the precision of RO-simulated TLS, *Ho et al.,* [2009b] has compared the COSMIC- calibrated AMSU TLS with those calibrated from CHAMP in the same month. Results shows that the mean biases between COSMIC-calibrated AMSU TLS and those of CHAMP-calibrated AMSU TLS can be as small as 0.07

K with a standard deviation of 0.1 K. The high precision RO-simulated TLS would be highly useful to calibrate the AMSU radiance biases (see below).

iv) Merging Procedures: Prior to the application of the linear calibration, daily means of the AMSU Ch9 brightness temperatures for each NOAA orbiter on a 2.5 degree × 2.5 degree grid are calculated. Only AMSU pixels with a satellite viewing angle ranging from -15 degrees to 15 degrees are included in the binning procedure. The calibration coefficients for each polar orbiter are then applied to the daily mean gridded values to obtain the daily-adjusted AMSU Ch9 brightness temperatures. Only high-quality TLS data from individual missions that passed their quality control tests (i.e., all quality flag bits equal to zero) are included in the daily files. The daily mean gridded AMSU Ch9 brightness temperatures from each AMSU mission in the same month are then averaged to compute the monthly means of the AMSU Ch9 brightness temperatures on a 2.5 degree × 2.5 degree grid.

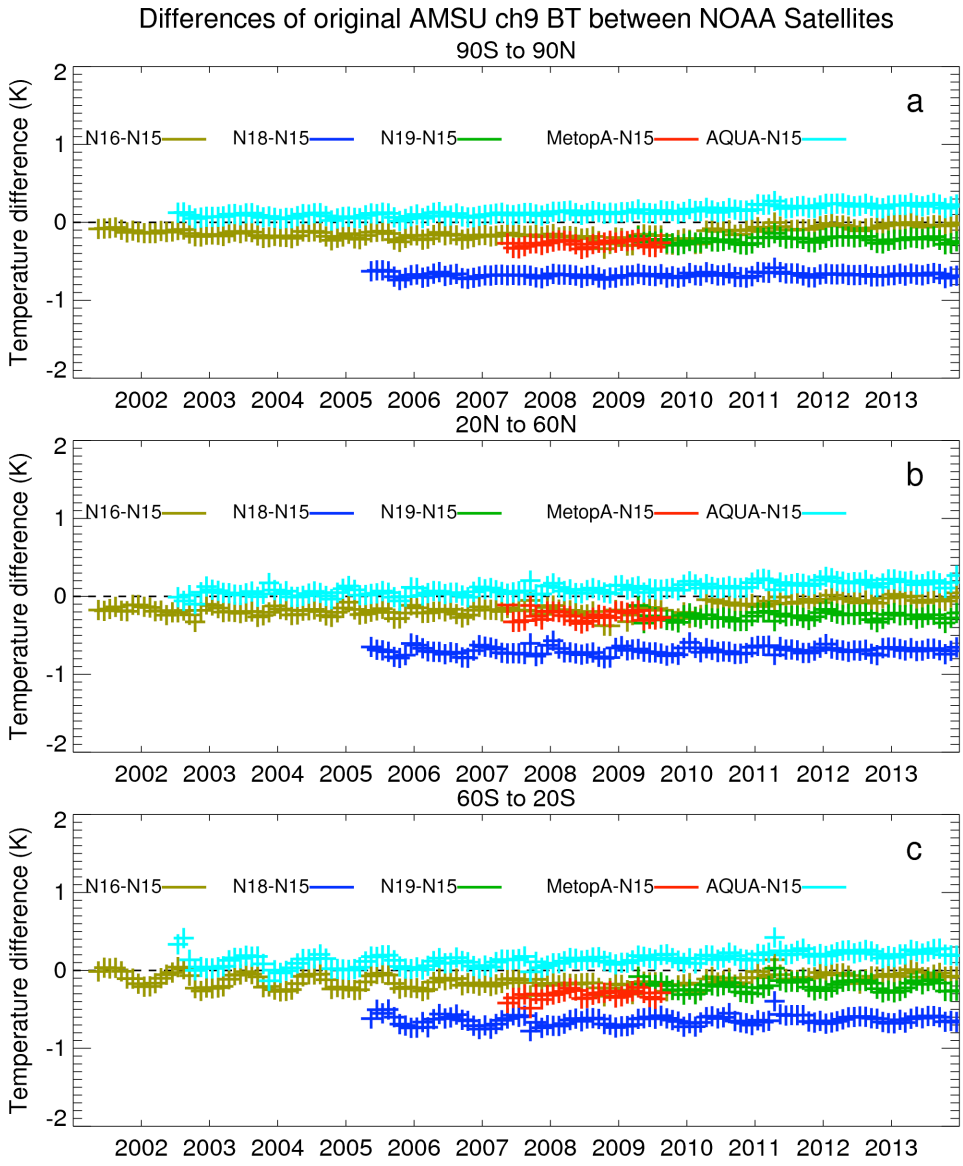


**Fig. 1. The time series of the monthly TLS mean differences for N16-N15, N18-N15, N19-N15, Metop-A – N15, and Aqua-N15 for (a) the entire globe (90ºN to 90ºS), (b) the 20ºN to 60ºN zone, and (c) the 60ºS to 20ºS zone.**

After applying the calibration method to all the AMSU brightness temperature from different NOAA, Aqua, and Metop-A missions, the time series of the inter-satellite biases of the calibrated TLS for different latitudinal zones are shown in Fig. 2.

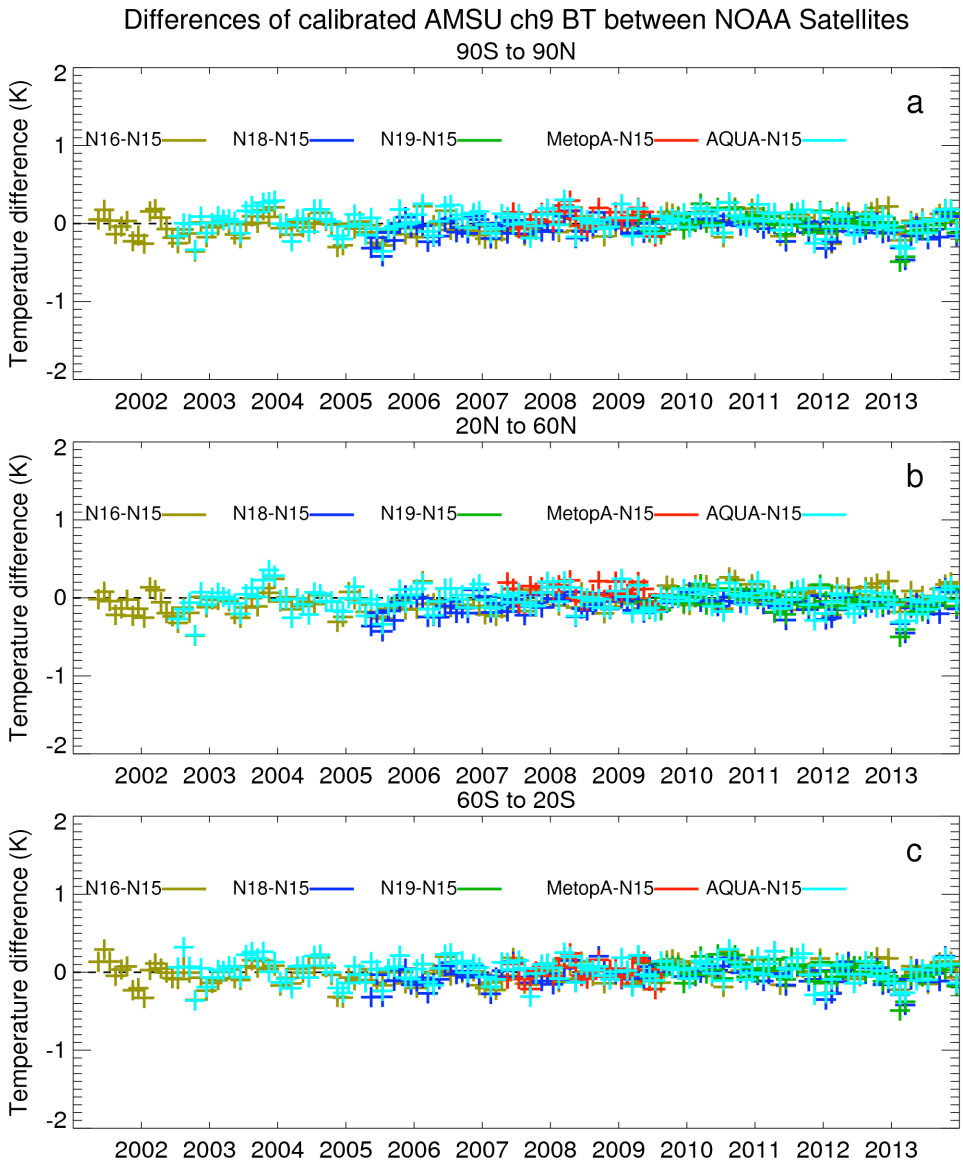


**Fig. 2. The time series of the monthly calibrated TLS mean differences for N16-N15, N18-N15, N19-N15, Metop-A – N15, and Aqua-N15 for (a) the entire globe (90ºN to 90ºS), (b) the 20ºN to 60ºN zone, and (c) the 60ºS to 20ºS zone.**

Fig. 3 depicts the anomaly of AMSU TLS calibrated by RO in December 2013. The monthly mean for AMSU TLS and the climatology of the AMSU TLS calibrated by RO data from 2002 to 2013 is also shown in Fig. 3.

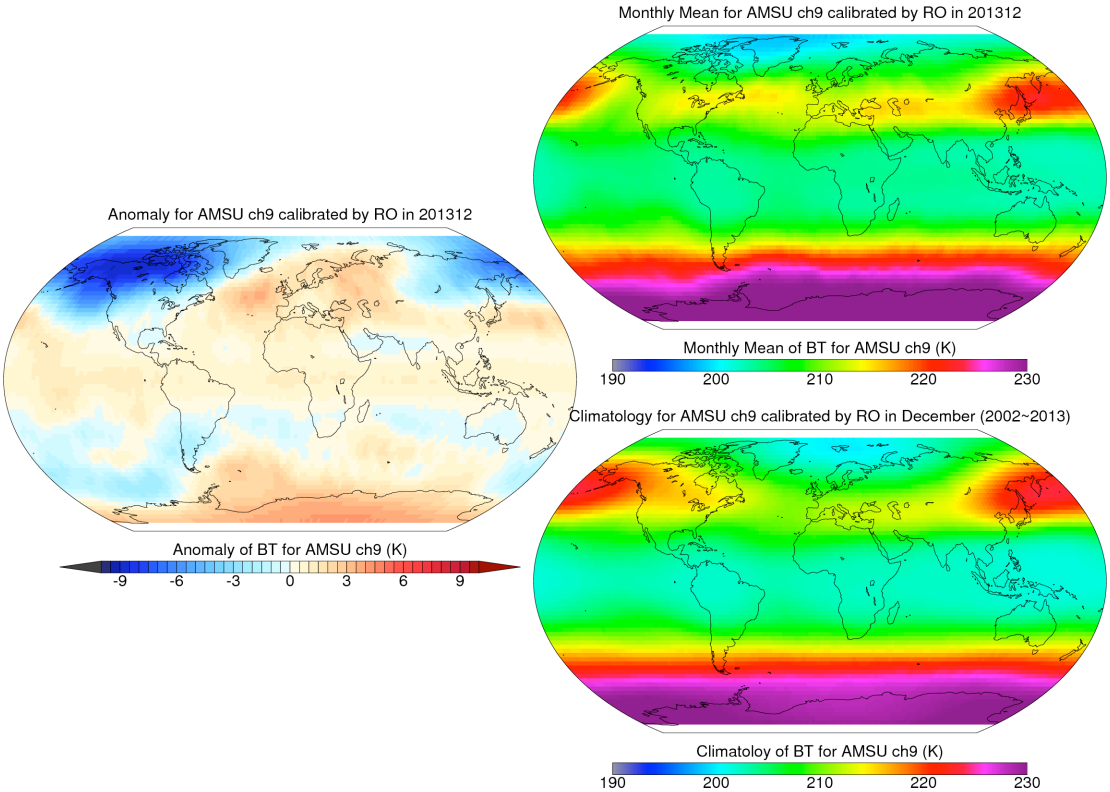


**Fig. 3. The left panel shows the anomaly of AMSU TLS calibrated by RO in December 2013. The right upper panel is the monthly mean for AMSU TLS. The right lower panel depicts the climatology of the AMSU TLS calibrated by RO data from 2002 to 2013.**

### 2.2 AMSU/MSU TLS Time Series form 1980 to 2013

We were using those AMSJU and MSU TLS calibrated by multiple RO missions from 2001 to 2013 to calibrate those overlapped AMSU and MSU TLS form 1978 to 2001. Fig. 4 depicts the inter-satellite biases between two missions when they are co-located. The inter-satellite biases between TIROS-N6, N6-N7, N7-N8, N8-N9, N10-N11, N11-N12, N12-N14, N14-N15, N16-N15, N19-N18, N14-RO, N15-RO, and Metop-A-N19 are generated.

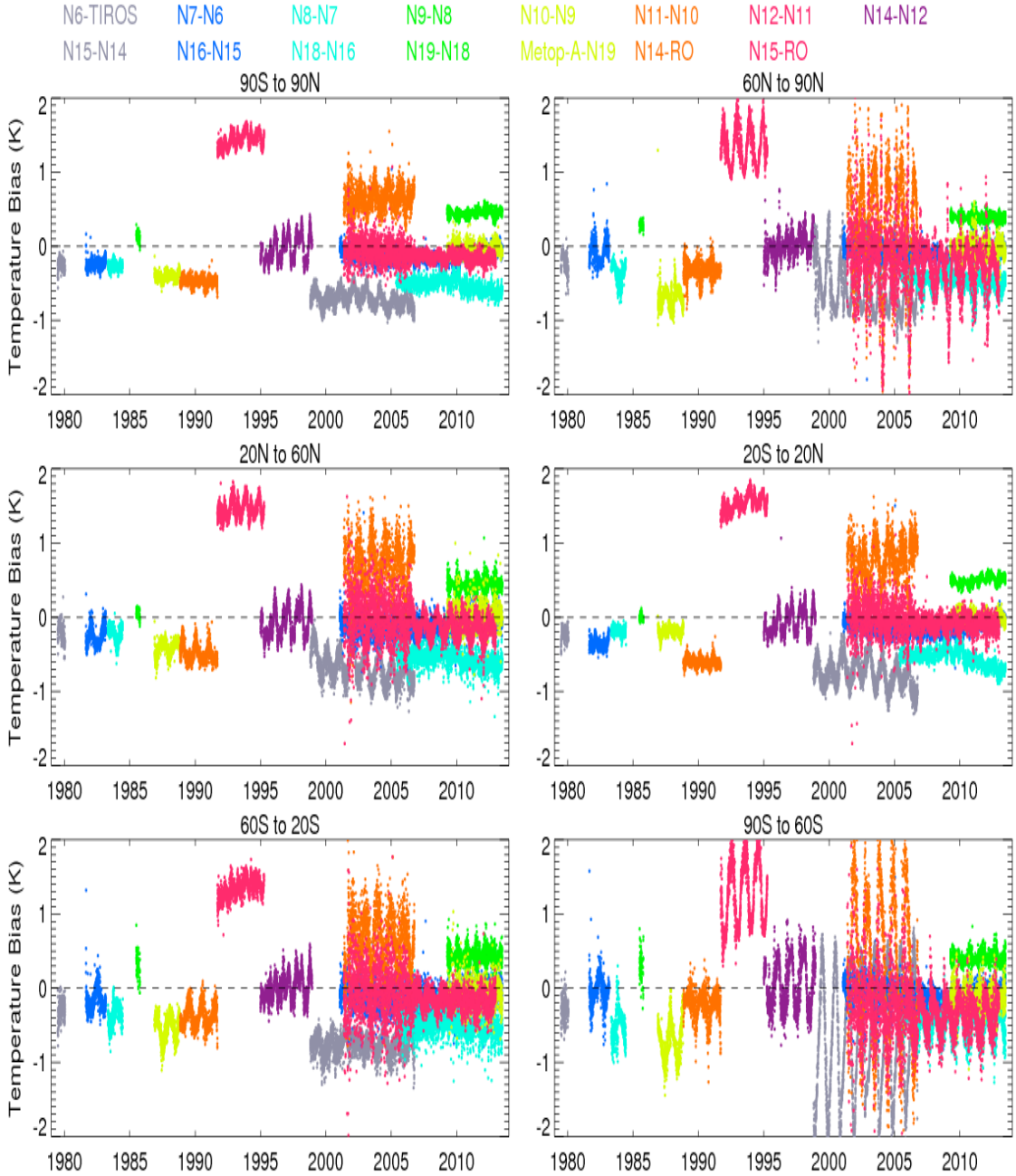


**Figure 4. The time series of the monthly TLS mean differences for TIROS-N6, N6-N7, N7-N8, N8-N9, N10-N11, N11-N12, N12-N14, N14-N15, N16-N15, N19-N18, N14-RO, N15-RO, and Metop-A-N19 for (a) the entire globe (90ºN to 90ºS), (b) the 90ºN to 60ºN zone, (c) the 20ºN to 60ºN zone, (d) the 20ºS to 20ºN zone, (e) the 60ºS to 20ºS zone, and (f) the 90ºS to 60ºS zone.**

Without detailing all the calibrated and construction procedures, we present the calibrated TLS from 1980 to 2013 in Fig. 5. The results show that the calibrated AMSU/MSU TLS between two overlapped NOAA or RO missions are all very close to zero degree K no matter they are before 2001 (no RO data) or after 2001 (RO data are used as calibration references).

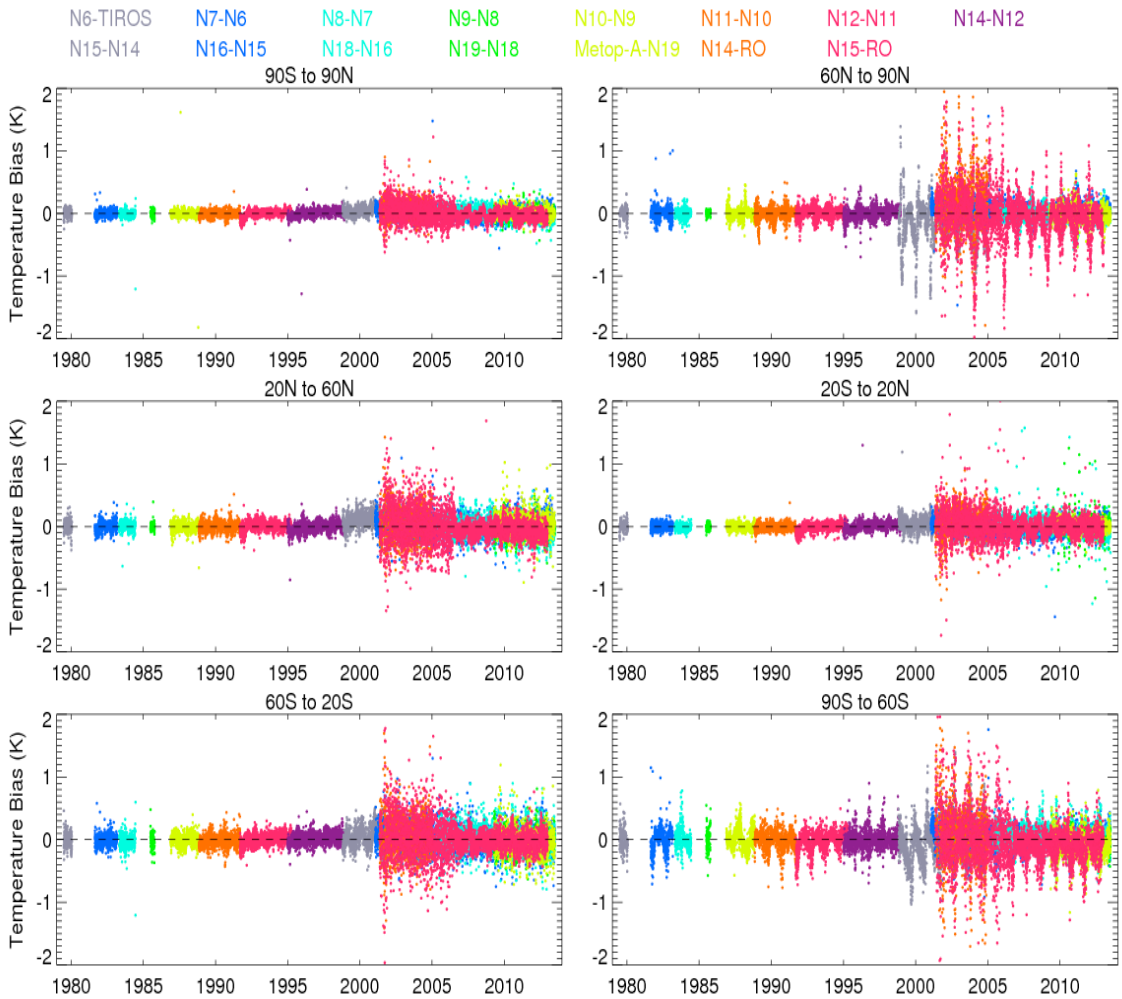


**Figure 5. The time series of the calibrated monthly TLS mean differences for TIROS-N6, N6-N7, N7-N8, N8-N9, N10-N11, N11-N12, N12-N14, N14-N15, N16-N15, N19-N18, N14-RO, N15-RO, and Metop-A-N19 for (a) the entire globe (90ºN to 90ºS), (b) the 90ºN to 60ºN zone, (c) the 20ºN to 60ºN zone, (d) the 20ºS to 20ºN zone, (e) the 60ºS to 20ºS zone, and (f) the 90ºS to 60ºS zone.**

### 2.3 AMSU/MSU TTS results from 2001 to 2013

We also used RO identified high quality radiosonde observations (RAOBs) as references to calibrate AMSU/MSU TTS results.

The method used for calibration of the TTS MSU/AMSU data from 1978 to 2010 us also applying for the AMSU/MSU TTS CDR from 1978 to 2010. Five types of Vaisala radiosonde data from the year of 2001 to 2010 were used to calibrate Temperatures of Tropopause/Stratosphere (TTS) taken from AMSU microwave measurements from different satellites for potential improvements of tropopause and Stratosphere temperature trend analysis. Details are described in the TTS CATBD and are not repeated here.

Fig. 6 depicts the inter-satellite TTS biases between two missions when they are co-located. No calibration procedures are implemented. The inter-satellite TTS biases between N16-N15, N18-N15, N19-N15, Metop-A – N15, and Aqua-N15 are generated.

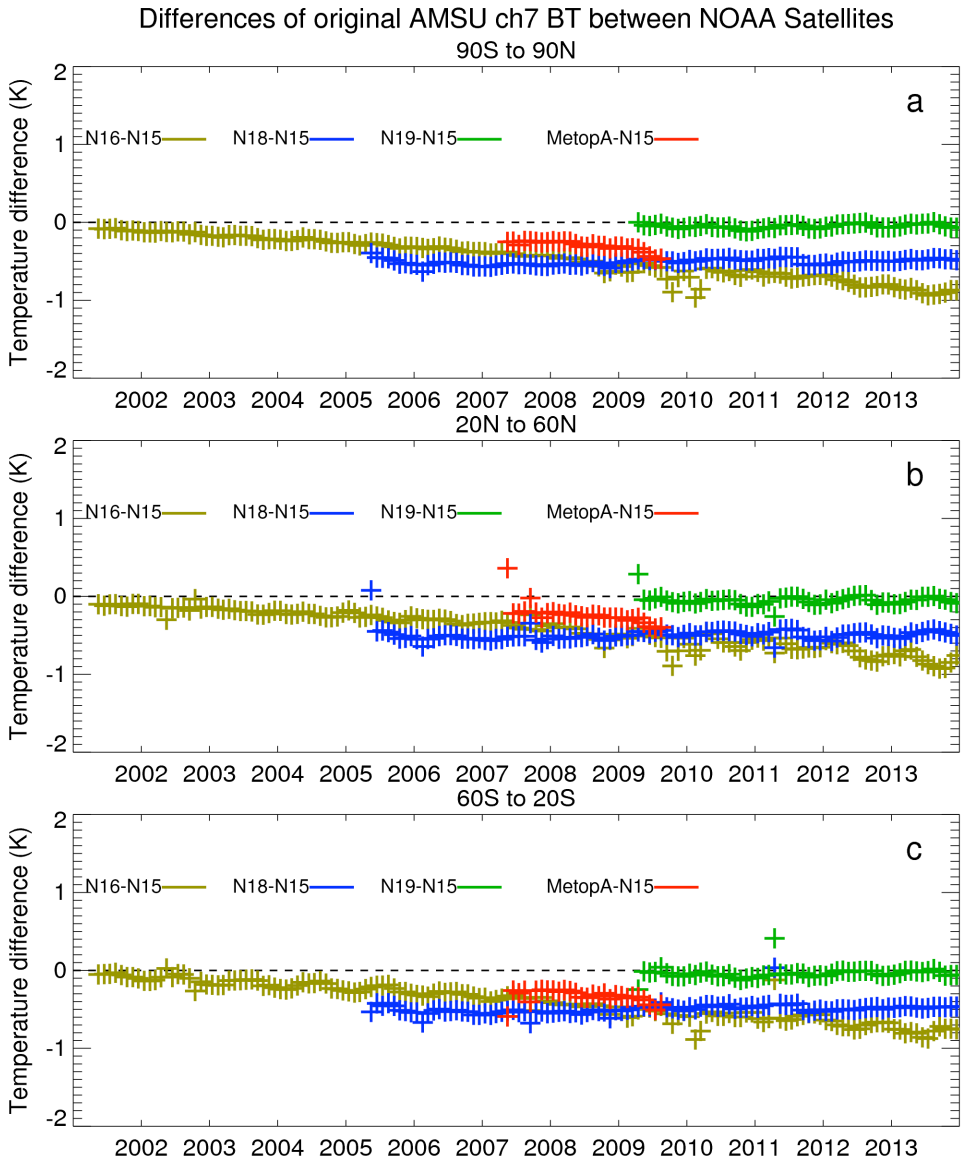


**Fig. 6. The time series of the monthly TTS mean differences for N16-N15, N18-N15, N19-N15, Metop-A – N!5, and Aqua-N15 for (a) the entire globe (90ºN to 90ºS), (b) the 20ºN to 60ºN zone, and (c) the 60ºS to 20ºS zone.**

After applying the calibration method to all the AMSU TTS from 2001 to 2013 from different NOAA, Aqua, and Metop-A missions, the time series of the inter-satellite biases of the calibrated TTS for different latitudinal zones are shown in Fig. 7.

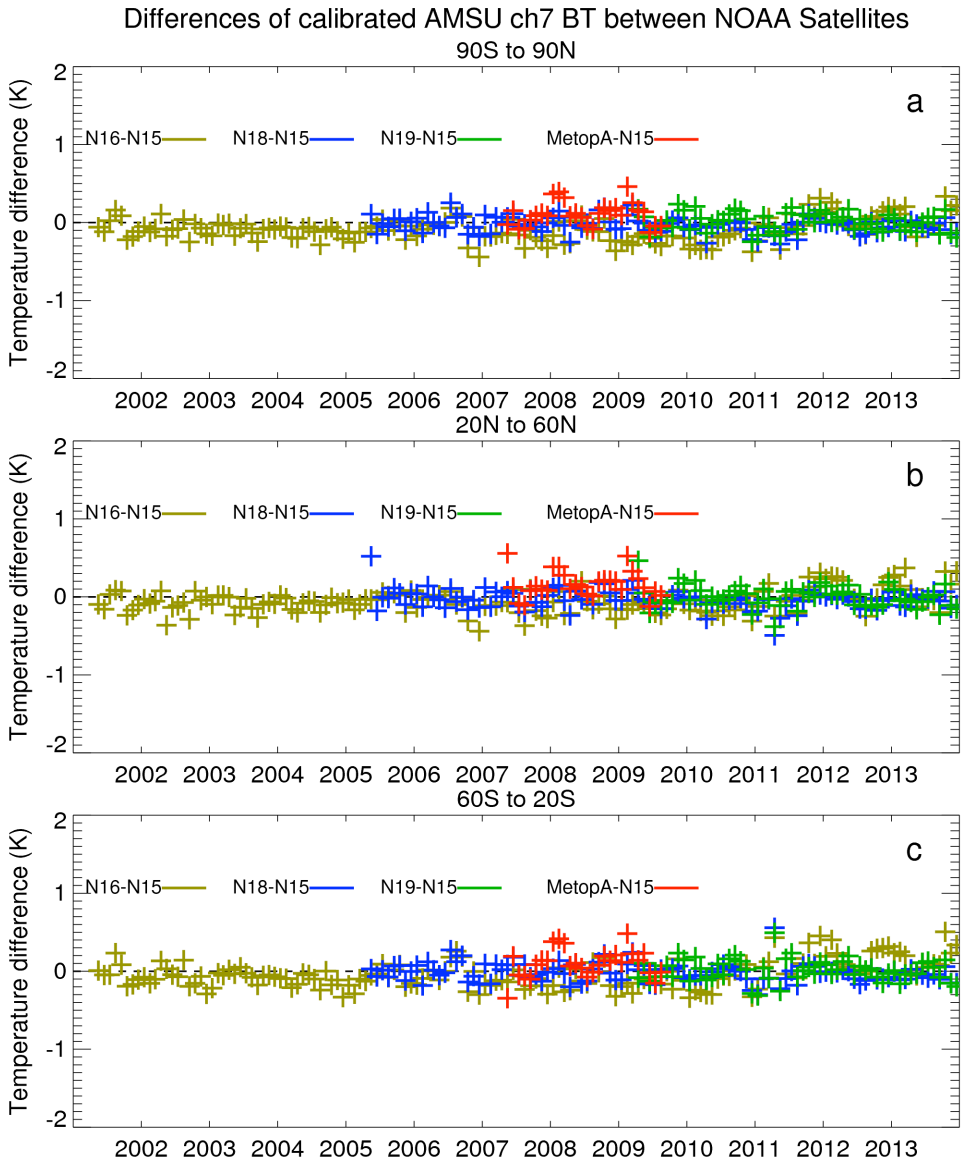


**Fig. 7. The time series of the monthly calibrated TTS mean differences for for N16-N15, N18-N15, N19-N15, Metop-A – N15, and Aqua-N15 for (a) the entire globe (90ºN to 90ºS), (b) the 20ºN to 60ºN zone, and (c) the 60ºS to 20ºS zone.**

Fig. 8 depicts the anomaly of AMSU TTS calibrated by RO identified RAOBs in December 2013. The monthly mean for AMSU TTS and the climatology of the AMSU TLS calibrated by RO data from 2002 to 2013 is also shown in Fig. 8.

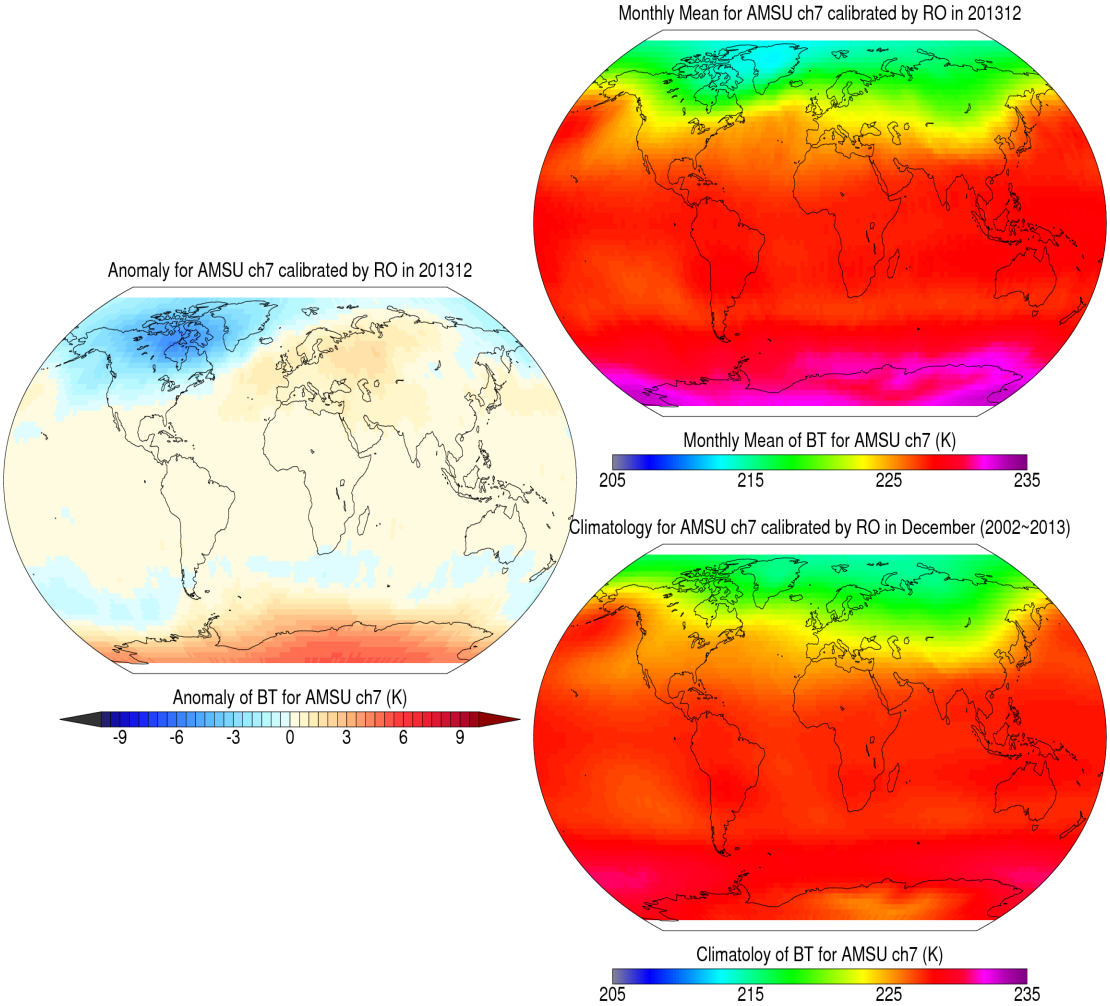


**Fig. 8. The left panel shows the anomaly of AMSU TTS calibrated by high quality RAOBs in December 2013. The right upper panel is the monthly mean for AMSU TTS. The right lower panel depicts the climatology of the AMSU TTS calibrated by RAOB data from 2002 to 2013.**

### 2.4 AMSU/MSU TTS results from 1980 to 2001

In this time period we also concentrated on developing methods to use the calibrated TTS after 2001 to calibrate those overlapped MSU TTS from 1980 to 2001 and to further construct consistent TTS from 1980 to 2013. Again, withour detailing all the refining procedures, we present the new TTS calibrated time series.

Figure 9 depicts the inter-satellite biases between two missions when they are co-located from 1980 to 2000. Figure 10 depicts the inter-satellite biases between two missions after the MSU TTS are calibrated.

We are still testing the method to merge the TTS results from 1980 to 2001 and those after 2001. The final results and detail description of the refining procedures will be summarized in the final project report.

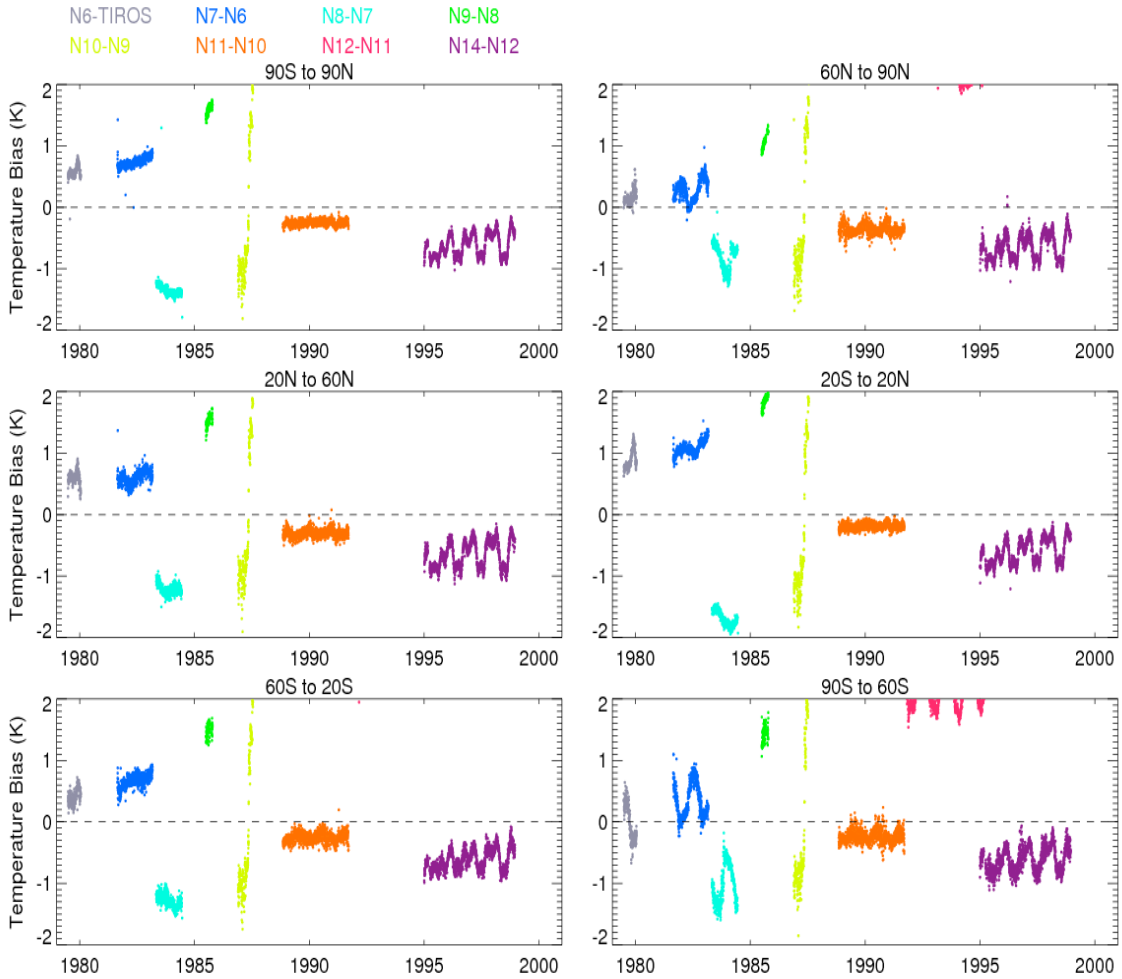


**Figure 9. The time series of the monthly TTS mean differences for N6-TIROS, N7-N6, N8-N7, N9-N8, N11-N10, N12-N11, N14-N12 for the global (upper left panel), 90º N to 60º N zone (upper right panel), 20º N to 60º N zone (middle left panel), 20º N to 20º S zone (middle right panel), 60º S to 20º S zone (lower left panel), and 90º S to 60º S zone (lower right panel).**

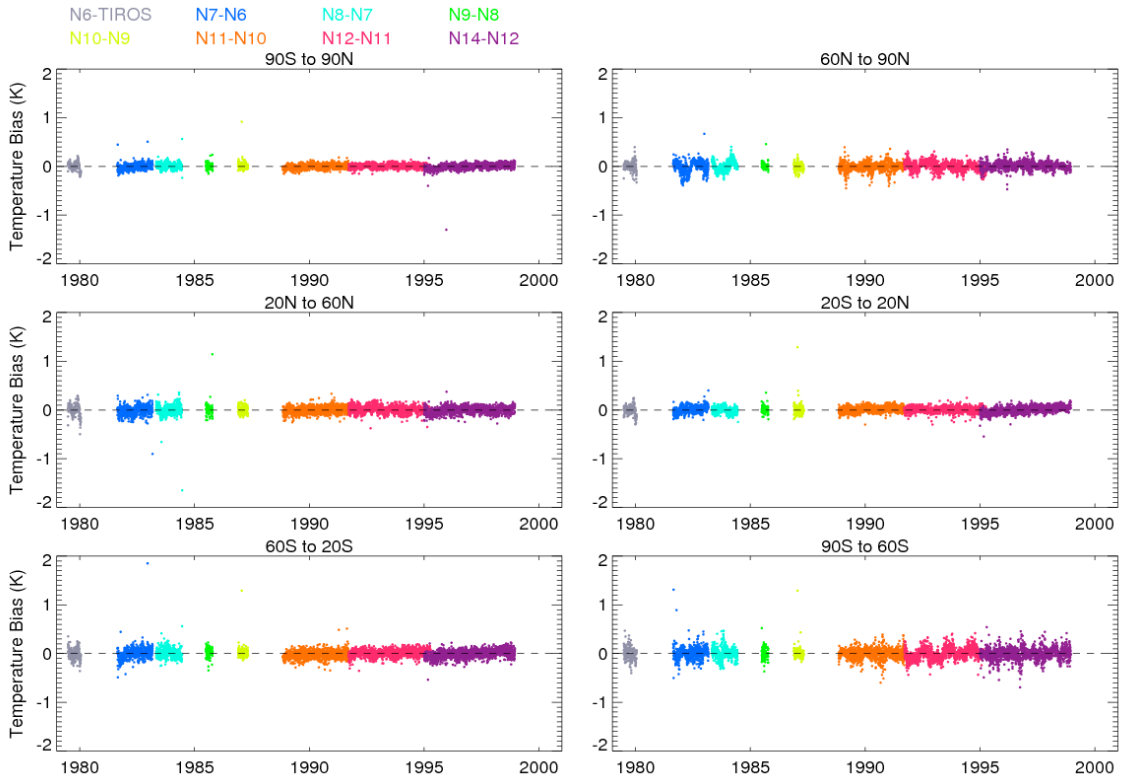


**Figure 10. The time series of the calibrated monthly TTS mean differences for N6-TIROS, N7-N6, N8-N7, N9-N8, N11-N10, N12-N11, N14-N12- for the global (upper left panel), 90º N to 60º N zone (upper right panel), 20º N to 60º N zone (middle left panel), 20º N to 20º S zone (middle right panel), 60º S to 20º S zone (lower left panel), and 90º S to 60º S zone (lower right panel).**

## 3. Presentations and Publications

Related publications and presentation from June 2013 to the current are listed:

1) Ho, S.-P., X. Yue, Z. Zeng, C. Ao, C.-Y. Huang, E. R. Kursinski, Y.-H. Kuo (2013), Applications of COSMIC Radio Occultation Data from the Troposphere to Ionosphere and Potential Impacts of COSMIC-2 Data, BAMS, doi: http://dx.doi.org/10.1175/BAMS-D-13-00035.1.

2) Mears, C., S.-P. Ho, L. Peng, Zhou, and J. Wang (2014), Total Column Water Vapor, [In "States of the Climate in 2013]. *Bul. Amer. Meteor. Sci.*, (*in press*).

3) Ho, S.-P., (section co-author) for IPCC AR5 report (invited)

4) Kumar, V., S. K. Dhaka, K. K. Reddy, A. Gupta, S. B. Surendra Prasad, V. Panwar, N. Singh, S.-P. Ho, and M. Takahashi (2014), Impact of Quasi-Biennial Oscillation on the inter-annual variability of the tropopause height and temperature in the tropics: A study using COSMIC/FORMOSAT-3 observations, Journal of Atmospheric Research (in press).

5) Huang, Ching-yuang, Wen-hsin Teng, S.-P. Ho, Y. H. Kuo (2013), Global Variation of COSMIC Precipitable Water over Land: Comparisons with Ground-based GPS Measurements and NCEP Reanalyses, GRL, DOI: 10.1002/grl.50885.

6) Blackwell, W. J., Rebecca Bishop, Clayton Crail, Kerri Cahoy, Brian Cohen, Lidia Cucurull, Pratik Dave, Michael DiLiberto, Neal Erickson, Chad Fish, shu-peng Ho, R. Vincent Leslie, Idahosa A. Osaretin, Radiometer Calibration Using Co-located GPS Radio Occultation Measurements, IEEE TRANSACTIONS ON GEOSCIENCE AND REMOTE SENSING, 2013 (*accepted*).

7) Mears, C., J. Wang, S.-P. Ho, L. Zhang, and X. Zhou (2013), Total Column Water Vapor, [In "States of the Climate in 2012]. *Bul. Amer. Meteor. Sci*.

8) Teng, Wen-Hsin, Ching-Yung Huang, S.-P. Ho, Ying-Hwa Kuo, and Xin-Jia Zhou (2013), Characteristics of Global Precipitable Water in ENSO Events Revealed by COSMIC Measurements, *J. Geophy. Research,* Vol. 118, 1–15, doi:10.1002/jgrd.50371.

9) Biondi, R., S.-P. Ho, W. Randel, T. Neubert and S. Syndergaard (2013), Tropical cyclone cloud-top heights and vertical temperature structure detection using GPS radio occultation measurements, *J. Geophy. Research,* VOL. 118, 1–13, doi:10.1002/jgrd.50448.

10) Steiner, A. K., D. Hunt, S.-P. Ho, G. Kirchengast, A. J. Mannucci, B. Scherllin-Pirscher, H. Gleisner, A. von Engeln, T. Schmidt, C. Ao, S. S. Leroy, E. R. Kursinski, U. Foelsche, M. Gorbunov, Y.-H. Kuo, K. B. Lauritsen, C. Marquardt, C. Rocken, W. Schreiner, S. Sokolovskiy, S. Syndergaard, and J. Wickert (2013), Quantification of Structural Uncertainty in Climate Data Records from GPS Radio Occultation, *ACP* doi:10.5194/acp-13-1469-2013.

11) Ho, S.-P., Liang Peng, Richard A. Anthes, Ying-Hwa Kuo, and Hsiao-Chun Lin, 2014, Marine Boundary Layer Heights and their Longitudinal, Diurnal and Inter-annual Variation in the Southeast Pacific using COSMIC, CALIOP, and Radiosonde Data, *J. of Climate* (submitted).

12) Ho, S.-P., L. Peng, X. J. Zhou, 2013: Calibration and Construction of Microwave Sensor Temperature Records in the Lower Stratosphere from 2001 to 2010 Using Global Positioning System Radio Occultation Data, *J. Geophy. Research (submitted).*

13) Dhaka, S. K., V. Kumar, R. K. Choudhary, S.-P. Ho, and K. K. Reddy (2014), Observation of strong remote dynamical connection between polar and tropical regions due to sudden stratospheric warming of 2009, *J. Geophy. Research* (submitted).

14) Kumar, V., S. K. Dhaka, R. K. Choudhary, S.-P. Ho, and K. K. Reddy (2014), On the occurrence of coldest temperature in stratospheric region and tropical tropopause stability: A study using COSMIC/ FORMOSAT-3 satellite measurements, Journal of Atmospheric and Solar-Terrestrial Physics (submitted).

15) Ho, S.-P., Enhancement of the AIRS Temperature and Water Vapor Retrievals using Global Positioning System Radio Occultation Data, AIRS science team, JPL, May 22, 2013.

16) Ho, S.-P., Construction of Consistent Microwave Sensor Temperature Records and Tropopause Height Climatology using MSU/AMSU Measurements, GPS RO Data, and Radiosonde Observations, NOAA's Climate Data Record Annual Meeting, July 30-31, August 1, 2013, Asheville, NC.

17) Ho, S.-P., Calibration of Temperature Troposphere / Stratosphere from Advanced Microwave Sounding Unit using High Quality Radiosonde Data Identified by Radio Occultation Data, Joint OPAC-5 and IROWG-3 workshop, September 5-11, 2013, Seggau Castle, Leibnitz, Austria.

18) Biondi, R. W. Randel, S.-P. Ho, and S. Syndergaard, Thermal structure of tropical cyclones and intense convective systems using GPS radio occultation measurements, Joint OPAC-5 and IROWG-3 workshop, September 5-11, 2013, Seggau Castle, Leibnitz, Austria.

19) Ho, S.-P., New Science opportunities on COSMIC-2/FORMOSAT-7, COSMIC annual retreat, Oct. 10, Boulder CO.

20) Ho, S.-P., Liang Peng, Rick Anthes, Ying-Hwa Kuo, and Hsiao-Chun Lin,Estimation of Planetary Boundary Layer Heights from COSMIC, CLIPSO, and High Resolution Radiosondes during the VOCALS-REx Conference Title: 18th Conference on Integrated Observing and Assimilation Systems for the Atmosphere, Oceans, and Land Surface (IOAS-AOLS) Meeting. Feb. 2-6, 2014, Atlanta, GA.

21) Ho, S.-P., Liang Peng, Rick Anthes, Ying-Hwa Kuo, and Hsiao-Chun Lin, Planetary Boundary Layer Heights from COSMIC and CALIOP over Ocean, Donald R. Johnson Symposium Meeting, 94th American Meteorological Society Annual Meeting, Feb. 2-6, 2014, Atlanta, GA.

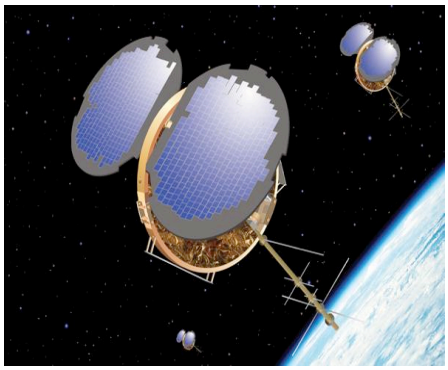

COSMIC

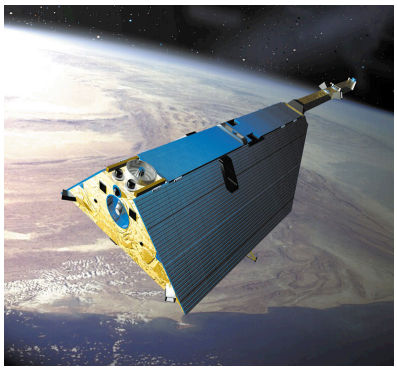

CHAMP

Final PROJECT REPORT (from 06/01/2010 - 05/31/2014)
NOAA Award number: NA10NES4400002

# Construction of Consistent Microwave Sensor Temperature Records and Tropopause Height Climatology using MSU/AMSU Measurements, GPS RO Data, and Radiosonde Observations


**Principal Investigator:**
Shu-Peng (Ben) Ho (303-497-2922, spho@ucar.edu)

**Co-Investigators:**
Cheng-Zhi Zou ((301) 763-8042 x156, cheng-zhi.zou@noaa.gov)
Ying-Hwa Kuo ((303) 497-8910, kuo@ucar.edu)

**National Center for Atmospheric Research**
**P.O. Box 3000, Boulder, CO 80307 USA**

## 1. Introduction

The monitoring and detecting of the vertical structure of atmospheric temperature trends are key elements in the climate change problem. In addition, the identifying of the long-term change of temperature and tropopause structure (i.e., tropopause height) in the upper troposphere and lower stratosphere (UTLS) is necessary to advance reliable predictions of trends in climate or global change. However, due to poor vertical resolution and/or measurement uncertainty, traditional in situ observations and most of satellite measurements in this region have not been well suited for these studies.

Recently, the Global Positioning System (GPS) Radio Occultation (RO) technique has been proven to be a mature global observation technique and is ideally suited for climate trend detection. GPS RO is the first satellite remote sensing technique where its fundamental observable, the delay of the occulted signal's phase due to the atmosphere and ionosphere, is accomplished via precise measurement of time that is traceable to ultra-stable international standards (SI traceability) on the ground (atomic clocks). This traceability makes GPS RO a strong candidate for a climate benchmark.

In this study, we propose to carry out three tasks:

- **Task 1: To use GPS RO data from 2001 to 2013 as climate benchmark datasets to quantify the Microwave Sounding Unit (MSU)/Advanced Microwave Sounding Unit (AMSU) temporal and spatial variation of temperature in the lower stratosphere (TLS) anomalies and to use the calibrated TLS after 2001 to calibrate the overlapped TLS before 2001 and to construct MSU/AMSU TLS records from 2001 to 2013;**

- **Task 2: To generate a long-term climate quality temperature dataset for of AMSU/MSU Temperatures of Tropopause/Stratosphere (TTS) by reprocessing thirty-three years (1980-2013) of MSU/AMSU data. The 'adjusted' MSU/AMSU data and identified RO-consistent radiosonde data in the period of 2001 to 2013 will serve as reference data to calibrate other overlapped MSU/AMSU data from 1980 to 2001;**

- **Task 3: To use GPS RO soundings collected from multi-RO missions but processed using a consistent processing package to construct tropopause height climatology from 2001 to 2013 that is consistent with changes in temperature and tropopause structure estimated by radiosondes.**

The work undertaken for construction of AMSU temperature in the TLS climate data records (CDRs) from 1980 to 2013 is detailed in section 2. The results and methods for construction of AMSU/MSU TTS CDRs s from 1980 to 2013 are detailed in Section 3. In Section 4, we summarized the work for construction of

Tropopause height CDRs from 2001 to 2013. The journal papers and presentations supported by this project are listed in Section 6.

## 2. Data Sources and Quantification of GPS RO data for climate monitoring

### 2.1 Data collection

We downloaded the following data from corresponding FTP and achieve sites:

- CHAMP data (from Jan. 2001 to April 2008) from UCAR CDAAC,
- COSMIC data (from June 2006 to April 2013) from UCAR CDAAC,
- GRACE data (from June 2006 to Dec. 2008) from UCAR CDAAC,
- MSU/AMSU data from NESDIS ($NESDIS_{OPR}$) for NOAA6, 7, 8, 9, 10, 11, 12 and 14 (MSU), NOAA 15, 16, 18, and 19 (AMSU) from 1980 to 2013,
- AMSU data from Aqua and Metop-A
- Global radiosonde data from NCAR archive

### 2.2 Data matching

To minimize the temporal/spatial/vertical-resolution mismatches among various datasets, we generated the following collocated data pairs:

- CHAMP-COSMIC, GRACE-COSMIC pairs (within 90 minutes, and 200 km).
- MSU/AMSU-RO pairs (within 15 minutes, and 50 km).
- RSS/UAH-RO pairs (monthly mean, 2.5×2.5 grid, we further bin each monthly mean MSU/AMSU and CHAMP 2.5 degree × 2.5 degree matched pairs into 10 degree × 10 degree grids).
- Radiosonde-RO pairs (temperature and moisture profiles obtained from radiosondes are interpolated onto RO locations within 3 hours and 200 km).
- ECMWF-RO pairs (ECMWF temperature and moisture profiles are interpolated onto RO locations within 3 hours and 200 km).
- To avoid AMSU vertical weighting function representation errors, instead of using a global fixed weighting function (WF), we apply a COSMIC/CHAMP dry temperature profile to an AMSU fast forward model from the Cooperative Institute for Meteorological Satellite Studies-CIMSS with 100 fixed pressure levels.

### 2.3 Reprocessing the RO data from Multiple RO Missions using Consistent inversion Procedures and Quantifying of the Reproducibility for using GPS RO Data for Climate Monitoring

#### *a. RO data Reprocessing*

A new RO inversion package is developed during the performance period. Several improvements to precise orbit determination (POD), excess atmospheric phase and neutral atmospheric inversion processes are developed. Now the consistent RO inversion algorithm is applied to several international RO missions to derive the vertical distribution of bending angle, refractivity, temperature, and geo-potential height. These RO missions include GPS/MET (from 1995 to 1997, no overlap with other RO missions), COSMIC (launched in April 2006), Challenging Mini-satellite Payload (CHAMP, from 2001 to 2008), Gravity Recovery And Climate Experiment (GRACE, launched in 2004), Satélite de Aplicaciones Científicas-C (SAC-C, launched in 2000), GNSS RO Receiver for Atmospheric Sounding (GRAS, launched in 2007), Communication/Navigation Outage Forecast System (C/NOFS, launched in 2008), and Terra Synthetic Aperture (SAR) Radar operating in the X-band (TerraSAR-X, launched in 2007).

#### *b. Quantification of the Comparability of RO data for Climate Research*

Since the instantaneous atmospheric truth profiles are not available, it is hard to quantify the absolute accuracy of GPS RO data. However, the precision of GPS RO data can be quantified by comparing closely located retrieved profiles derived from independent GPS RO missions (or among different receivers) and the precision can be quantified where the GPS RO signals travel through nearly the same atmospheric paths. Here we quantified the differences of inverted profiles among different RO missions whenever the newly processed RO data from different RO missions are available. We continue to conduct the following studies:

**i). Quantify the Uncertainty of the Long-term Stability of GPS RO Data for Climate Monitoring by conducting profile-to-profile comparisons**

To quantify not only the mean difference but also the uncertainty to the mean difference between RO missions, we continue to inter-compare the co-located RO data among CHAMP, COSMIC, SAC-C, GRACE, GRAS, C/NOFS, TerraSAR-X, and possible new RO missions beyond 2011.

**ii) Documenting traceable standards for GPS RO metadata including the change of observing practices, the bending angle, phase, amplitude, and time delay of radio signals.**

**iii) Subseting the data into latitude bands as well as land and ocean subsets, which will show whether this comparability is regionally**

**dependent. We also examine differences of viewing geometry, rising/setting, thermal noise, ionospheric calibration, and orbit error among different missions.**

Results show that the mean temperature biases from 8 km to 30 km between two close collocated RO missions are in general less than 0.1 K. No further results are reported.

***c. Reproducibility of RO Sounding Results: profile-to-profile comparisons of RO data processed by different RO centers***

In addition, because although the raw RO phase delay is traceable to the SI unit, the derived atmospheric variables temperature are not. The derived temperature profiles may vary when different initial conditions and implementation methods are used. To examine the claim that GPS RO data are useful as a benchmark data set for climate monitoring, the structural uncertainties of retrieved profiles that result from different processing methods are quantified.

To quantify the reproducibility of RO data among different RO processing centers, we conduct profile-to-profile comparisons among different RO centers. This is to quantify the structural uncertainty of RO parameters derived at each of the following processing step:

a. Precise Orbit Determinations and Excess Atmospheric Phase Processing
b. Calculation of L1 and L2 Bending Angles
c. Ionospheric Correction
d. Abel Integral Upper Boundary
e. Derivation of Dry temperature
f. Derivation of geo-potential height
g. Derivation of pressure
h. Quality Control Methods

***Approaches:***

i) Collect CHAMP data (2001 to 2008) processed by UCAR, JPL, GFZ, DMI, EUM, and Wegc.
ii) In order to match the exact the same profiles processed by different centers, we first used UCAR routines to rename the filename from individual centers so that they are consistent with the UCAR filename.
iii) Using the profile information from the filename, we match all the individual profile processed by different processing centers.

***Comparison results:***

- We compare the GPS RO-derived vertical profiles of bending angle, refractivity, and dry temperature derived by six different centers.

- **Figure 1** shows the time series of refractivity anomalies (relative to the mean refractivity for all five centers) from January, 2002 to December, 2008 among six centers.

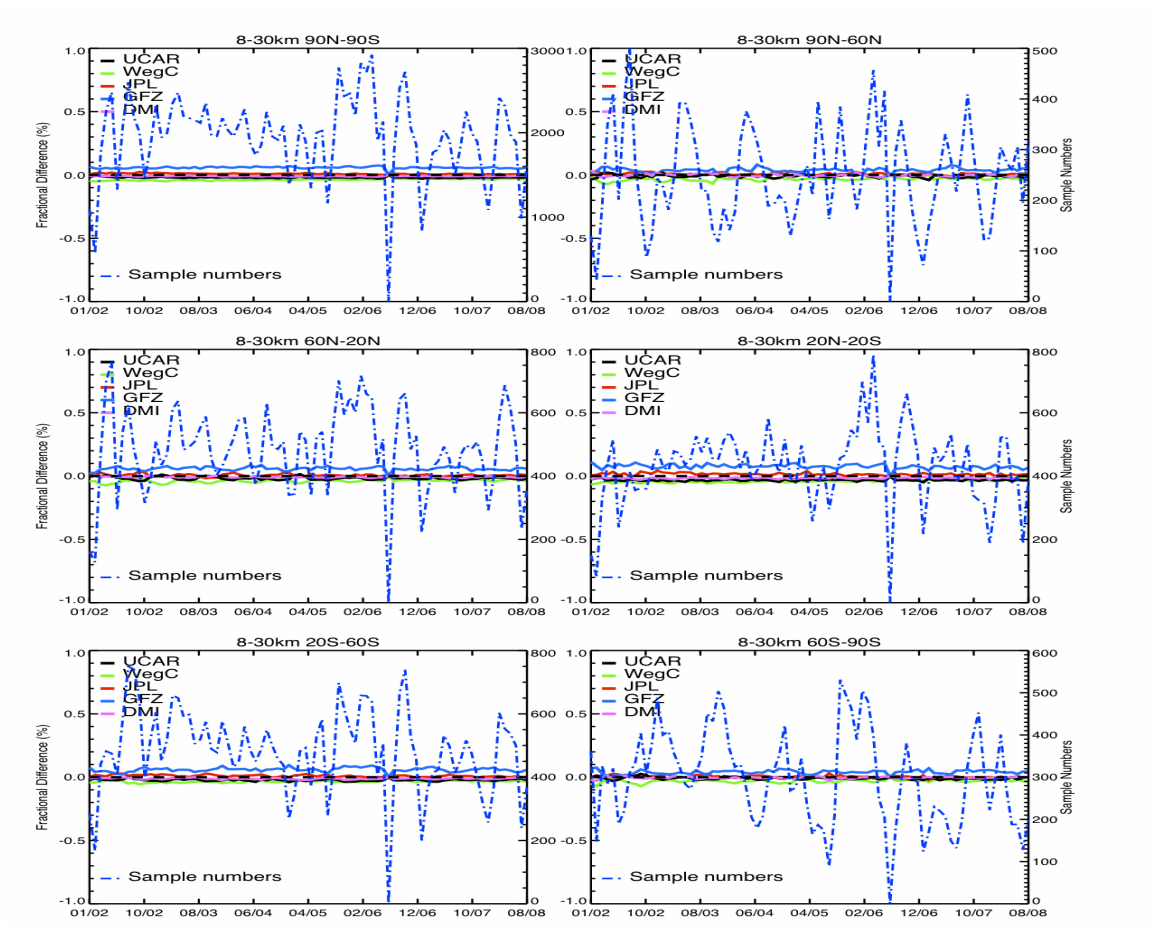


**Figure 1. The time series of refractivity anomalies (relative to the mean refractivity for all five centers) from January, 2002 to December, 2008 among six centers for the 8-30 km layer for (a) the entire globe (82.5ºN-82.5ºS, the left upper panel), b) the 82.5ºN-60ºN zone (the upper right panel), (c) the 60ºN-20ºN zone (the middle left panel), (d) the 20ºN-20ºS zone (the middle right panel), (e) the 20ºS-60ºS zone (the bottom left panel), and (f) the 60ºS-82.5ºS zone (the bottom right panel).**

Research results from above research studies are summarized in several journal papers and national and international conferences, which are listed in Section 5.

# 3. AMSU/MSU temperature in the lower stratosphere (TLS) Climate Data Records

## 3.1 AMSU temperature in the lower stratosphere (TLS) Climate Data Records from 2001 to 2013

Using RO temperature profiles derived from multiple RO missions, the AMSU ch9 brightness temperatures (TLS) are calibrated.

Currently, more than 10 year of RO data from multiple RO missions including CHAllenging Minisatellite Payload (CHAMP, launched in 2001), COSMIC (launched in 2006), Gravity Recovery And Climate Experiment (GRACE, launched in 2004), and MetOp/GRAS (launched in 2006) are consistently processed by the COSMIC Data Analysis and Archive Center (CDAAC). The COSMIC, CHAMP, GRACE dry temperature profiles (atmPrf) downloaded from UCAR CDAAC (http://cosmic.cosmic.ucar.edu/cdaac/index.html) are used.

**Figure 2** depicts the inter-satellite biases between two missions when they are co-located. No calibration procedures are implemented. The inter-satellite biases between N16-N15, N18-N15, N19-N15, Metop-A - N15, and Aqua-N15 are generated.

A sequence of processing steps is implemented to use the RO data to calibrate the AMSU TLS and merge the calibrated TLS among multiple AMSU missions. The procedure consists of the following steps:

i) Forward calculation of the AMSU TLS using RO temperature profiles: The AMSU fast-forward model from the Cooperative Institute for Meteorological Satellite Studies–CIMSS, $MWF_{CIMSS}$ (Hal Woolf, CIMSS, personal communication, 2005), is used in this study. The validation of the microwave transmittance of this model is described in *Woolf et al.,* [1999]. All the available temperature profiles for COSMIC, CHAMP, and GRACE are first extracted from the CDAAC level2 data and interpolated to the 100 pressure levels of the AMSU fast-forward model. The interpolated temperature profiles from GPS RO missions are then applied to the AMSU fast-forward model to calculate the AMSU Ch9 brightness temperatures. The water vapor profiles are set to zero in the forward calculation.

ii) Data Matching: To avoid the spatial and temporal representation errors, we collocate AMSU pixels with each RO profile within 30 minutes and 100 km. AMSU pixels with a satellite viewing angle ranging from -15 degrees to 15 degrees are all included in this study to increase the number of AMSU pixels in our comparison. To avoid anomalous values due to missing data, differences among the brightness temperatures that are larger than 10 degrees are omitted. To have enough RO profiles, which contain reasonable temporal and spatial coverage, we use three consecutive months of CHAMP data to represent the TLS variation for the middle month. Three monthly running CHAMP-AMSU pairs are used before June 2006, whereas the available CHAMP, COSMIC, and

GRACE RO data in the same month are used to match up with the AMSU data after June 2006. Collectively, these matching criteria balance the tradeoff between the quality and the number of the matched measurements.

iii) Calculation of the calibration coefficients: The quality of the RO temperatures over the vertical range of AMSU Ch9 weighting function leads to comparable brightness temperatures $TLS^{RO}$. The highly linear relationship between $TLS^{RO}$ and the measured AMSU brightness temperatures ($TLS^{AMSU}$) permits calibration via a simple linear fit:

$$TLS^{RO} = \text{SLOPE} \times TLS^{AMSU} + \text{OFFSET} \qquad (2),$$

where the SLOPE and OFFSET values for each month are calculated by minimizing the root mean square between the coincident $TLS^{RO}$ and $TLS^{AMSU}$ values. Hereafter, the RO- simulated TLS for N15, N16, N18, N19, Aqua, and Metop-A are denoted as $TLS^{RO}_{N15}$, $TLS^{RO}_{N16}$, $TLS^{RO}_{N18}$, $TLS^{RO}_{N19}$, $TLS^{RO}_{Aqua}$, and $TLS^{RO}_{Metop-A}$, respectively. The AMSU TLS for N15, N16, N18, N19, Aqua, and Metop-A are denoted as $TLS_{N15}$, $TLS_{N16}$, $TLS_{N18}$, $TLS_{N18}$, $TLS_{Aqua}$, and $TLS_{Metop-A}$, respectively. The calibrated AMSU TLS (i.e., $TLS^{Cal}$) can be obtained by applying the defined slope and offset to the $TLS^{AMSU}$ for the same month. Note that although the derived RO variables (bending angle, refractivity, and dry temperature) are not synchronized to the ultra-stable atomic clocks on the ground, the high precision nature of the raw RO observables is preserved in the inversion chain [*Ho et al.,* 2012]. Since the AMSU fast-forward model cannot introduce additional variability, the precision of these temperature measurements at the altitudes sensitive to AMSU Ch9 results in stable reference values for Ch9 brightness temperatures. To quantify the precision of RO-simulated TLS, *Ho et al.,* [2009b] has compared the COSMIC- calibrated AMSU TLS with those calibrated from CHAMP in the same month. Results shows that the mean biases between COSMIC-calibrated AMSU TLS and those of CHAMP-calibrated AMSU TLS can be as small as 0.07 K with a standard deviation of 0.1 K. The high precision RO-simulated TLS would be highly useful to calibrate the AMSU radiance biases (see below).

iv) Merging Procedures: Prior to the application of the linear calibration, daily means of the AMSU Ch9 brightness temperatures for each NOAA orbiter on a 2.5 degree × 2.5 degree grid are calculated. Only AMSU pixels with a satellite viewing angle ranging from -15 degrees to 15 degrees are included in the binning procedure. The calibration coefficients for each polar orbiter are then applied to the daily mean gridded values to obtain the daily-adjusted AMSU Ch9 brightness temperatures. Only high-quality TLS data from individual missions that passed their quality control tests (i.e., all quality flag bits equal to zero) are included in the daily files. The daily mean gridded AMSU Ch9 brightness temperatures from each AMSU mission in the same month are then averaged to compute the monthly means of the AMSU Ch9 brightness temperatures on a 2.5 degree × 2.5 degree grid.

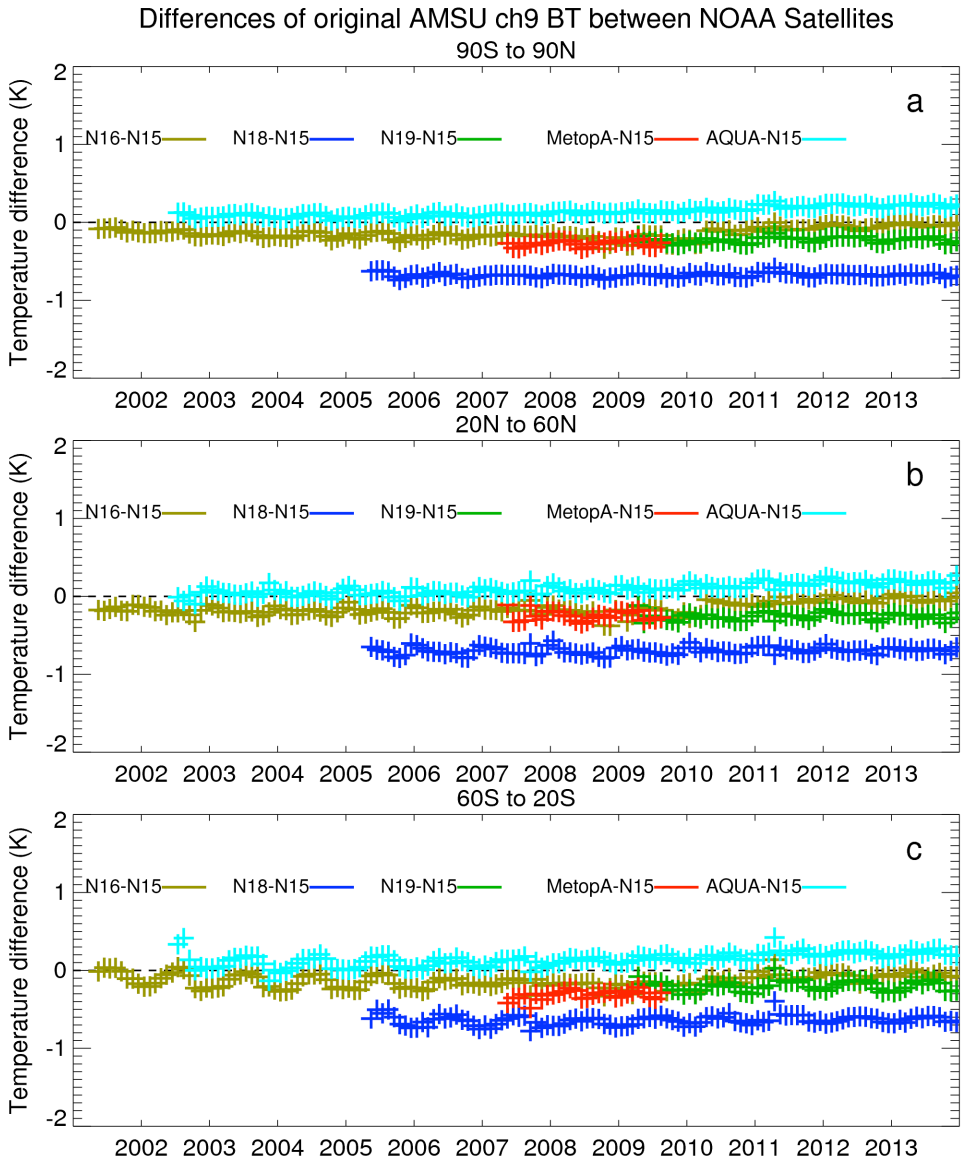


**Figure 2. The time series of the monthly TLS mean differences for N16-N15, N18-N15, N19-N15, Metop-A – N15, and Aqua-N15 for (a) the entire globe (90ºN to 90ºS), (b) the 20ºN to 60ºN zone, and (c) the 60ºS to 20ºS zone.**

After applying the calibration method to all the AMSU brightness temperature from different NOAA, Aqua, and Metop-A missions, the time series of the inter-satellite biases of the calibrated TLS for different latitudinal zones are shown in **Fig. 3**.

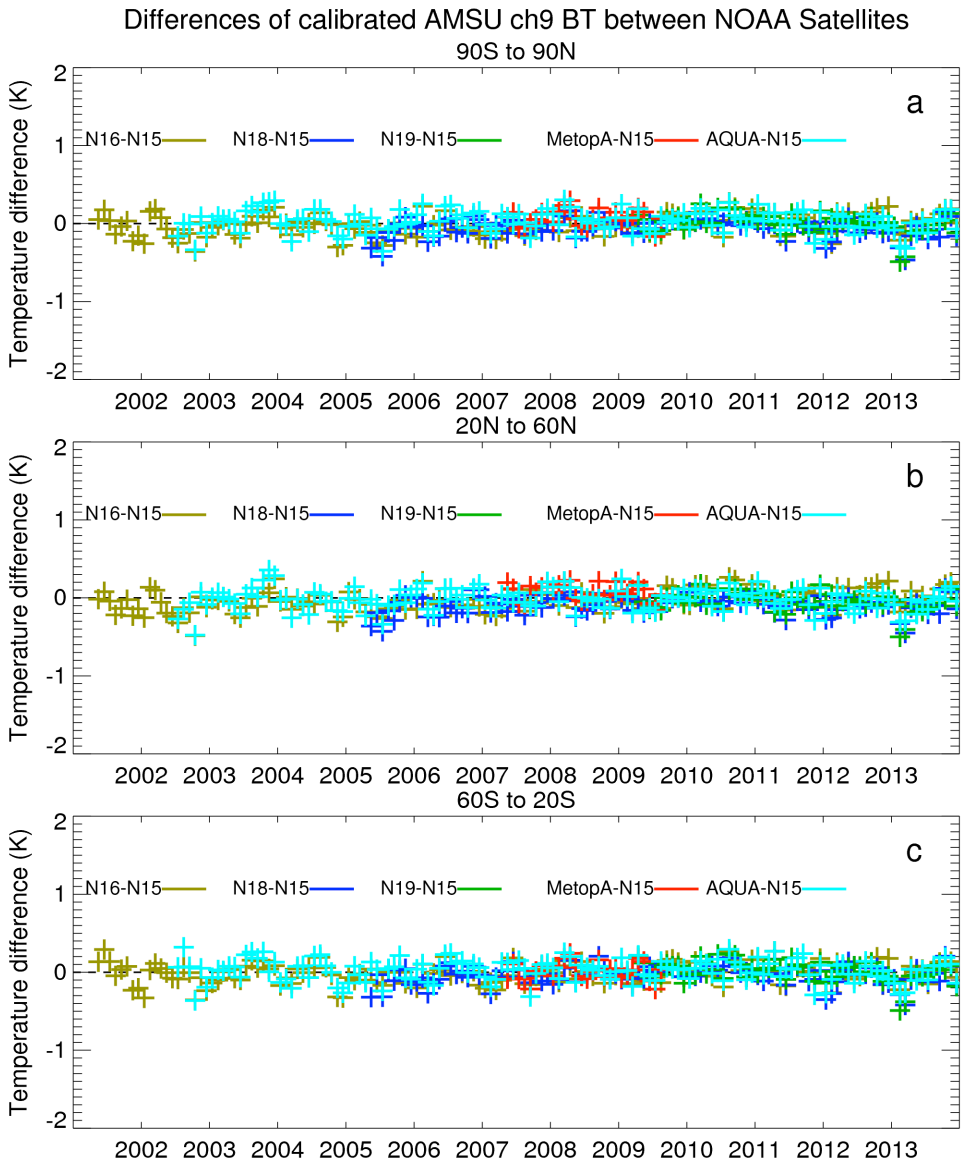


**Figure 3. The time series of the monthly calibrated TLS mean differences for N16-N15, N18-N15, N19-N15, Metop-A – N15, and Aqua-N15 for (a) the entire globe (90ºN to 90ºS), (b) the 20ºN to 60ºN zone, and (c) the 60ºS to 20ºS zone.**

**Fig. 4** depicts the anomaly of AMSU TLS calibrated by RO in December 2013. The monthly mean for AMSU TLS and the climatology of the AMSU TLS calibrated by RO data from 2002 to 2013 is also shown in **Fig. 4**.

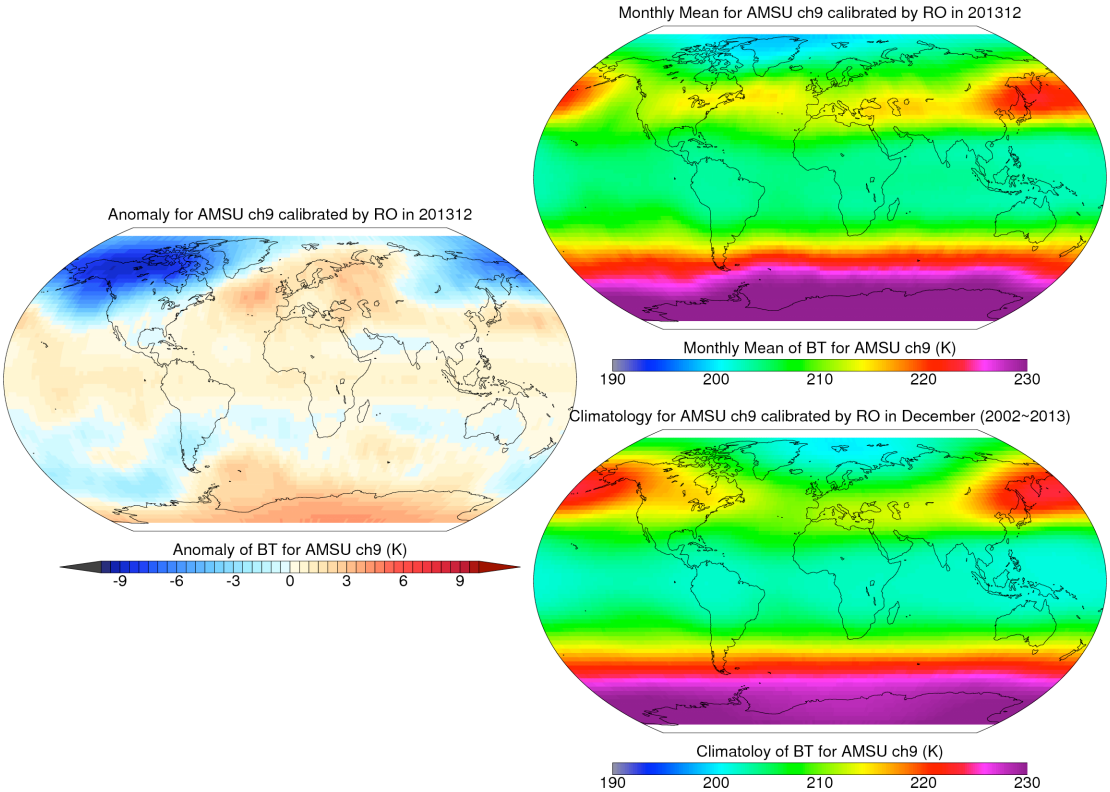


**Figure 4. The left panel shows the anomaly of AMSU TLS calibrated by RO in December 2013. The right upper panel is the monthly mean for AMSU TLS. The right lower panel depicts the climatology of the AMSU TLS calibrated by RO data from 2002 to 2013.**

### 3.2 AMSU/MSU TLS Time Series form 1980 to 2013

We were using those AMSU and MSU TLS calibrated by multiple RO missions from 2001 to 2013 to calibrate those overlapped AMSU and MSU TLS form 1978 to 2001. **Fig. 5** depicts the inter-satellite biases between two missions when they are co-located. The inter-satellite biases between TIROS-N6, N6-N7, N7-N8, N8-N9, N10-N11, N11-N12, N12-N14, N14-N15, N16-N15, N19-N18, N14-RO, N15-RO, and Metop-A-N19 are generated.

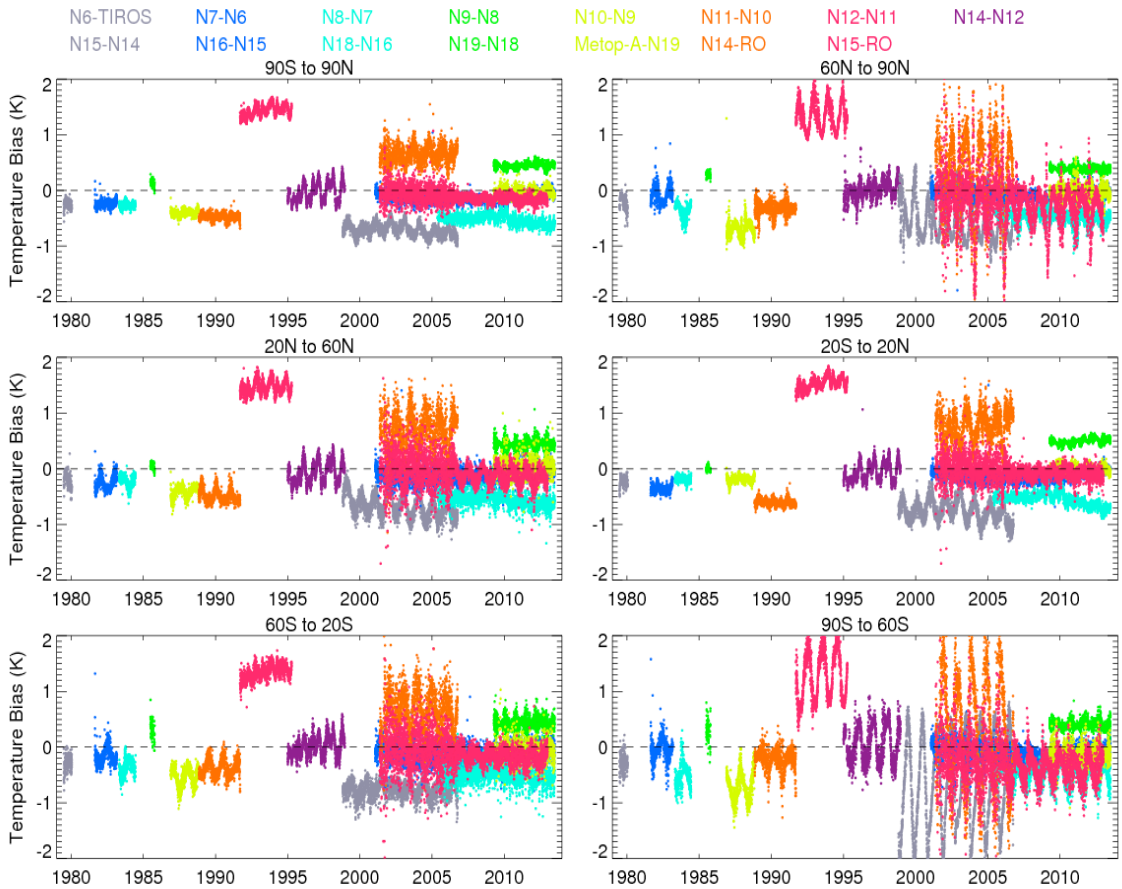


**Figure 5. The time series of the monthly TLS mean differences for TIROS-N6, N6-N7, N7-N8, N8-N9, N10-N11, N11-N12, N12-N14, N14-N15, N16-N15, N19-N18, N14-RO, N15-RO, and Metop-A-N19 for (a) the entire globe (90ºN to 90ºS), (b) the 90ºN to 60ºN zone, (c) the 20ºN to 60ºN zone, (d) the 20ºS to 20ºN zone, (e) the 60ºS to 20ºS zone, and (f) the 90ºS to 60ºS zone.**

Applying the RO calibrated MSU NOAA 14 data as references to calibrate overlapped NOAA 12 MSU and repeating the procedures, we were able to calibrate MSU data before 2001 and construct consistent AMSU/MSU TLS climate data records from 1980 to 2013. The calibrated TLS from 1980 to 2013 in is shown **Fig. 6**. The results show that the calibrated AMSU/MSU TLS between two overlapped NOAA or RO missions are all very close to zero degree K no matter they are before 2001 (no RO data) or after 2001 (RO data are used as calibration references).

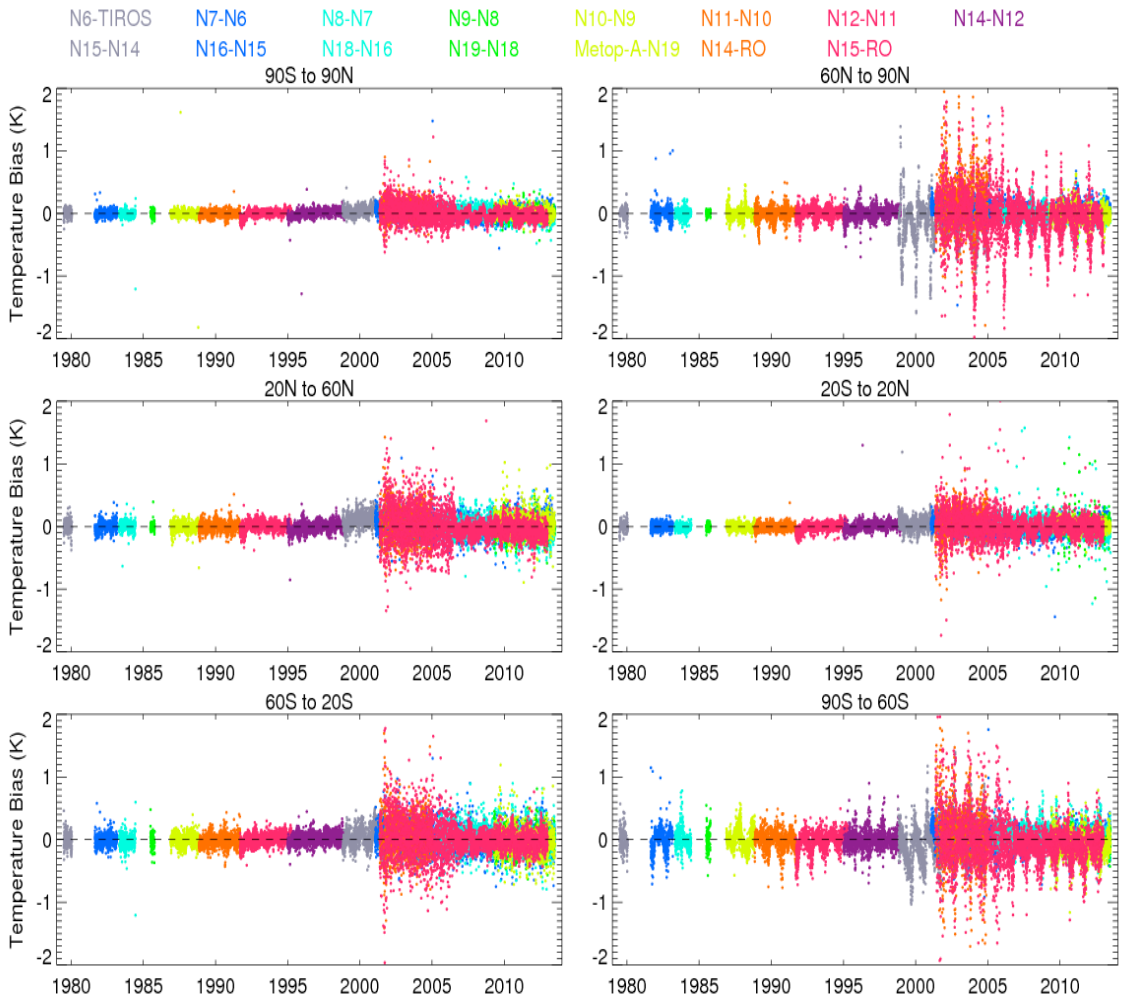


**Figure 6. The time series of the calibrated monthly TLS mean differences for TIROS-N6, N6-N7, N7-N8, N8-N9, N10-N11, N11-N12, N12-N14, N14-N15, N16-N15, N19-N18, N14-RO, N15-RO, and Metop-A-N19 for (a) the entire globe (90ºN to 90ºS), (b) the 90ºN to 60ºN zone, (c) the 20ºN to 60ºN zone, (d) the 20ºS to 20ºN zone, (e) the 60ºS to 20ºS zone, and (f) the 90ºS to 60ºS zone.**

### 3.3 Data maturity analysis: Inter-comparison of RO-AMSU TLS with other TLS datasets

To improve the maturity of the derived TLS CDRs, in situ data, reanalysis data, and TLS datasets derived from different groups were compared with the derived TLS CDRs. Many insightful results have been obtained and are used to demonstrate the maturity of the RO calibrated TLS CDTRs. Since the RO derived TLS CDRs shall also be consistent with RO temperatures in terms of stability and shall have no geo-location dependent biases, the comparison results also demonstrate the potential future applications of the RO derived CDRs. Many comparison details are not summarized in this report. In this report, we present comparisons of time series TLS anomalies among datasets (**Figure 7**).

The derived TLS record is compared with the newly available TLS datasets provided by Remote Sensing Systems (RSS) and University of Alabama in Huntsville (UAH), and TLS processed by NOAA STAR (SNO method) since 2001 to 2010. **Figure 7** shows that the time series of the TLS anomalies of the four centers vary with different latitudinal zones. The TLS anomalies from UAH and STAR generally agree well with those from RO calibrated AMSU TLS in all latitudinal zones.

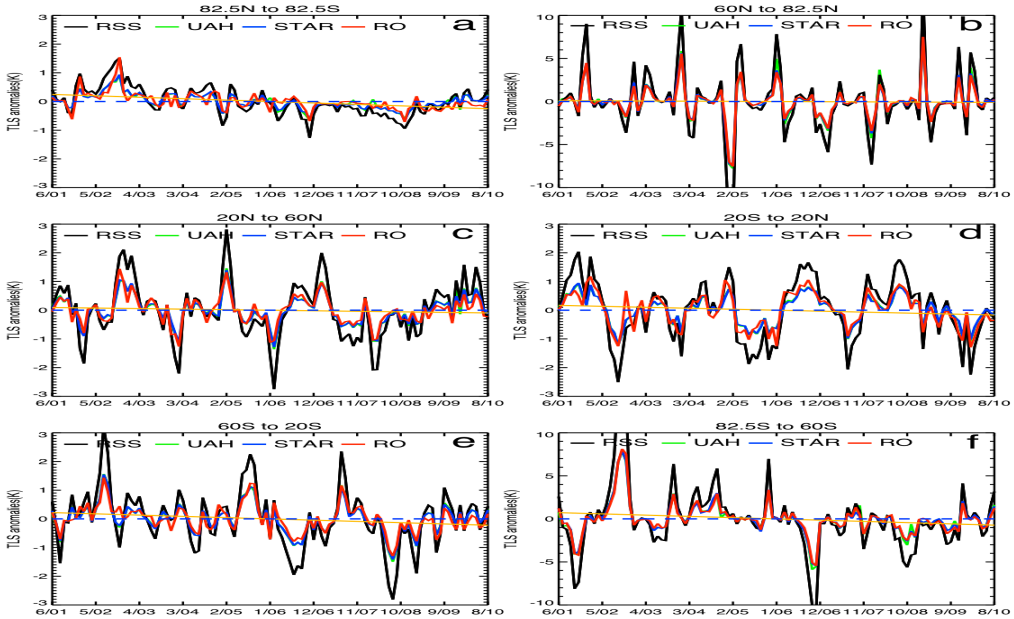


**Figure 7. TLS anomalies of RSS, UAH, STAR, and RO_AMSU for (a) the entire globe (82.5ºN-82.5ºS, the left upper panel), b) the 82.5ºN-60ºN zone (the upper right panel), (c) the 60ºN-20ºN zone (the middle left panel), (d) the 20ºN-20ºS zone (the middle right panel), (e) the 20ºS-60ºS zone (the bottom left panel), and (f) the 60ºS-82.5ºS zone (the bottom right panel). The orange line indicates the mean trend for RO_AMSU.**

# 4. AMSU/MSU TTS Climate Data Records from 1980 to 2013

## 4.1 Using GPS RO Data to Identify High Quantify Radiosonde data

GPS RO data were used to assess the systematic biases of the global radiosonde temperature measurements. The goal is to use RO temperature data to identify high quality radiosonde types and use those radiosonde types to calibrate AMSU/MSU TTS.

***Approaches:*** Globally, there are roughly 850 radiosonde stations using about fourteen different types of radiosonde systems. The RO atmPrf data from COSMIC, CHAMP, and GRACE are first interpolated into the mandatory pressure level of the radiosondes. The horizontal resolution for RO measurements is around 200 km with a less than 100 km horizontal drift at the height of its tangent point. Radiosondes may also drift horizontally with wind after launch. To minimize the temporal and spatial mismatches between RO data and radiosonde observations (RAOBs), the RO atmPrf data within 2 hours and 300 km with those radiosonde data are collected for different ROAB instrument types. The position of COSMIC sounding is defined at the altitude around 5 km altitude. The RO-RAOB ensembles for different instrument type are collected from 2001 to 2010. Detail results are summarized in a journal paper and are not further described in this report. To demonstrate the feasibility to use GPS RO temperature to assess solar zenith angle (SZA) dependent biases, we compared the binned temperature biases at 50 hPa for RS92 ($\Delta T_{RS92(ID=81)}$), AVK-MRZ ($\Delta T_{AVK-MRZ(ID=27)}$), VIS-B2 ($\Delta T_{VIZ-B2(ID=51)}$), and Shanghai ($\Delta T_{Shanghai(ID=32)}$), respectively in **Figure 8**. **Figure 8** shows that the temperature biases from different radiosondes relative to RO temperature are consistent with known SZA dependent biases for each f individual radiosonde types.

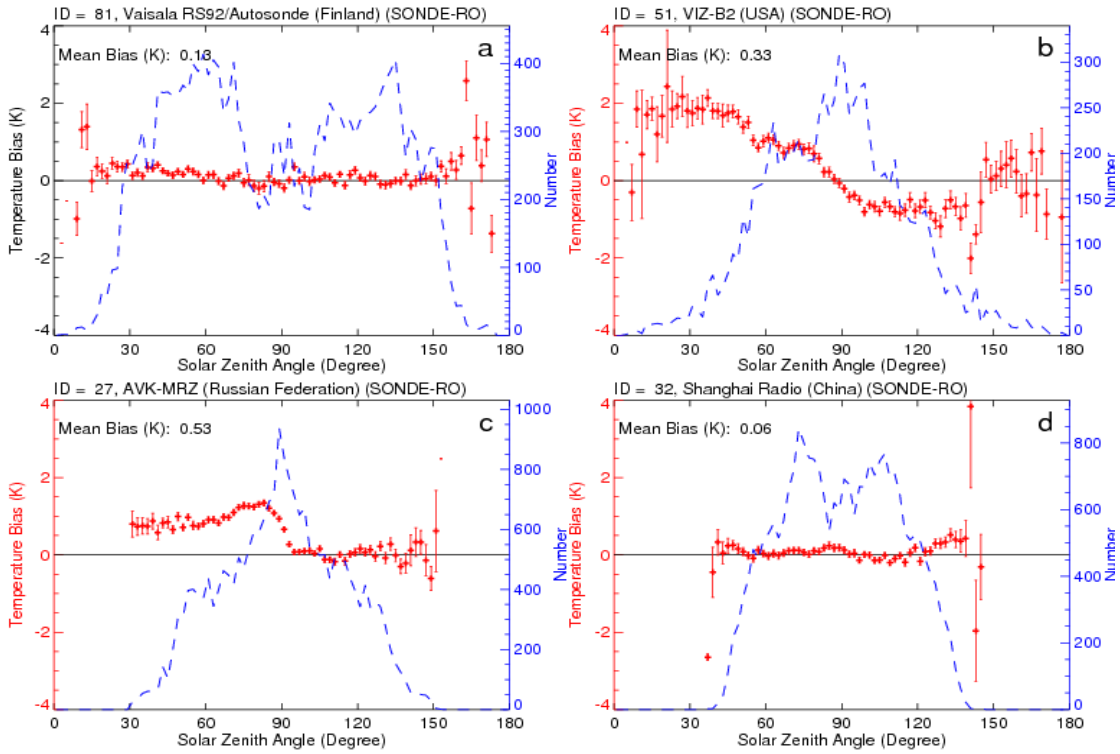


**Figure 8, the binned temperature biases for different SZA bins at 50 hPa for (a) RS92 ($\Delta T_{RS92(ID=81)}$), (b) AVK-MRZ ($\Delta T_{AVK-MRZ(ID=27)}$), (c) VIS-B2 ($\Delta T_{VIZ-B2(ID=51)}$), and (d) Shanghai ($\Delta T_{Shanghai(ID=32)}$).**

### 4.2 AMSU/MSU TTS results from 2001 to 2013

We also used RO identified high quality radiosonde observations (RAOBs) as references to calibrate AMSU/MSU TTS results. Five types of Vaisala radiosonde data from the year of 2001 to 2013 were used to calibrate TTS taken from AMSU microwave measurements from different satellites for potential improvements of tropopause and stratosphere temperature trend analysis. Details are described in the TTS CATBD and are not repeated here.

**Fig. 9** depicts the inter-satellite TTS biases between two missions when they are co-located. No calibration procedures are implemented. The inter-satellite TTS biases between N16-N15, N18-N15, N19-N15, Metop-A – N15, and Aqua-N15 are generated.

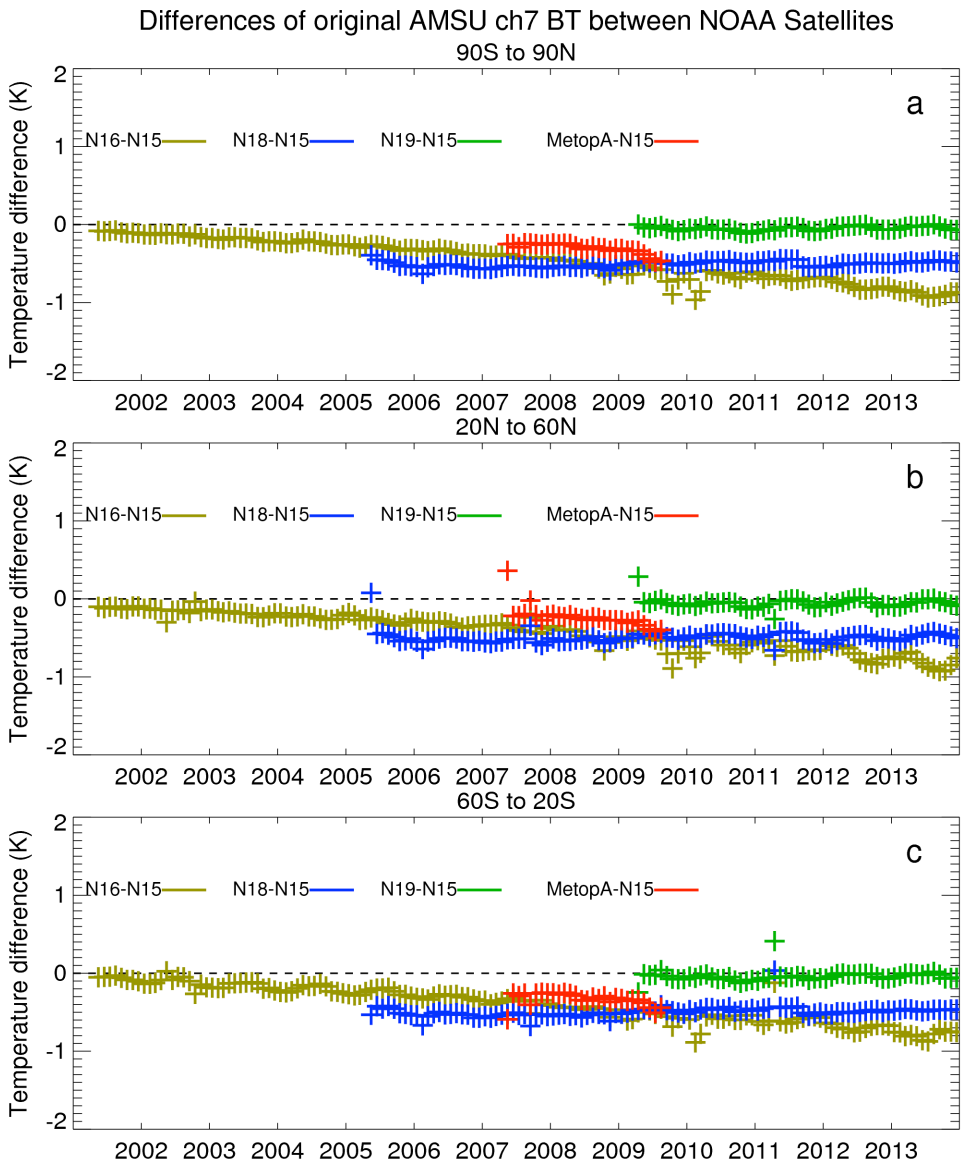


**Figure 9. The time series of the monthly TTS mean differences for N16-N15, N18-N15, N19-N15, Metop-A – N15, and Aqua-N15 for (a) the entire globe (90ºN to 90ºS), (b) the 20ºN to 60ºN zone, and (c) the 60ºS to 20ºS zone.**

After applying the calibration method to all the AMSU TTS from 2001 to 2013 from different NOAA, Aqua, and Metop-A missions, the time series of the inter-satellite biases of the calibrated TTS for different latitudinal zones are shown in **Fig. 10**.

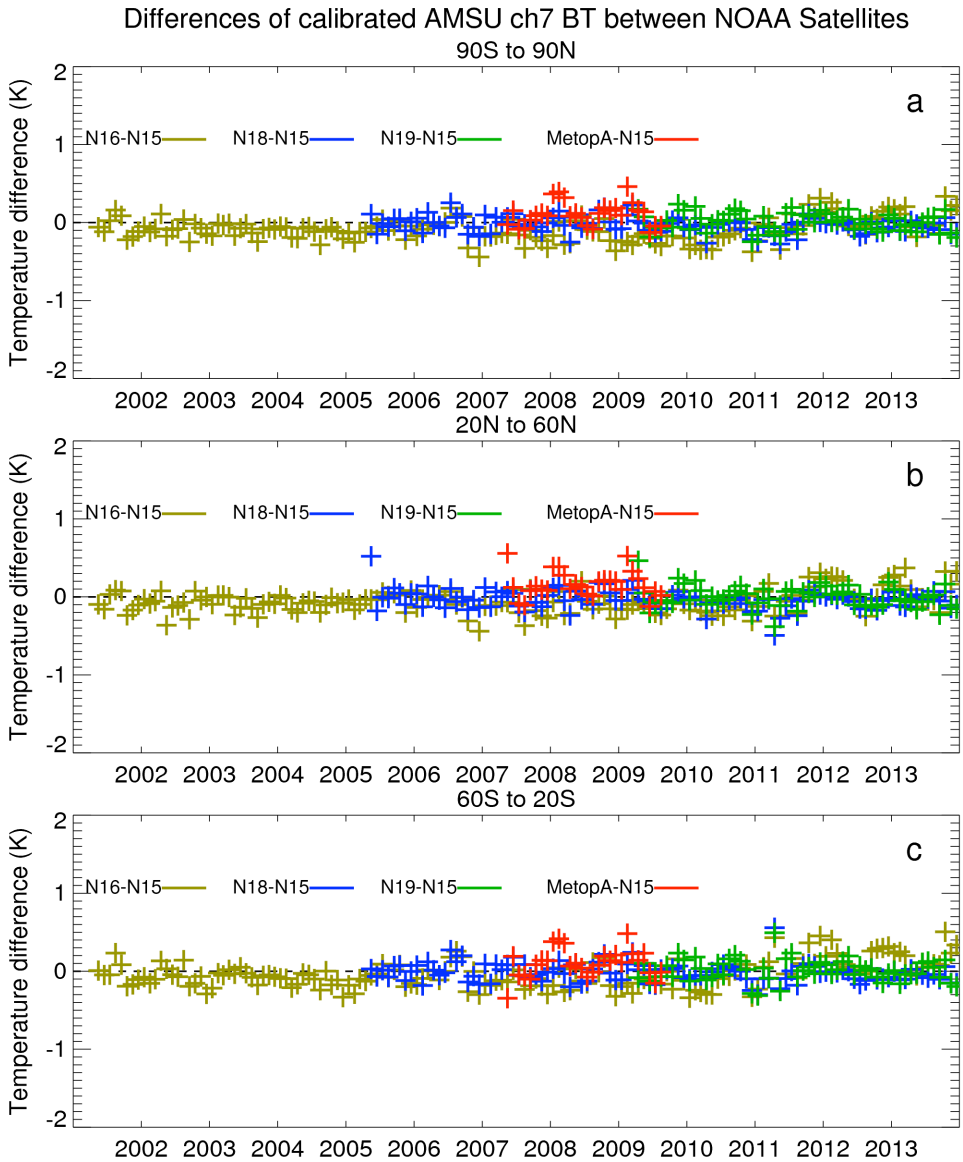


**Figure 10. The time series of the monthly calibrated TTS mean differences for for N16-N15, N18-N15, N19-N15, Metop-A – N15, and Aqua-N15 for (a) the entire globe (90ºN to 90ºS), (b) the 20ºN to 60ºN zone, and (c) the 60ºS to 20ºS zone.**

**Fig. 11** depicts the anomaly of AMSU TTS calibrated by RO identified RAOBs in December 2013. The monthly mean for AMSU TTS and the climatology of the AMSU TLS calibrated by RO data from 2002 to 2013 is also shown in **Fig. 11**.

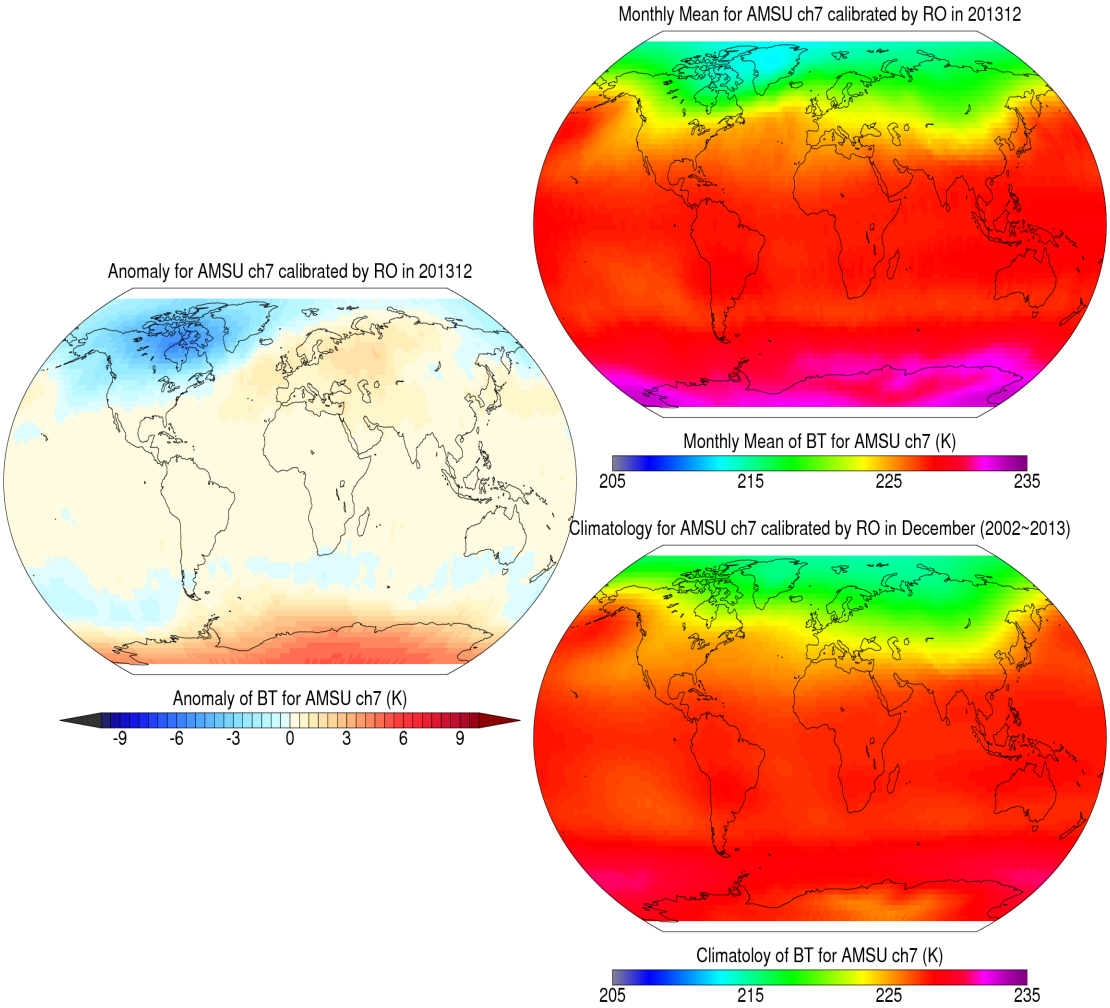


**Figure 11. The left panel shows the anomaly of AMSU TTS calibrated by high quality RAOBs in December 2013. The right upper panel is the monthly mean for AMSU TTS. The right lower panel depicts the climatology of the AMSU TTS calibrated by RAOB data from 2002 to 2013.**

### 4.3 Using calibrated AMSU/MSU TTS results before 2001 to calibrate those overlapped data from 1980 to 2000

We used the calibrated TTS after 2001 to calibrate MSU TTS and used those overlapped MSU TTS from 1980 to 2001 to further construct consistent TTS from 1980 to 2001. Again, without detailing all the refining procedures, we present the new TTS calibrated time series. **Figure 12** depicts the inter-satellite biases between two missions when they are co-located from 1980 to 2000. **Figure 13** depicts the inter-satellite biases between two missions after the MSU TTS are calibrated.

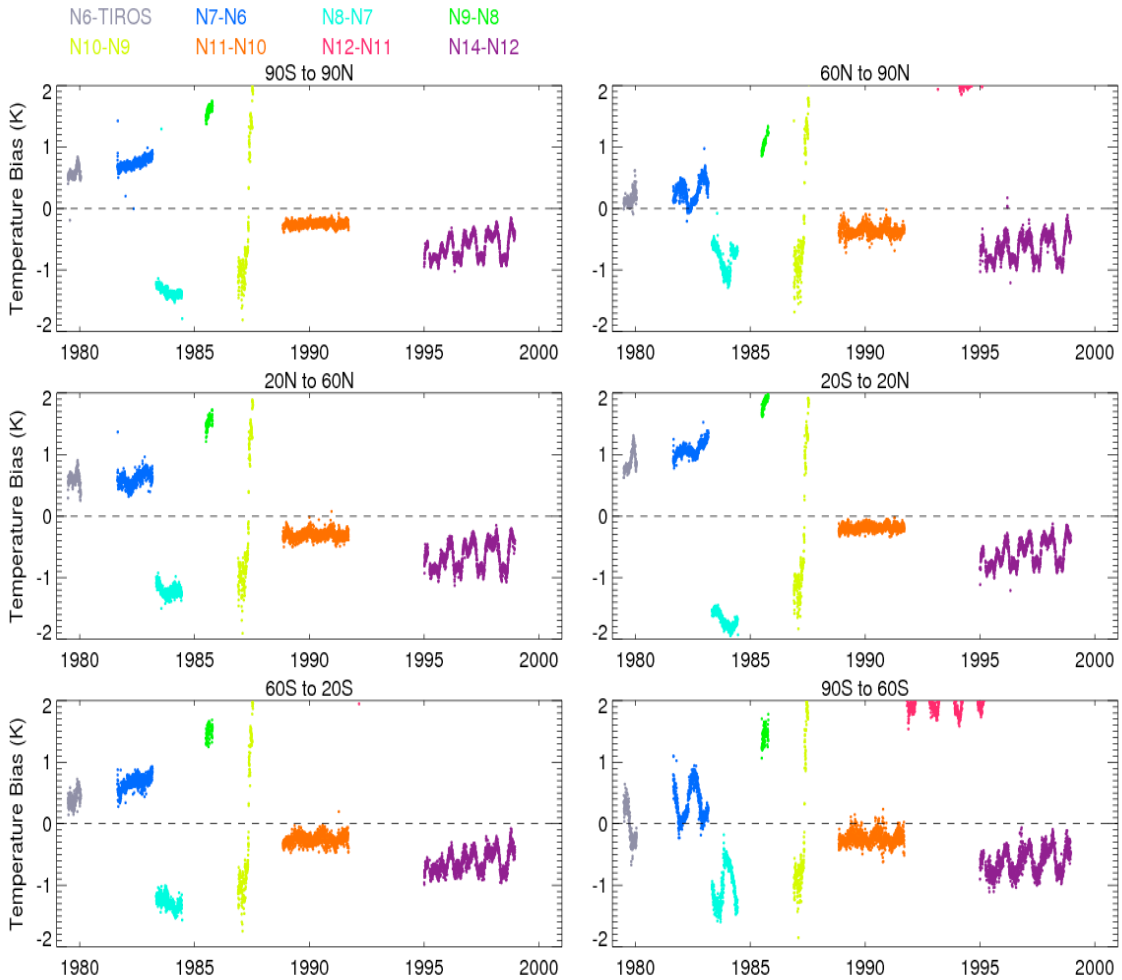


**Figure 12. The time series of the monthly TTS mean differences for N6-TIROS, N7-N6, N8-N7, N9-N8, N11-N10, N12-N11, N14-N12 for the global (upper left panel), 90º N to 60º N zone (upper right panel), 20º N to 60º N zone (middle left panel), 20º N to 20º S zone (middle right panel), 60º S to 20º S zone (lower left panel), and 90º S to 60º S zone (lower right panel).**

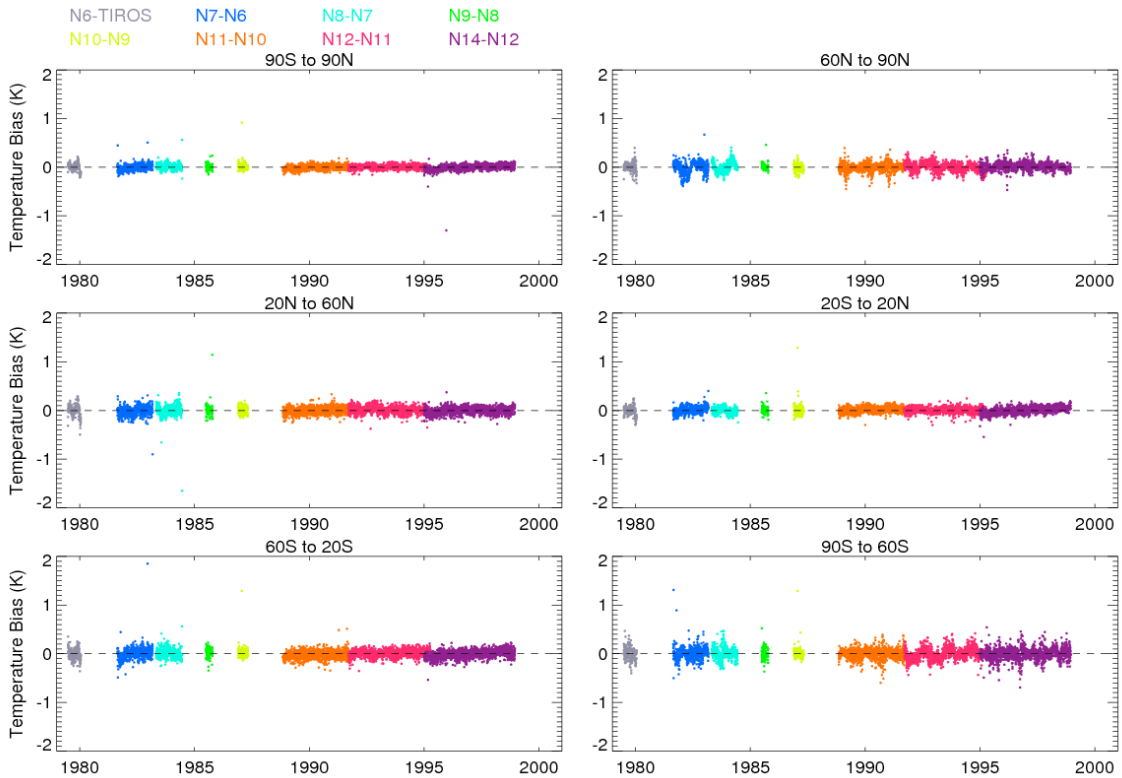


**Figure 13. The time series of the calibrated monthly TTS mean differences for N6-TIROS, N7-N6, N8-N7, N9-N8, N11-N10, N12-N11, N14-N12- for the global (upper left panel), 90º N to 60º N zone (upper right panel), 20º N to 60º N zone (middle left panel), 20º N to 20º S zone (middle right panel), 60º S to 20º S zone (lower left panel), and 90º S to 60º S zone (lower right panel).**

## 5. Tropopause Height Climate Data Records from 2001 to 2013

### 5.1 Detection of the Tropopause Height using COSMIC and CHAMP Temperature Profiles

The tropopause represents the boundary between the troposphere and stratosphere. It is an important region of the atmosphere often been examined to understand the stratosphere-troposphere exchange and coupling. The tropopause is defined as lapse rate tropopause (LRT) in this study. According to the standard World Meteorological Organization (WMO) [1957] definition, the tropopause is defined as “the lowest level at which the lapse rate decreases to 2°C/km or less, and the average lapse rate from this level to any level within the next higher 2°C/km does not exceed 2°C/km”. The procedures and criteria for using GPS RO temperature profiles to identify tropopause heights are:

(a) The lowest level between 500 mb and 70 mb at which lapse rate is less than -2$^{o}$C/km is calculated.

(b) The average lapse rate between this lowest level and all higher levels within 2 km does not exceed -2 K/km.

(c) None of the levels from this lowest level up to 2 km above has lapse rate less than -2 K/km.

(d) Mean lapse rate from the layers below this lowest layer is greater than -2 K/km. This minimizes the influence of outliers in the temperature profiles.

**Figure 14** depicts the mean tropopause height climatology and the monthly anomalies relatively to the mean climatology.

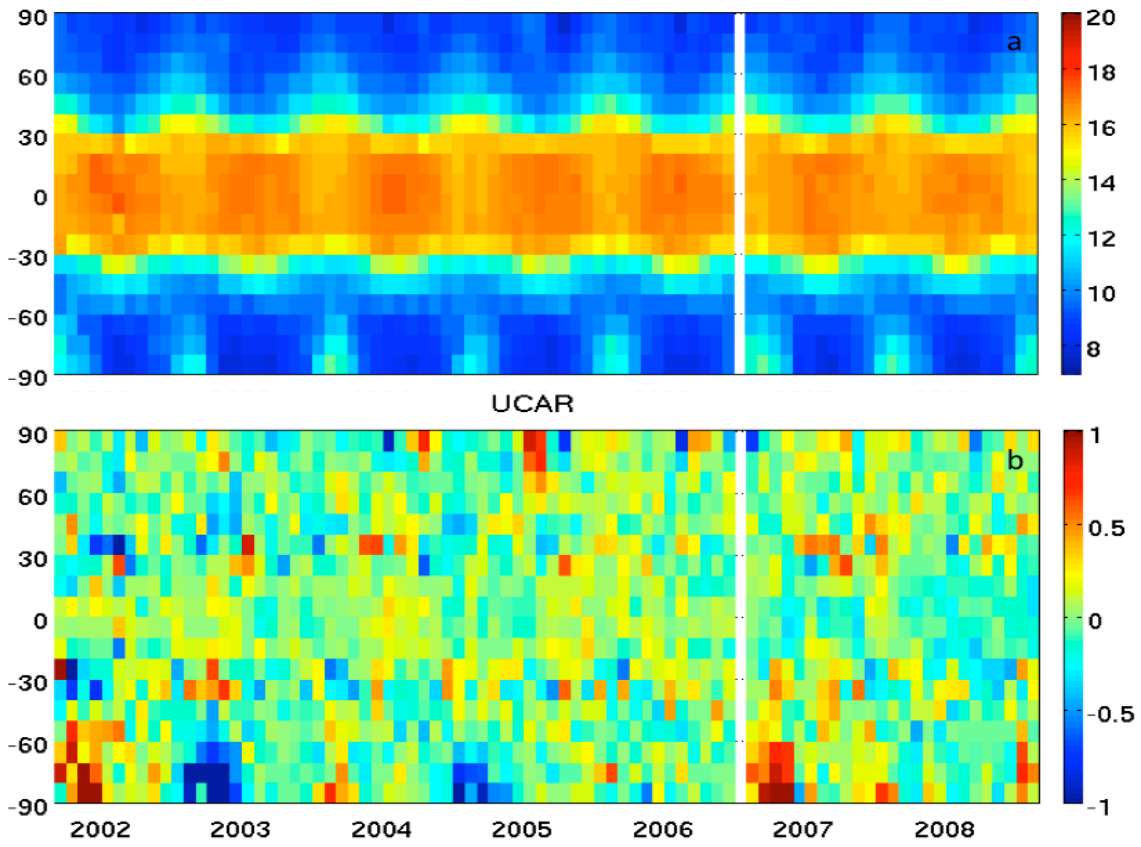


**Figure 14, a) mean tropopause height climatology (in km) generated by using CHAMP data from June 2001 to August 2008, and b) the corresponding monthly tropopause height anomalies (in km).**

## 5.2 Constriction of Tropopause Height Climatology and Quantification of its Sampling Errors

To construct tropopause height climatology, we need to first quantify and remove the sampling errors from different RO missions. According to the research of Ho et al. (2009), the reanalysis data such as NCEP can reproduces synoptic short-term (less than one month) changes and spatial variation which are the dominant cause of sampling error in GPS RO data especially for CHAMP. **Fig. 15** summarizes the results for the time series of tropopause height calculated from the temperature climatology. As mentioned above, we use NCEP, ERA-Interim and MERRA reanalysis data interpolated to RO profiles to compute the sampling errors.

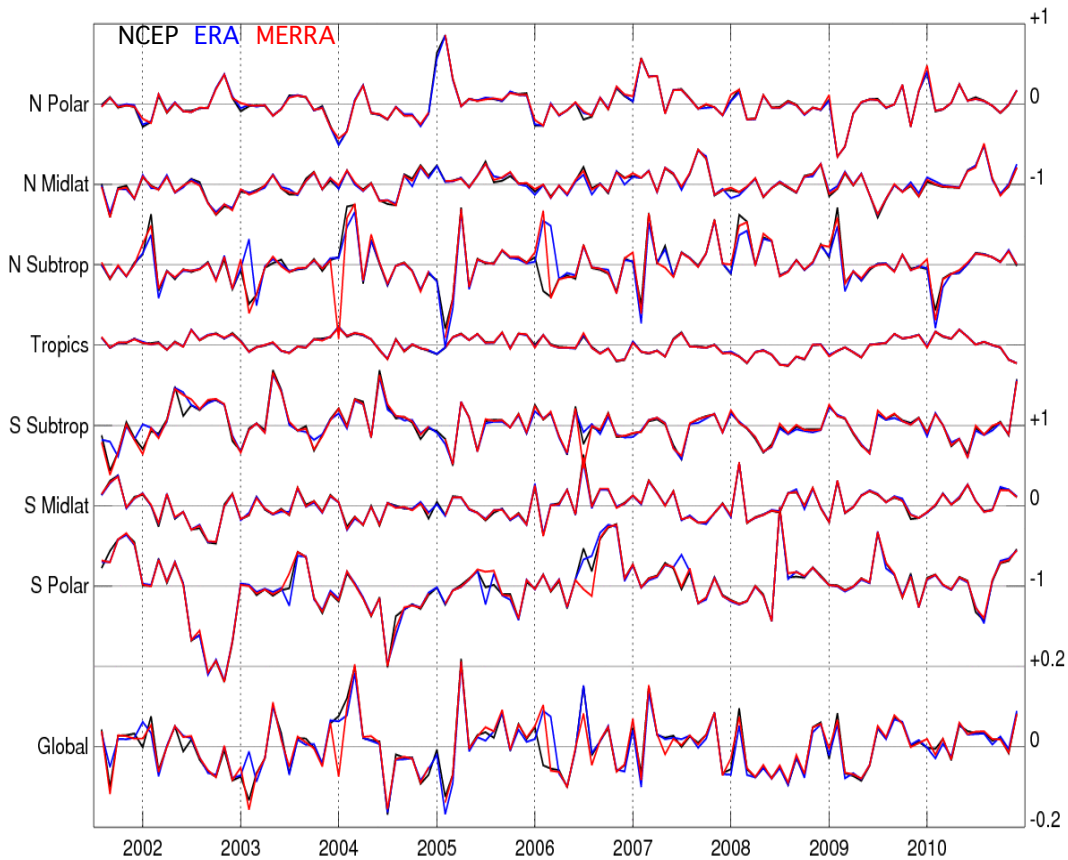


**Figure 15. Monthly anomalies of tropopause heights for different geographical regions and global. Each tick mark on the vertical axis represents 1 km (0.1 km for the global time series, black, NCEP; blue, ERA-Interim; red, MERRA).**

The Tropopause height trends [m/yr] based on GPS RO data from May 2001–December 2007 (80 months) from temperature calibrated by different models. (black, NCEP; blue, ERA-Interim; red, MERRA) is shown in **Fig. 16**.

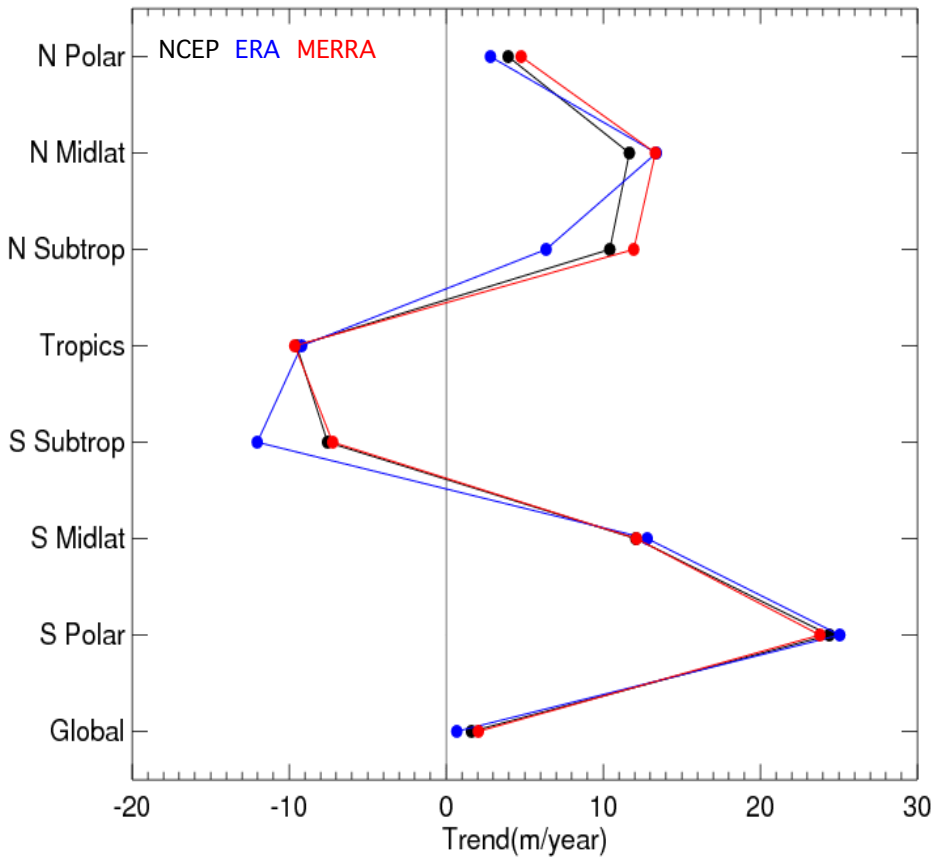


**Figure 16. Tropopause height trends [m/yr] based on GPS RO data from May 2001–December 2007 (80 months) from temperature calibrated by different models. (black, NCEP; blue, ERA-Interim; red, MERRA).**

### 5.3 Studies to improve the Maturity of the Tropopause Climatology

#### *a. Quantification of the Differences of Tropopause Height Climatologies derived from Different Tropopause Definitions*

Here we continue deriving tropopause height (lapse rate tropopasue (LPT) and cold point tropopause (CPT)) cliamtolgies from individual RO missions. These include CHAMP (2001 to 2008), GPS/Meteorology (GPS/MET, from 1995 to 1997), COSMIC (launched in April 2006), Gravity Recovery And Climate

Experiment (GRACE, launched in 2004), Satélite de Aplicaciones Científicas-C (SAC-C, launched in 2000), MetOp/GRAS (launched in 2006), Communication/Navigation Outage Forecast System (C/NOFS, launched in 2008), and Terra Synthetic Aperture Radar (SAR) operating in the X-band (TerraSAR-X, launched in 2007). **Figure 17** show the monthly mean tropopasue height differences between COSMIC and CHAMP from June 2006 to the September 2008.

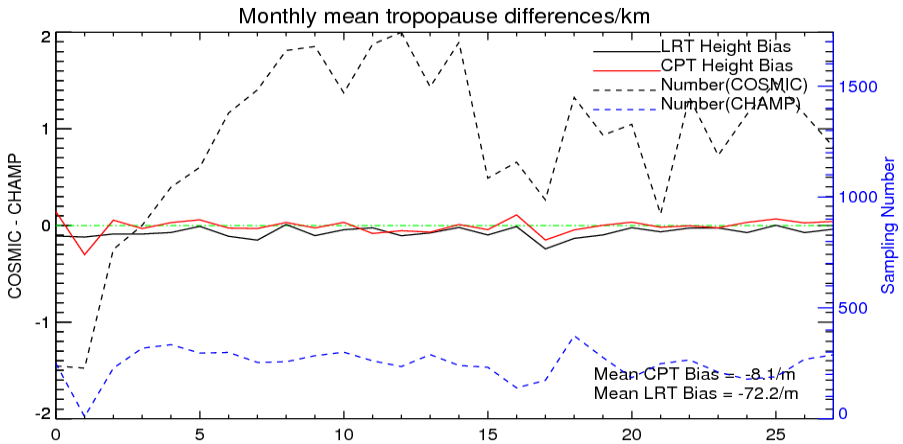


**Figure 17. The monthly mean CPT and LRT differences between COSMIC and CHAMP during the period from June 2006 to September 2008.**

### *b. Estimating the Structural Uncertainty of Tropopause Height Derived from GPS RO Data*

We continue quantifying the structural uncertainty of tropopause height derived from GPS radio occultation data. This is to inter-compare the of CHAMP tropopause height derived from DMI, EUM, GFZ, JPL, UCAR, and WEGC. **Figure 18** illustrates the results for the LRT height trends for the different binning methods and RO data centers. Results show that at most latitudes the LRT height trend is more sensitive to the binning method than the data centers. Although independent inversion algorithms and different quality control methods are used among centers, the difference among centers either for 5° or 10° binning method agree to within ±10m/yr except in the polar region (**Fig. 19**). Polar region show the largest difference between data centers for 5° binning methods (especially in the south polar region). This can be explained with the small sampling number and not apparent minimum values for temperature profiles in polar region.

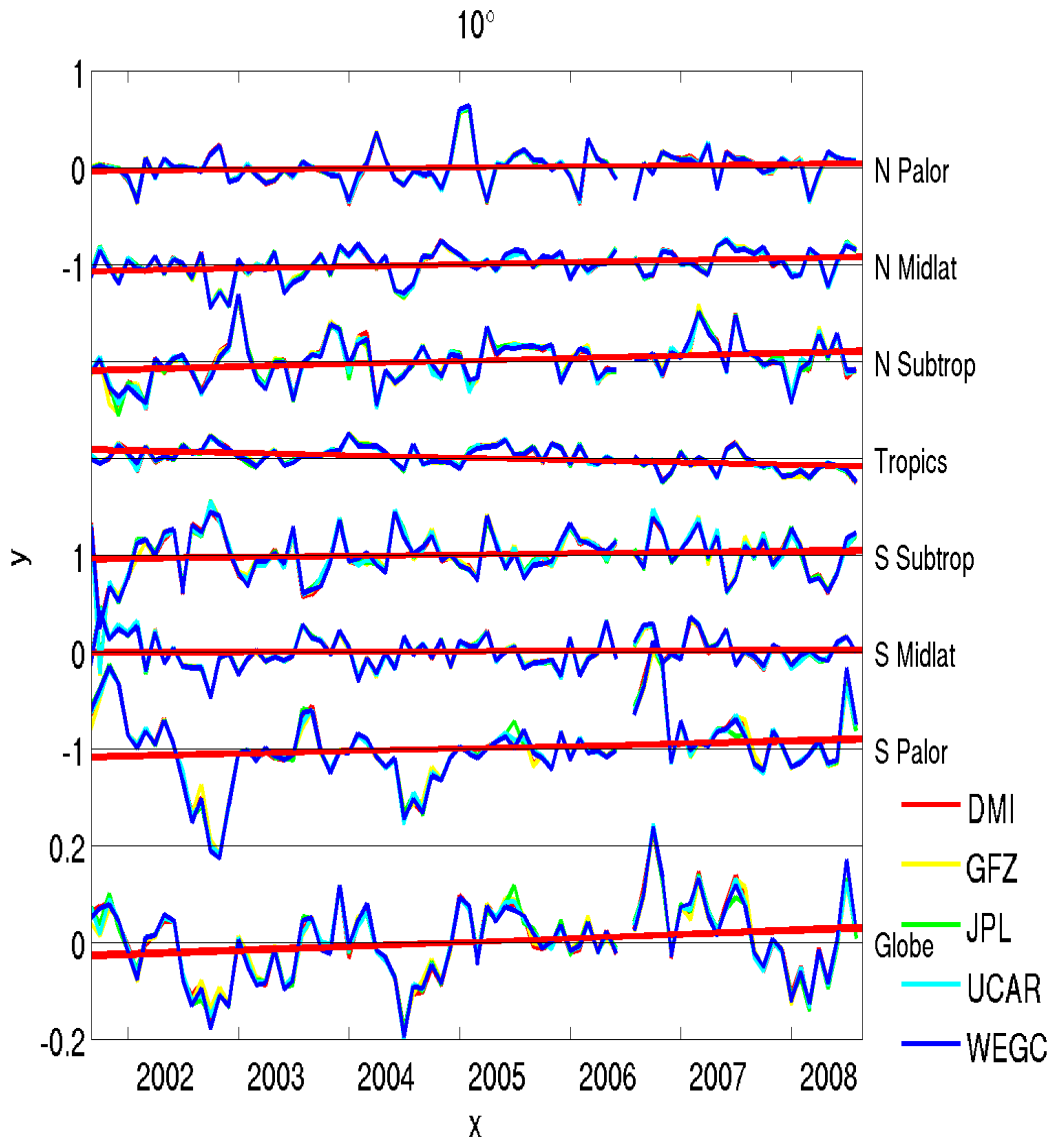


**Figure 18. The LRT time series from October 2001 to October 2008 for DMI, GFZ, JPL, UCAR and WEGC for different latitudinal zones.**

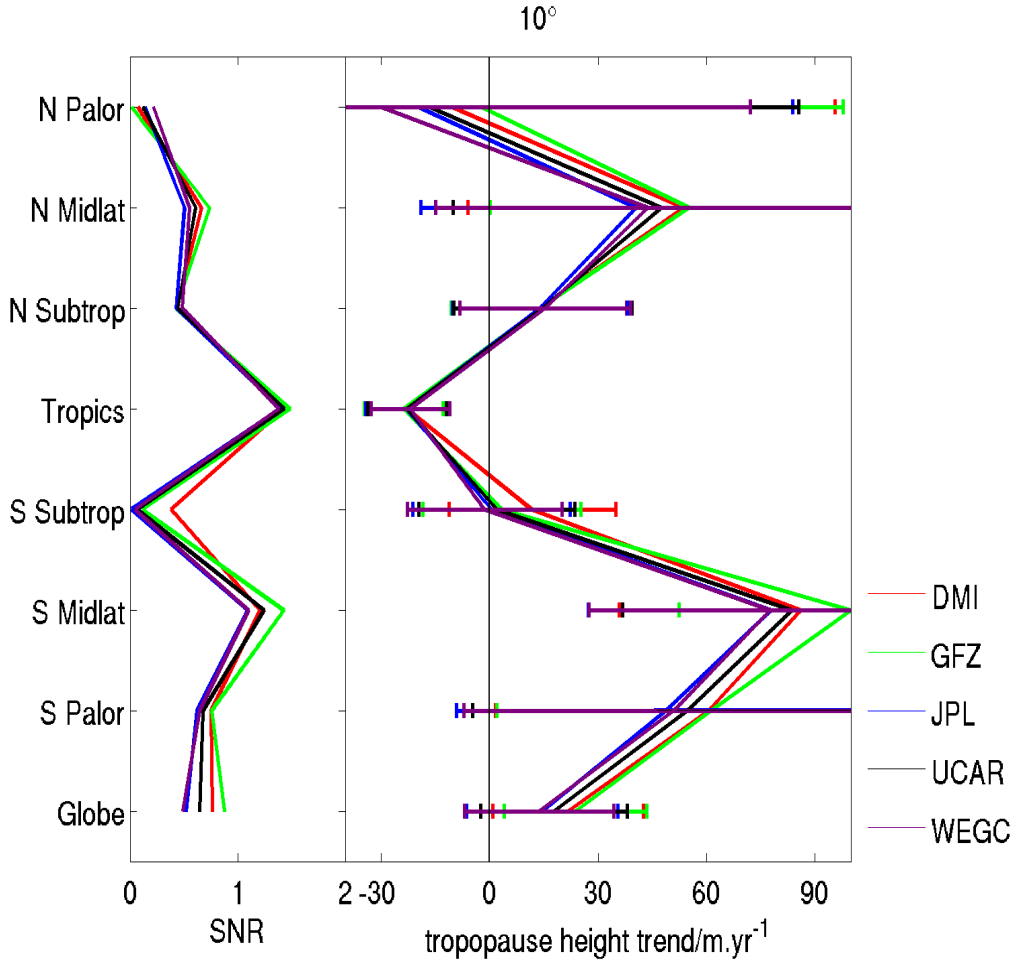


**Figure 19. The LRT trends (meter/yr) from October 2001 to October 2008 for DMI, GFZ, JPL, UCAR and WEGC for different latitudinal zones.**

### c. Quantification of the Impacts of QBO on the Global Tropopause Climatology

To demonstrate how the QBO will affect the global tropopause climatology, we compare time series of temperature anomalies (in K) from 8 km to 30 km in height and from 10 degree N to 10 degree S derived from UCAR CHAMP with the corresponding time series of the trend of tropopause height (in km/year) also computed by using UCAR CHAMP data (**Fig. 20**).

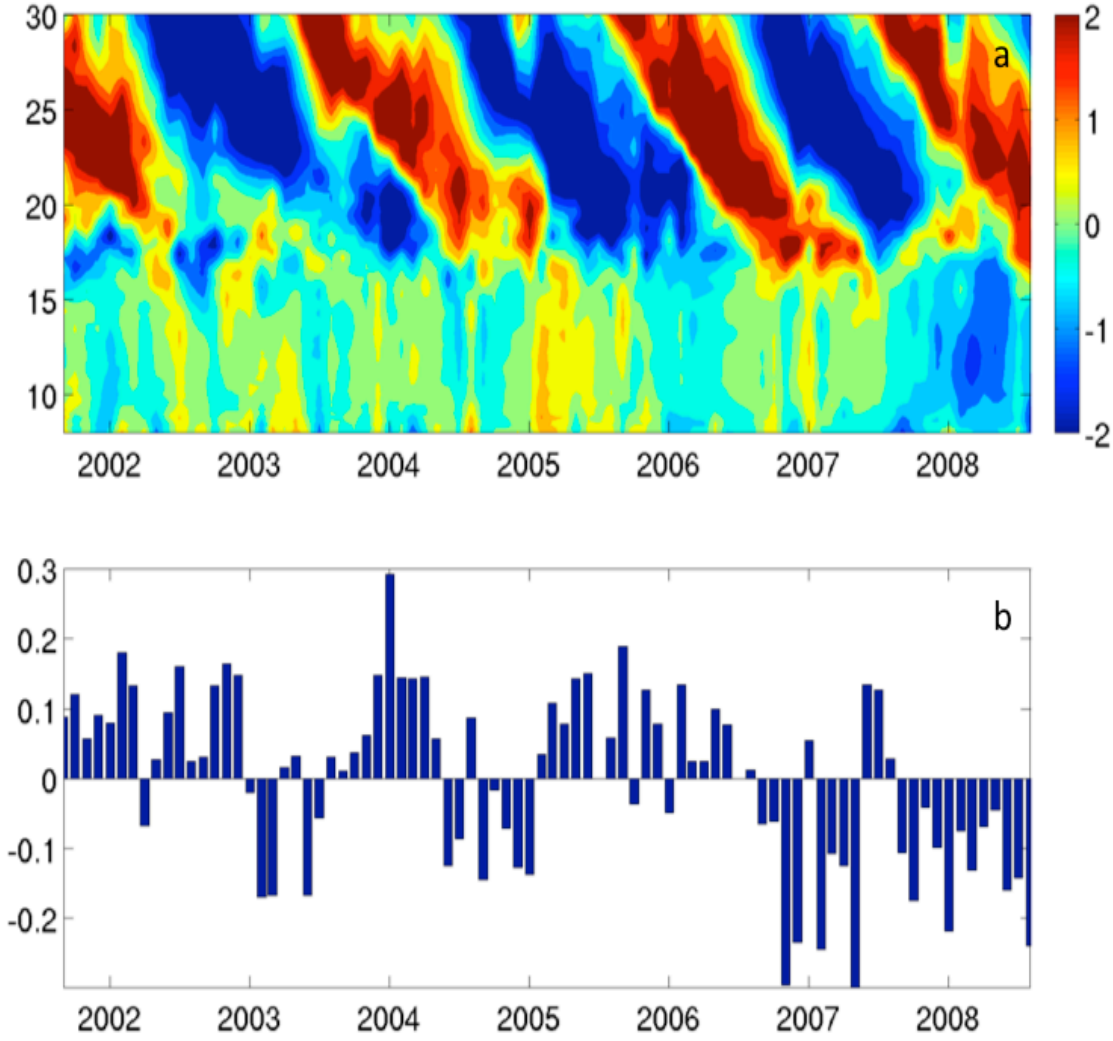


**Figure 20. a) time series of temperature anomalies (in K) from 8 km to 30 km in height and from 10 degree N to 10 degree S that are constructed by using UCAR CHAMP data, b) the corresponding time series of the trend of tropopause height (in km/year) also computed by using UCAR CHAMP data.**

## 6. Presentations and Publications

Publications and presentations related to the project are listed:


1) **Ho, S.-P.**, X. Yue, Z. Zeng, C. Ao, C.-Y. Huang, E. R. Kursinski, Y.-H. Kuo (2013), Applications of COSMIC Radio Occultation Data from the Troposphere to Ionosphere and Potential Impacts of COSMIC-2 Data, BAMS, doi: http://dx.doi.org/10.1175/BAMS-D-13-00035.1.

2) Mears, C., **S.-P. Ho**, L. Peng, Zhou, and J. Wang (2014), Total Column Water Vapor, [In "States of the Climate in 2013]. *Bul. Amer. Meteor. Sci.*, (*in press*).

3) **Ho, S.-P**., (section co-author) for IPCC AR5 report (invited)

4) Kumar, V., S. K. Dhaka, K. K. Reddy, A. Gupta, S. B. Surendra Prasad, V. Panwar¸ N. Singh, **S.-P. Ho**, and M. Takahashi (2014), Impact of Quasi-Biennial Oscillation on the inter-annual variability of the tropopause height and temperature in the tropics: A study using COSMIC/FORMOSAT-3 observations, Journal of Atmospheric Research (in press).

5) Huang, Ching-yuang, Wen-hsin Teng, **S.-P. Ho**, Y. H. Kuo (2013), Global Variation of COSMIC Precipitable Water over Land: Comparisons with Ground-based GPS Measurements and NCEP Reanalyses, GRL, DOI: 10.1002/grl.50885.

6) Blackwell, W. J., Rebecca Bishop, Clayton Crail, Kerri Cahoy, Brian Cohen, Lidia Cucurull, Pratik Dave, Michael DiLiberto, Neal Erickson, Chad Fish, **shu-peng Ho**, R. Vincent Leslie, Idahosa A. Osaretin, Radiometer Calibration Using Co-located GPS Radio Occultation Measurements, IEEE TRANSACTIONS ON GEOSCIENCE AND REMOTE SENSING, 2013 (*accepted*).

7) Mears, C., J. Wang, **S.-P. Ho**, L. Zhang, and X. Zhou (2013), Total Column Water Vapor, [In "States of the Climate in 2012]. *Bul. Amer. Meteor. Sci*.

8) Teng, Wen-Hsin, Ching-Yung Huang, **S.-P. Ho**, Ying-Hwa Kuo, and Xin-Jia Zhou (2013), Characteristics of Global Precipitable Water in ENSO Events Revealed by COSMIC Measurements, *J. Geophy. Research,* Vol. 118, 1–15, doi:10.1002/jgrd.50371.

9) Biondi, R., **S.-P. Ho**, W. Randel, T. Neubert and S. Syndergaard (2013), Tropical cyclone cloud-top heights and vertical temperature structure detection using GPS radio occultation measurements, *J.*

*Geophy. Research,* VOL. 118, 1–13, doi:10.1002/jgrd.50448.

10) Steiner, A. K., D. Hunt, **S.-P. Ho**, G. Kirchengast, A. J. Mannucci, B. Scherllin-Pirscher, H. Gleisner, A. von Engeln, T. Schmidt, C. Ao, S. S. Leroy, E. R. Kursinski, U. Foelsche, M. Gorbunov, Y.-H. Kuo, K. B. Lauritsen, C. Marquardt, C. Rocken, W. Schreiner, S. Sokolovskiy, S. Syndergaard, and J. Wickert (2013), Quantification of Structural Uncertainty in Climate Data Records from GPS Radio Occultation, *ACP* doi:10.5194/acp-13-1469-2013.

11) **Ho, S.-P**., Liang Peng, Richard A. Anthes, Ying-Hwa Kuo, and Hsiao-Chun Lin, 2014, Marine Boundary Layer Heights and their Longitudinal, Diurnal and Inter-annual Variation in the Southeast Pacific using COSMIC, CALIOP, and Radiosonde Data, *J. of Climate* (submitted).

12) **Ho, S.-P**., L. Peng, X. J. Zhou, 2013: Calibration and Construction of Microwave Sensor Temperature Records in the Lower Stratosphere from 2001 to 2010 Using Global Positioning System Radio Occultation Data, *J. Geophy. Research (submitted).*

13) Dhaka, S. K., V. Kumar, R. K. Choudhary, **S.-P. Ho**, and K. K. Reddy (2014), Observation of strong remote dynamical connection between polar and tropical regions due to sudden stratospheric warming of 2009, *J. Geophy. Research* (submitted).

14) Kumar, V., S. K. Dhaka, R. K. Choudhary, **S.-P. Ho**, and K. K. Reddy (2014), On the occurrence of coldest temperature in stratospheric region and tropical tropopause stability: A study using COSMIC/ FORMOSAT-3 satellite measurements, Journal of Atmospheric and Solar-Terrestrial Physics (accepted).

15) **Ho, S.-P.**, Y.-H. Kuo, X.-J. Zhou, P. Callaghan (2011), The Use of the COSMIC/FORMOSAT-3 Global Positioning System Radio Occultation Data as Global Reference Observations in Orbit and Their Applications in Meteorology, *Horizons in Earth Science Research, Vol. 5*, B. Veress and J. Szigehty, Eds. NOVA Publishers, in press (invited)

16) **Ho, S.-P.**, Zhou X., Kuo Y.-H., Hunt D., Wang J.-H., (2010a), Global Evaluation of Radiosonde Water Vapor Systematic Biases using GPS Radio Occultation from COSMIC and ECMWF Analysis. *Remote Sensing*. 2010; 2(5):1320-1330. [Cited by 19]

17) **Ho, S.-P.**, Ying-Hwa Kuo, William Schreiner, Xinjia Zhou (2010b), Using SI-traceable Global Positioning System Radio Occultation Measurements for Climate Monitoring [In “States of the Climate in 2009]. *Bul. Amer. Meteor. Sci*., **91** (7), S36-S37. (invited).

18) **Ho, S.-P.**, G. Kirchengast, S. Leroy, J. Wickert, A. J. Mannucci, A. K. Steiner, D. Hunt, W. Schreiner, S. Sokolovskiy, C. O. Ao, M. Borsche, A. von Engeln, U. Foelsche, S. Heise, B. Iijima, Y.-H. Kuo, R. Kursinski, B. Pirscher, M. Ringer, C. Rocken, and T. Schmidt (2009a), Estimating the Uncertainty of using GPS Radio Occultation Data for Climate Monitoring: Inter-comparison of CHAMP Refractivity Climate Records 2002-2006 from Different Data Centers, *J. Geophys. Res.*, doi:10.1029/2009JD011969. [Cited by 48]

19) **Ho, S.-P.**, M. Goldberg, Y.-H. Kuo, C.-Z Zou, W. Schreiner (2009b), Calibration of Temperature in the Lower Stratosphere from Microwave Measurements using COSMIC Radio Occultation Data: Preliminary Results, Terr. Atmos. Oceanic Sci., Vol. 20, doi: 10.3319/TAO.2007.12.06.01(F3C). [Cited by 32] (ranked one of the top 50 most popular papers for TAO)

20) **Ho, S.-P**., Enhancement of the AIRS Temperature and Water Vapor Retrievals using Global Positioning System Radio Occultation Data, AIRS science team, JPL, May 22, 2013.

21) **Ho, S.-P**., Construction of Consistent Microwave Sensor Temperature Records and Tropopause Height Climatology using MSU/AMSU Measurements, GPS RO Data, and Radiosonde Observations, NOAA's Climate Data Record Annual Meeting, July 30-31, August 1, 2013, Asheville, NC.

22) **Ho, S.-P**., Calibration of Temperature Troposphere / Stratosphere from Advanced Microwave Sounding Unit using High Quality Radiosonde Data Identified by Radio Occultation Data, Joint OPAC-5 and IROWG-3 workshop, September 5-11, 2013, Seggau Castle, Leibnitz, Austria.

23) Biondi, R. W. Randel, **S.-P. Ho**, and S. Syndergaard, Thermal structure of tropical cyclones and intense convective systems using GPS radio occultation measurements, Joint OPAC-5 and IROWG-3 workshop, September 5-11, 2013, Seggau Castle, Leibnitz, Austria.

24) **Ho, S.-P.**, New Science opportunities on COSMIC-2/FORMOSAT-7, COSMIC annual retreat, Oct. 10, Boulder CO.

25) **Ho, S.-P.**, Liang Peng, Rick Anthes, Ying-Hwa Kuo, and Hsiao-Chun Lin,Estimation of Planetary Boundary Layer Heights from COSMIC, CLIPSO, and High Resolution Radiosondes during the VOCALS-REx Conference Title: 18th Conference on Integrated Observing and Assimilation Systems for the Atmosphere, Oceans, and Land Surface (IOAS-AOLS) Meeting. Feb. 2-6, 2014, Atlanta, GA.

26) **Ho, S.-P**., Liang Peng, Rick Anthes, Ying-Hwa Kuo, and Hsiao-Chun Lin, Planetary Boundary Layer Heights from COSMIC and CALIOP over Ocean, Donald R. Johnson Symposium Meeting, 94th American Meteorological Society Annual Meeting, Feb. 2-6, 2014, Atlanta, GA.